LOCKHEED MARTIN ENERGY RESEARCH LIBRARIES
3 4456 0514257 4

CENTRAL RESEARCH LIBRARY
DOCUMENT COLLECTION

OAK RIDGE NATIONAL LABORATORY
operated by
UNION CARBIDE CORPORATION • NUCLEAR DIVISION
for the
U.S. ATOMIC ENERGY COMMISSION

ORNL-TM-3148

Copy 68

DATE - March 28, 1972

Neutron Physics Division

NONELASTIC INTERACTIONS OF NUCLEONS AND π-MESONS WITH COMPLEX NUCLEI AT ENERGIES BELOW 3 GeV*

Hugo W. Bertini, Miriam P. Guthrie,
and Arline H. Culkowski†

Abstract

Nonelastic interactions corresponding to continuum state transitions are calculated using the intranuclear-cascade-evaporation approach. Spallation yields, energy- and angular-dependent spectra, particle multiplicities, and nonelastic cross sections are calculated for incident nucleons and π-mesons with energies below 3 GeV on complex nuclei. Comparisons with experimental data are made and, in general, the agreement is good. Discrepancies in these comparisons are discussed with respect to the deficiencies in the model.

NOTE:
Research partially funded by the
National Aeronautics and Space Administration
under Order H-38280A

OAK RIDGE NATIONAL LABORATORY
CENTRAL RESEARCH LIBRARY
DOCUMENT COLLECTION
LIBRARY LOAN COPY
DO NOT TRANSFER TO ANOTHER PERSON
If you wish someone else to see this document, send in name with document and the library will arrange a loan.
UCN-7969
(3 3-67)

*Submitted for journal publication.

†Mathematics Division.

NOTICE This document contains information of a preliminary nature and was prepared primarily for internal use at the Oak Ridge National Laboratory. It is subject to revision or correction and therefore does not represent a final report.

This report was prepared as an account of work sponsored by the United States Government. Neither the United States nor the United States Atomic Energy Commission, nor any of their employees, nor any of their contractors, subcontractors, or their employees, makes any warranty, express or implied, or assumes any legal liability or responsibility for the accuracy, completeness or usefulness of any information, apparatus, product or process disclosed, or represents that its use would not infringe privately owned rights.

INTRA-LABORATORY CORRESPONDENCE

OAK RIDGE NATIONAL LABORATORY

August 7, 1972

To: Recipients of Subject Report

Report No.: ORNL-TM-3148 Classification: Unclassified

Author(s): Hugo W. Bertini, Miriam P. Guthrie & Arline H. Culkowski

Subject: Nonelastic Interactions of Nucleons and π -Mesons with Complex Nuclei at Energies Below 3 GeV.

Request compliance with indicated action:

In the above report, the zero energy p-n cross section that is used in the intranuclear cascade calculation (MECC-7) was incorrectly tabulated in Table I, page 35. It was given as 196.5 mb and it should be 1965 mb. Please make this correction in your copy(ies) of the report.

N. T. Bray, Supervisor
Laboratory Records Department
Information Division

NTB:we

lev
9/18/72

UCN-430
(3 5-61)

TABLE OF CONTENTS

	Page No.
ABSTRACT	1
INTRODUCTION	1
COMPARISON WITH GLAUBER THEORY	3
THE NUCLEAR MODEL	6
PARTICLE-PARTICLE INPUT DATA	6
General Features	6
Nucleon-Nucleon Reactions	7
Pion-Nucleon Reactions	9
The Isobar Model	11
COMPARISON WITH PREVIOUS CALCULATION	12
COMPARISONS WITH EXPERIMENT	13
Statistical Error	13
Total Nonelastic Cross Sections	13
Secondary Particle Multiplicities	14
Secondary Particle Spectra	16
Spallation Products	18
Incident Pions	25
CONCLUSIONS	26
PROGRAM INFORMATION	28
ACKNOWLEDGMENTS	29
REFERENCES	30
TABLES I through XXII	35-56
FIGURES 1 through 37	57-93
APPENDIX	94

LOCKHEED MARTIN ENERGY RESEARCH LIBRARIES

3 4456 0514257 4

Nonelastic Interactions of Nucleons and π-Mesons with Complex Nuclei at Energies Below 3 GeV*

Hugo W. Bertini, Miriam P. Guthrie,
and Arline H. Culkowski†
Oak Ridge National Laboratory, Oak Ridge, Tennessee, 37830

ABSTRACT

Nonelastic interactions corresponding to continuum state transitions are calculated using the intranuclear-cascade evaporation approach. Spallation yields, energy- and angular-dependent spectra, particle multiplicities, and nonelastic cross sections are calculated for incident nucleons and π-mesons with energies below 3 GeV on complex nuclei. Comparisons with experimental data are made and, in general, the agreement is good. Discrepancies in these comparisons are discussed with respect to the deficiencies in the model.

INTRODUCTION

Over the years there has evolved a powerful method for calculating nonelastic reactions of nucleons and π-mesons with complex nuclei. This is the method of intranuclear cascades followed by evaporation. In this approach, the continuum state transitions of high-energy particles ($E \geqslant 100$ MeV) on nuclei are treated as a two-step process. The first step is the fast cascade where the reaction is described by a series of individual particle-particle reactions that occur within the nucleus, and the second is the evaporation of particles from the excited nucleus

*Research partially funded by the National Aeronautics and Space Administration, Order H-38280A, under Union Carbide Corporation's contract with the U. S. Atomic Energy Commission.

†Mathematics Division.

remaining after the cascade. Monte Carlo calculational techniques are generally employed. The method has proven to be successful in the energy region below that where pion production is important,[1-4] and it has been shown to be valid in predicting the high-energy[5] and low-energy[6] spectra of secondary nucleons for incident nucleons on complex nuclei at energies $\lesssim$ 3 GeV.

The work described in this paper is an extension of earlier work presented elsewhere.[5] The present model incorporates better data pertaining to all of the particle-particle reactions in which pions are involved. The validity of the present model is tested by comparing predicted values with experimental results for the following: (a) pion-nucleus nonelastic cross sections; (b) secondary nucleon and pion multiplicities from reactions involving incident nucleons and π-mesons; (c) angle-energy correlated pion spectra for incident nucleons, and (d) spallation product cross sections for incident nucleons and π-mesons. It is shown that the predictions of the theory are in reasonable agreement with most of the experimental data, and where consistent discrepancies are observed, they can usually be attributed to specific deficiencies of the model. It was deemed necessary to carry out these extensive comparisons for a variety of energies, incident particles, and target elements in order to ferret out the deficiencies that might be overlooked in a cursory survey.

The fact that so much experimental data can be subjected to theoretical interpretation illustrates the extreme power of the approach, particularly when there are no arbitrary constants that can be adjusted to fit the particle-nucleus data. To be sure, not all of the particle-particle data that have been incorporated into the model are free of

constants. But adjustments were only made to fit the experimental data for free particle-particle reactions. An example of this is the angular distribution of the isobars, which will be discussed later.

COMPARISON WITH GLAUBER THEORY

It is interesting to compare the basic assumptions generally used in the intranuclear-cascade model with those of the high-energy collision theory formulated by Glauber[7] and to compare the effects that are incorporated in each.

Basic to both approaches is that $ka \gg 1$, where k is the wave number of the incident beam and a is the range of the nuclear forces. In the Glauber theory one assumes that $(V/E) \ll 1$, where V is the nuclear potential and E is the kinetic energy of the incident particle. This is not necessary in the theory of intranuclear cascades, and hence the cascade theory can be applied at lower energies. In the Glauber theory it is assumed that all scatterings with bound nucleons are at small angles, and consequently only small momentum transfers are permitted. Attempts to modify this restriction somewhat have been made with reasonable success.[8,9] However, in the theory of intranuclear cascades, all scattering angles and momentum transfers consistent with the exclusion principle are permitted. In the formulation of a time-dependent Glauber theory, the time dependence of particular operators is neglected (this is consistent with small momentum transfers), which is equivalent to neglecting the differences in relative energies between the incident beam and the various moving but bound nucleons. These differences are accurately calculated in the cascade theory, which leads to more reasonable

estimates of the pion-production thresholds for incident particles on complex nuclei.

Effects that are included in the Glauber theory but not in the cascade theory are the interference from multiple scattering, the correlations of the bound nucleons, and, if desired, spin-dependent and velocity-dependent interactions can be included. The velocity dependence of the interactions has been tested in the cascade theory, and the effects were found to be small.[10] A particular correlation effect arising from the hard core of the nucleon-nucleon potential was investigated by Chen *et al.*[4] Because the core is hard, successive collisions cannot take place within its spatial region, and to approximate this effect successive collisions were forbidden to take place within about 1 F of each other in the cascade. The effect was found to be significant, and it compensated for the discrepancy with particle-nucleus data that was introduced when refraction effects were included in the cascade calculation.[4] In the model used here, neither the hard core effects nor the refraction effects are included. The only correlation effect that is taken into account is that of the absorption of pions on nucleon pairs.

The main difference between the Glauber theory and that of intranuclear cascades is that in the former, all of the nuclear effects are used to modulate the incident wave. Pion production, for example, is treated as an absorption. The modulated wave is used to describe the elastic and nonelastic differential cross sections for the incident beam. In the cascade theory there is no modulation. This is equivalent to giving arbitrary phase to the waves that are scattered off of each bound nucleon, and hence the method is not applicable to those reactions

where the Glauber theory has its greatest strength, i.e., in the calculation of the forward peaked elastic and nonelastic scattering amplitudes.

In the incoherent region of momentum transfers, i.e., beyond the elastic scattering peak and beyond the region containing structure, the Glauber model is inappropriate whereas the cascade model becomes applicable, and hence it appears that the two calculations are, in fact, complementary.

A few additional remarks should be made on some of the recent extensions of the Glauber theory. By keeping the small-angle approximation but including closure (i.e., assuming all final states of the nucleus are excited), Trefil has extended the inelastic scattering cross section into the incoherent region.[11] Using the same formalism he calculated the forward differential cross section for producing a K*, for example, by making use of the fact that the nucleus cannot return to its ground state in a reaction such as this. Later, Fishbane and Trefil[12] included multiple particle production at the collision sites within the nucleus.

There are several restrictions involved in each extension. The small-angle approximation is common to all. In extending the region of applicability of the inelastically scattered particles into the incoherent region (restricted in extent by the small-angle approximation) one is still dealing with the incident particle. When a particle such as a K* is introduced, its production is similar to a single knockout reaction where the K* is produced by the collision of an incident pion with a nucleon, and it and the resulting Λ escapes from the nucleus.[13] When

multiple production is included, it is assumed that the target nucleus remains constantly in its groud state.[12] All of the restrictions are necessitated by the difficulties encountered in attempting to solve these very complicated problems analytically.

As a final word, the Glauber high-energy theory is inappropriate for calculating the excited states of the residual nucleus following the nonelastic reactions, and hence it has shed no light (so far) on the spallation products resulting from high-energy interactions.

THE NUCLEAR MODEL

The details of the nuclear model are described elsewhere,[2,5] It is sufficient to say that the diffuseness of the nuclear edge, the motion of the bound nucleons, the exclusion principle, and a local potential for nucleons and pions are included, but reflection and refraction of the incident particles[3] and nuclear correlations[4] are not. The latter are included only in that pions are assumed to be absorbed on nucleon-nucleon pairs within the nucleus.[2]

PARTICLE-PARTICLE INPUT DATA

General Features

Wherever possible free-particle experimental cross sections were employed, and where these data were lacking, they were estimated by the use of isotopic spin concepts or phase shift analyses. Scattering reactions, and single π-meson and double π-meson production reactions were included in nucleon-nucleon collisions. In pion-nucleon collisions, scattering, charge exchange, absorption, and single π-meson production

reactions were taken into account. Pion absorption was assumed to take place on nucleon pairs.[2] The Sternheimer-Lindenbaum isobar model was used to describe the branching ratios and the kinematics in all of the pion-production reactions.[14] The isobar was assumed to decay at the space point where it was created. All kinematics calculations were carried out relativistically. A cross section at any required energy was obtained by linear interpolation of the cross sections that were tabulated at specific energies. Further details and discussions of some of these points, for example, the neglect of pion absorption via isobar reactions, is given elsewhere.[5]

Nucleon-Nucleon Reactions

The nucleon-nucleon cross sections that were utilized are illustrated in Figs. 1-6 and in Table I. The elastic proton-neutron cross section at energies from 360 to 920 MeV was calculated using the difference $\sigma_t(pn) - \sigma_{sp}(pn)$ (the total and single production cross sections, respectively) while at energies > 1200 MeV it was calculated from the relation

$$\sigma_{el}(pn) = \frac{1}{2}\left[\frac{\sigma_t(I=0)}{\sigma_t(pp)} \times \sigma_{el}(pp)\right] + \frac{1}{2}\sigma_{el}(pp) \quad ,$$

which comes from isotopic spin considerations. $\sigma_t(I=0)$ is the contribution to the total cross section from the isotopic spin I=0 state, which was taken from the paper by Bugg *et al.*[15] To fill in between 920 and 1200 MeV a smooth curve was arbitrarily drawn. The values of the cross sections at zero were calculated so that the trapezoid formed by connecting a straight line from the cross section at zero to that at 20 MeV would

yield the same integral from 1 MeV to 20 MeV as

$$\int_{1}^{20} \sigma_{NN}(E)\, dE$$

where σ_{NN} is the n-p or p-p cross section determined by experimental data.[16] Only on rare occasions would a particle-particle reaction occur in which the relative kinetic energy would be below 1 MeV, and since the cross section is evaluated in the calculation by linear interpolation between values tabulated at 20-MeV intervals, this method was deemed appropriate. A lower-energy limit was not used in order to avoid the extreme inefficiencies of the sampling techniques[17] when large peaks occur in the cross sections.

The p-p single π-meson production cross section (Fig. 3) was taken to be the sum of the experimental cross sections for the $p+p \rightarrow p+p+\pi^{o}$ and $p+p \rightarrow p+n+\pi^{+}$ reactions. The p-n cross section for producing one π-meson was taken to be $\sigma(p+n \rightarrow p+n+\pi^{o}) + 2\sigma(p+n \rightarrow p+p+\pi^{-})$ where these partial cross sections, along with the single production cross section, are illustrated in Fig. 4. Because there were no experimental data above 1 GeV, the cross sections at the higher energies were estimated as follows: the slope of the $p+n \rightarrow p+p+\pi^{-}$ cross section curve was taken to be equal to that for the $p+p \rightarrow p+p+\pi^{o}$ reaction and the curve of the $p+p+\pi^{-}$ cross section was simply extended beyond 1 GeV with this slope. The equality

$$\sigma(p+n \rightarrow p+n+\pi^{o}) = \frac{1}{2}\,\sigma(p+p \rightarrow n+p+\pi^{+}) + \sigma(p+n \rightarrow p+p+\pi^{-}) - \sigma(p+p \rightarrow p+p+\pi^{o})$$

was used to evaluate the π^o production cross section above 1 GeV. The justification for these procedures comes from isotopic spin considerations.

The p-p and p-n cross sections for producing two π-mesons (Fig. 5) were calculated by subtracting the sum of the elastic and single production cross sections from the total cross sections. All of the data described above were tabulated at every 20-MeV interval.

The differential cross section in the center-of-mass system for p-p elastic scattering below 500 MeV was assumed to be isotropic.[2] Between 0.5 and 1 GeV the data were taken from Ref. 18 and tabulated at six energy intervals. Above 1000 MeV the data were taken from Ref. 19.

The differential cross section for elastic p-n scattering in the center-of-mass system below 740 MeV was unchanged.[2] At the higher energies, data exist for either forward scattering or backward scattering, and, in general, the data for the scattering in the forward directions are at different energies from those for the backward directions. Hence the data in the forward direction were treated as a separate distribution from those in the backward direction. To utilize these data an estimate was made of the fraction of the scattering that is backward by integrating the differential cross sections, and the result is illustrated in Fig. 6. The forward and backward scattered data were taken from Ref. 20.

Pion-Nucleon Reactions

Figures 7 through 11 illustrate the pion-nucleon elastic scattering, charge-exchange scattering, and single-pion-production data that were used in the calculation. The $\pi^o p$ scattering data (Fig. 10) were calculated from the relation

$$\sigma_{el}(\pi^o p) = \frac{1}{2}\,[\sigma_{el}(\pi^+ p) + \sigma_{el}(\pi^- p) - \sigma_{ex}(\pi^- p)] \quad ,$$

where σ_{ex} is the charge-exchange cross section. The single-pion-production cross sections for the $\pi^+ p$ and the $\pi^- p$ reactions were calculated by subtracting the elastic cross section from the total cross section for the $\pi^+ p$ case and by subtracting the sum of the elastic and exchange cross sections from the total in the $\pi^- p$ reactions. The $\pi^o p$ single-production cross section was calculated from

$$\sigma_{sp}(\pi^o p) = \frac{1}{3}\,\sigma_{11} + \frac{2}{3}\,\sigma_{31} \quad ,$$

where σ_{11} and σ_{31} are the cross sections for producing single pions through the total isotopic spin 1/2 and 3/2 states, respectively, and were taken to be

$$\sigma_{31} = \sigma_{sp}(\pi^+ p)$$

and

$$\sigma_{11} = \frac{3}{2}\,\sigma_{sp}(\pi^- p) - \frac{1}{2}\,\sigma_{sp}(\pi^+ p) \quad .$$

Pion reactions with neutrons were taken to be the same as the charge symmetrical reactions with protons.

All of the pion-nucleon elastic and charge-exchange differential cross sections were calculated from the energy-dependent phase shifts of Donnachie, Kirsopp, and Lovelace.[21] Some criticism of this phase-shift data has been published,[22] but the small discrepancies observed in the differential cross sections would be totally masked by the statistics of the calculation. The phase-shift analysis used in calculating the differential cross sections includes angular momentum states up to

ℓ=4. The details of this calculation are published elsewhere.[23] The phase shifts of Donnachie *et al.* covered the energy range from 0 to 2 GeV. They were arbitrarily extrapolated to 2500 MeV by using both the plots of phase shifts vs energy and the Argand diagrams as a guide.[21]

The Isobar Model

All pion-production processes were assumed to be described by the Sternheimer-Lindenbaum isobar model,[14] and with the exceptions described below, its implementation is as described previously.[5]

The major improvement in the use of this model is that the angular distribution of the isobars were determined phenomenologically by comparing the calculated results with experimental data.[24] This distribution had been previously assumed to be energy independent and such that the isobars were distributed isotropically 50% of the time, straight forward 25%, and straight backward 25% of the time. The new distributions are given in Tables II and III.

Several variables, not given by the isobar model itself, are needed to determine the final charge states in all but the p-p or π^+p collisions. One is k_o, defined by

$$k_o = \frac{\sigma_2(I=0)}{\sigma_2(I=1)} \quad ,$$

where the cross sections are those for producing two isobars through the total isotopic spin 0 and 1 states. The variable k_o was calculated from the relationship

$$\sigma_{2\pi}(np) = \frac{\sigma_{2\pi}(pp)}{2} \quad (1 + k_o) \quad ,$$

where the cross sections are the double π-meson production cross sections for p-p and n-p reactions illustrated in Fig. 5. In order to calculate the final charge states in n-p double production reactions, k_o must be determined.

The variables a and ρ, defined below, must be calculated in order to specify the final states in pion-nucleon reactions other than π^+p.

$$\rho = \frac{\sigma_{31}}{2\sigma_{11}} \quad , \qquad a = 2\sqrt{\rho/5} \quad \cos\phi \quad .$$

The cross sections σ_{31} and σ_{11} were defined previously, and ϕ is the phase angle between the matrix elements for producing an isobar through the isotropic spin 3/2 and 1/2 states. These variables were calculated using

$$\rho = \frac{\sigma_{sp}(\pi^+p)}{2\sigma_{11}}$$

and

$$a = \frac{2}{5} + \frac{17}{25}\rho - \frac{27}{10} \frac{\sigma(\pi^- + p \rightarrow \pi^- + p + \pi^o)}{\sigma_{11}} \quad ,$$

where $\sigma(\pi^- + p \rightarrow \pi^- + p + \pi^o)$ is an experimentally determined cross section.[25] The values of k_0, ρ, $\sigma(\pi^- + p \rightarrow \pi^- + p + \pi^o)$, and a vs energy are illustrated elsewhere.[26]

COMPARISON WITH PREVIOUS CALCULATION

It was stated in the earlier work[5] that the lack of accurate pion data would not greatly influence the secondary nucleon spectra from

incident nucleons on complex nuclei. A comparison of the results of a typical case in which the less accurate pion data were used[5] with those from the present calculation is illustrated in Fig. 12 for the secondary proton spectra from 660-MeV protons on copper. There is little difference. Other comparisons of this type are also illustrated elsewhere.[26] Comparisons with the calculations of Metropolis *et al.*[1] were shown in Ref. 5.

COMPARISONS WITH EXPERIMENT

Statistical Error

All error limits on the theoretical results represent the limits of the standard 68% confidence interval, i.e., plus or minus one standard deviation. They appear solely because of the statistical nature of the calculation (Monte Carlo).

Total Nonelastic Cross Sections

Comparisons of the theoretical total nonelastic cross sections for incident neutrons and protons with experimental data have been made elsewhere,[5] and reasonable agreement was found. Comparisons of the theoretical nonelastic cross sections with experimental data for incident π^-- and π^+-mesons on several elements at various energies are illustrated in Tables IV and V. The comparisons for π^- on carbon and lead are illustrated graphically in Fig. 13. The comparisons indicate that the agreement of the theoretical predictions with the experimental data is quite reasonable.

Secondary Particle Multiplicities

Neutrons

The average number of neutrons emitted per interaction is shown in Figs. 14-16 for protons below 1 GeV on elements ranging from carbon to uranium. The agreement of the theoretical values with the experimental data is quite good. In the case of a copper target (Fig. 14), the calculations were performed for a ^{65}Cu target, and the calculated multiplicities from this neutron-rich isotope overestimates the experimental data. The calculation was repeated at 500 MeV for a ^{63}Cu target, and the result agrees with the experimental value. The theoretical values somewhat overestimate the neutron multiplicities for lead (Fig. 15), but they are in reasonable agreement with the data for uranium. However, if the theoretical values were about 4 neutrons less at all energies for the heavy elements, the agreement would still be reasonable. This point will be discussed in more detail in the section on spallation products.

Since the effect of fission is not included in the present calculation, the agreement with the experimental data for uranium may indicate that the residual excitation energy, whether residing in a nonfissioned nucleus or shared by fission fragments, is lost by the evaporation of approximately the same number of neutrons. This point will be discussed in another paper.[27]

The experimental results of Vasilkov *et al.*[28] at 400, 500, and 660 MeV did not include neutrons emitted into a 20° forward cone. All of the theoretical results illustrated at these energies were calculated by including all evaporation neutrons but excluding the cascade neutrons that went into a forward 20° cone. The total solid angle subtended

by this cone is small, and the number of evaporation neutrons, assumed to be emitted isotropically in the lab system, would not be greatly altered if those emitted therein were excluded. This assumption is reasonable for these reactions. Table VI contains a breakdown of the contribution to the multiplicities from the cascade and from the evaporation, and it is clear that the major contribution for the heavy targets is from the evaporation.

Charged Particles

Tables VII to IX illustrate the multiplicities of various charged particles emitted in the reactions of protons and π^--mesons with heavy emulsion nuclei. The theoretical numbers of singly charged particles from the cascade and those from the cascade-plus-evaporation are in good agreement with the experimental data, as shown in Tables VII and VIII.

The predicted number of alpha particles, however, is underestimated (Table VIII). There are two probable deficiencies in the model that lead to this discrepancy. One is that the direct knockout of alpha particles in the cascade is not taken into account,[29] and the other is that at the higher energies the evaporation model employed in this calculation[30] is not sufficiently appropriate. The high angular momenta transferred to the nucleus enhances the evaporation of alpha particles,[31] and this angular-momentum effect is not presently included.

The predicted number of charged pions is smaller than that from the experimental data, Table IX. This is probably due to the fact that only single π-meson production has been included in the calculation. This discrepancy will again be manifest in the (π^-,π^-n) reactions that are

described in the section on spallation products.

π^o-Mesons

Table X and Fig. 17 illustrate the π^o cross sections from reactions of protons with various elements, and the agreement is found to be fair with the theoretical values somewhat overestimating the experimental data in general.

Secondary Particle Spectra

The energy spectra of secondary charged pions that are emitted from the interaction of protons with carbon, copper, and lead are illustrated in Figs. 18-28. In general, the agreement of the theoretical predictions with the experimental data is quite reasonable. Additional comparisons are illustrated elsewhere.[26]

A typical discrepancy in the comparisons with the data of Lillethun[32] is shown in Fig. 18 for 450-MeV protons on carbon. The experimental values are about as large as those from 660-MeV protons on carbon (Fig. 21) at the same angle, but the theoretical results do not reflect this energy independence, being lower at 450 MeV than at 660 MeV.

For 660-MeV protons on carbon and copper, the shape of the low-energy π^- spectra is significantly different from that for the π^+. This was noted by Hert *et al.*[33] who argued that this difference was real by systematically eliminating all potential experimental causes for it. It is interesting to note that this difference is indeed predicted by the theory. The cause for it is postulated to be as follows:[34] The π^+-mesons, which are produced at relatively high energies and in greater numbers than

the π^- for incident protons, undergo secondary collisions within the nucleus in which low-energy pions are produced. Hence these produced pions, both π^+ and π^-, cause a low-energy peak in both spectra. But the low-energy peak in the π^+ spectra is not as significant as that in the π^- spectra because there are many more π^+ than π^- in general. The high-energy π^--mesons also contribute to the secondary production process, but since their numbers are small, this contribution is negligible. Figures 20-22 illustrate the changing character of the π^- spectrum with angle.

By comparing ratios and magnitudes of the π^+ and π^- spectra for beryllium and carbon Haddock *et al.*[35] suggest that the effect of the neutron shell in beryllium is visible from the experimental data. This effect is masked by the statistics of theoretical results. The theoretical spectra for beryllium are illustrated elsewhere.[26]

To examine the effect that the diffuseness of the nuclear edge may have on the spectra, a case was run in which the nucleon density was uniform and the nucleus had the rms radius of the continuous charge distribution.[36] The resulting π^- spectra are illustrated in Fig. 26 and can be compared with those in Fig. 25. It is clear that the effect at the edge of the nucleus for these reactions is significant.

The agreement with experiment for a lead target (Figs. 27 and 28) is not as good as for the carbon and copper targets.

Spallation Products

Incident Protons

Spallation yields from protons on ^{27}Al, ^{75}As, ^{108}Ag, and ^{209}Bi will be discussed briefly in this section, and comparisons with experiment will be made. Also, (p,pn) and $(p,p\pi^+)$ reactions will be discussed. Comparisons of the calculated yields with experimental data for protons on carbon and iodine are illustrated elsewhere,[26] but the results will be described here. The effects of fission on spallation yields from heavy elements are discussed in another paper.[27]

^{12}C. In the proton energy range from about 0.3 to 3 GeV the theoretical spallation cross sections for producing ^{11}C, ^{10}C, and ^{9}Li from protons on ^{12}C were calculated and compared with experimental data. The ^{11}C cross sections are overestimated by about 60%, the ^{10}C cross sections are in good agreement, and the ^{9}Li cross sections are in fair agreement. The term "good" implies that most of the data points show overlapping error bars for one standard deviation, while "fair" implies that there is an overlap for two standard deviations. The calculations were repeated using a uniform nucleon density distribution with the rms radius for the continuous charge distribution,[36] and it was found that the resulting cross sections were about a factor of five to ten smaller than when the diffuse nuclear edge is included. With the diffuse edge, the theoretical cross section for producing $^{7}_{4}Be$ was about a factor of 10 smaller than the measured value,[37] and it made little difference whether ^{8}Be instantaneous breakup was included[30] in the evaporation calculation or not. This indicates a probable need to include fragmentation effects in the evaporation calculation.

^{27}Al. Spallation product cross sections for protons from 0.5 to 3 GeV on aluminum are shown in Fig. 29 and in Table XI. As illustrated in the figure, the agreement is excellent for the ^{22}Na and ^{18}Fl products, but a discrepancy of factors of 2 to 4 exist for the ^{24}Na and ^{15}O. Larger discrepancies exist for the more infrequently produced products (Table XI), but the discrepancies are not systematic. These cross sections are quite small, and, as indicated previously,[38] the theory does not accurately reproduce these data.

Probably the most interesting product from these reactions is that of ^{27}Mg. Others have assumed that this isotope was produced predominantly through the $(p,p\pi^+)$ mode,[39] and this was confirmed theoretically in that the theoretical cross section for any other possible mode of production [for example, $(p,p\pi^+\pi^o)$ or (p,π^+) followed by proton evaporation] was either zero or completely insignificant compared to the direct $(p,p\pi^+)$ mechanism.

As with the carbon target, the predicted cross section for producing ^{7}Be completely underestimates the experimental data.[40] The results from the calculation, as before, are insensitive to the inclusion or exclusion of instantaneous ^{8}Be breakup in the evaporation calculation.[30] This calculation does not include the evaporation of particles heavier than ^{4}He. Evaporation models that were modified to permit the evaporation of heavier clusters such as ^{7}Be and ^{13}N have been fairly successful in predicting their yields from medium- to heavy-weight targets.[41] Although the validity of the concept may be questionable for a lighter weight target, a test of the applicability of the evaporation concept for ^{7}Be in these reactions would be worthwhile since the present model fails in this regard.

Table XII illustrates the results for the forward momentum transferred in the $(p,p\pi^+)$ reaction, and the agreement with the experimental data is fairly reasonable. However, the theoretical results include all cascade $(p,p\pi^+)$ reactions, i.e., even those in which high excitation energy is transferred to the residual nucleus, and hence the calculated forward momentum transferred should be somewhat greater than the experimental values, rather than smaller. This discrepancy is difficult to explain.

^{75}As. The spallation product yields for 2.9-GeV protons on arsenic are shown in Table XIII, and the theoretical cross sections are in good agreement with the experimental data. The cross sections vs $Z-Z_A$, where Z_A is the charge of the most stable element for a given mass,[42] are plotted in Fig. 30 for the products with mass number 72, and the expected Gaussian variation is observed. Plots such as these are sometimes used in determining the total mass yields of nuclides with mass numbers near those for which data are obtained; i.e., the curve is assumed to be universal for neighboring mass regions.[43] For example, Kaufman estimates that the region of constant mass yield from the reaction under consideration ranges from 66 to 73.[42] However, indications from the data in Table XIV are that this region might be much narrower, and hence considerable care must be exercised in the extrapolation of cross-section values into regions in which the mass yield is not completely determined.

^{108}Ag. Reasonable agreement is again found in the comparison of theoretical and experimental total mass yields from 3-GeV protons on silver, as is shown in Fig. 31. Although somewhat masked by statistics,

the calculated values appear to overestimate the data in the mass region from about 20 to 60 mass units, and the shapes of the distributions in the low-mass region appear to diverge. The prediction from the model is that the cross section tends to zero for low masses while the experimental data show an increase for decreasing mass, and hence this indicates a need to include fragmentation reactions in the model.

^{127}I. Illustrated elsewhere[26] are reactions of the type "(p,pxn)" vs proton energy over the range 0.1 to 2 GeV. There are usually several paths to forming the final spallation product when reaction energies are greater than the pion threshold, and hence the reactions are not true (p,pxn) reactions. In these cases, the notation is symbollic designating the final product and not the reaction path. The agreement of the theoretical values with the experimental data of Ladenbauer and Winsberg[44] is excellent for x up to 7, but the values differ from the data of Kuznetsova *et al.*[45] for a few products. Table XV shows the effects of the diffuse nuclear edge.

Table XVI illustrates comparisons with the data of Ladenbauer and Winsberg[44] for reactions leading to tellurium, and the agreement is only fair.

^{209}Bi. A significant discrepancy with the experimental data for 660-MeV protons in bismuth is illustrated in Fig. 32. (One should be aware of the shifting scale of the abscissa in this figure.) The predicted mass yield for a given Z peaks at masses quite far removed from the valley of stability as the atomic number of the spallation product becomes smaller. One reason for this may be a breakdown of the evaporation model presently employed[30] for the spallation products in question. On the

average, one gets $^{207}_{82}Pb$ from the cascade phase for this reaction, which is in the valley of stability. The average excitation energy following the cascade is 179 MeV. The average momentum of the residual nuclei following the cascade is 59 $\hbar$. On the average, the number of evaporation particles is 11.7 for neutrons, 1.5 for protons, and only 0.11 for alpha particles. A mechanism for enhancing the emission of alpha and other charged particles would help in alleviating this discrepancy, and the method suggested that includes the effects of high angular momentum[31] should be explored further. As mentioned before, the theoretical neutron multiplicities for the heavy elements could be smaller without affecting the agreement with experimental data.

Another reason for the discrepancy may be the lack of a process for direct knockout of alpha particles in the cascade. If these alpha particles were emitted at high energies, they would leave a "cooler" nucleus that would evaporate fewer neutrons.

"(p,pn)" Reactions. Reactions of the type "(p,pn)" for incident protons on several targets are shown in Fig. 33. The calculation overestimates the cross section in these reactions for the light target elements, and the reason for this is completely obscure. Good agreement is obtained for the other targets. The experimentally determined ^{181}Ta cross section was measured for transitions to the metastable state only and hence is smaller than would be expected if transitions to the ground state were included.[46]

Calculations were carried out for 400-MeV protons on targets in the mass range 54 to 65 to investigate the ability of the model to predict the significantly different (p,pn) cross sections[46] for ^{54}Fe and ^{50}Ni

as opposed to ^{63}Cu, ^{65}Cu, and ^{64}Zn. No differences, other than statistical, were found. As discussed by Markowitz *et al.*,[46] these differences might be due to shell-structure effects that are not included in the model.

"$(p,p\pi^+)$" Reactions. The cross sections for reactions of protons on ^{65}Cu leading to a ^{65}Ni final state are shown in Fig. 34 where a discrepancy between the calculated values and the experimental data is illustrated. The difference in magnitude is not as disturbing as the difference in shape because such a simple mechanism would appear amenable to reproduction by the cascade theory. One would expect that the cross section for this reaction would roughly assume the shape of the free particle p-p cross section for single-pion-production reactions (Fig. 3) as is the case for the experimental data as shown in Fig. 34. However, this is not the case for the theoretical results.

Several possible causes for the discrepancy were examined, and a satisfactory explanation was not found in any. For example, Table XVII contains the theoretical cross sections following the cascade, and following the cascade and evaporation. The cross section following the cascade more nearly resembles the desired shape, but this is not reflected in the product yield. The contribution of the cross sections from paths other than the $(p,p\pi^+)$ path was examined and their contributions, shown in Table XVIII are negligible. Finally, the effect of the exclusion principle was examined. The connection between this principle and the discrepancy is that at low energies, the reaction might be inhibited by the exclusion principle since the energies of the emerging nucleons from particle-particle production reactions would be small, and at higher energies this effect would essentially vanish. The calculations were

repeated with the exclusion principle bypassed in the program for nucleon-nucleon single production events only, and the resulting cross sections are illustrated by the dashed line in Fig. 34. There is only a slight improvement in the shape, and hence the cause of the discrepancy when the cascade theory is used remains unknown. Remsberg has been able to better reproduce the shape of this curve by employing one pion exchange theory (OPE).[47] The main difference between the OPE approach and the cascade theory is that the latter uses the isobar model while the former uses OPE theory to describe the details of the pion production through the individual particle-particle reactions. In both approaches the energy dependence of the cross section should be the same, and hence it is difficult to see why a somewhat different description of the details of the reaction should yield such differences in the energy dependence of the $(p,p\pi^+)$ cross section.

An additional comparison between the predictions of the cascade theory and the OPE for this reaction is in the predictions of the average forward kinetic energy of the ^{65}Ni shown in Table XIX. Even though the OPE results require normalization, they predict the experimental shape[47] better than does the cascade theory. For the cascade results, the average forward energy was assumed to be given by

$$\langle T \cos\theta \rangle = \frac{\langle p \cos\theta \rangle \langle p \rangle}{2A} \quad ,$$

where p is the recoil momentum of the residual nucleus from the cascade for the $(p,p\pi^+)$ reaction only, and A is the mass of ^{65}Ni. As before, this reaction can be readily calculated from the computer programs for the cascade phase only, and this might be a cause for the discrepancy.

Further theoretical analysis of these results in order to determine

the cause of the different predictions from the two theories appears worthwhile.

Incident Pions

The results of a significant experiment have been published recently where light elements were bombarded by π^+ and π^- mesons with energies at 180 MeV, the peak of the 3/2, 3/2 resonance.[48] Cross sections for the $^{12}C \rightarrow {}^{11}C$, $^{14}N \rightarrow {}^{13}N$, and $^{16}O \rightarrow {}^{15}O$ reactions were determined, and the ratio of the π^+ to the π^- cross section for each element was found to be 1, within a 10% experimental error. The impulse approximation predicts this ratio to be about 1/3. Chivers *et al.* argue that the cross section for coherent inelastic scattering could be a large contributor.[48] However, one must essentially give up the theory of direct interactions with single particles in order to explain the cross-section ratios of unity. Clearly these results should be experimentally confirmed.

Table XX illustrates the comparison of the theoretical predictions from the cascade theory with the experimental data, and the theoretical ratios are consistent with the impulse approximations, as is to be expected.

Spallation yields from π^- on carbon, aluminum, and argon are illustrated in Figs. 35 and 36, and in Table XXI. The agreement of the theoretical results with the experimental data is generally poor to fair. Probably the most significant deficiency in the model that contributes to these discrepancies is the lack of a mechanism for producing more than one pion in the individual pion-nucleon collisions.

Since only the end product is determined in spallation-product experiments, one must merely speculate as to which is the dominant path leading to the formation of the end product. In order to shed some light on this problem for a specific case, the reaction leading to ^{11}C from π^- on ^{12}C was studied in some detail. Table XXII illustrates the predicted cross sections for all cascade paths that might lead to ^{11}C. Although it is generally assumed that the (π^-,π^-n) reaction dominates, note the significant contribution from the $(\pi^-,\pi^-\pi^0n)$ mode. Figure 37 shows the excitation energy distribution for the residual nuclei for these two reactions. Integration over these curves from 0 to 9 MeV, which is the binding energy of the most loosely bound nucleon (a proton for ^{11}C),[49] gives the fraction of the cascade cross sections that lead to ^{11}C. Hence, both reactions contribute about equal fractions of their cross sections to the final state.

CONCLUSIONS

The intranuclear-cascade evaporation model can predict the nonelastic cross sections, the nucleon multiplicities, the secondary nucleon and pion angle-energy correlated spectra, and the yield of many spallation products with reasonable accuracy for the continuum state transitions involving incident pions and nucleons on complex nuclei at interaction energies ranging from about 100 MeV to 3 GeV. One computer program, without adjustable parameters, can be used in the calculation of these quantities, which indicates the power of the method.

The following are discrepancies observed between the theoretical predictions and experimental data that appear to be direct reflections of deficiencies in the model: (a) the theoretical results grossly

underestimate the production of ^{7}Be from high-energy protons on carbon and aluminum. This situation might be ameliorated by the inclusion of ^{7}Be evaporations in the model, or the adoption of some other method for calculating fragmentation reactions. Besides this particular discrepancy, there is experimental evidence that light elements, such as chlorine, are emitted from 1- to 3-GeV protons on targets such as lead,[43,50] while the theory incorporating the evaporation of single nucleons and small clusters of nucleons fails to yield these light elements. (b) The theoretical results overestimate the cross sections for the relatively simple reactions of the type (π^-,π^-n) at high energies, while the total pion multiplicity for incident pions is underestimated. Both discrepancies can be attributed to the lack, within the model, of a means of producing more than 1 pion in the individual pion-nucleon reactions that occur within the nucleus. (c) The theoretical results underestimate the alpha-to-proton yield ratio for high-energy protons on heavy targets, and furthermore the mass yield curves for given Z's, which are several protons removed from the target, peak at nuclide values that are very neutron deficient. The suggested method of enhancing alpha-particle emissions by Gilat and Grover[31] should serve as a guide to explore the resolution of these discrepancies. Additionally, the effect of direct knockout of alpha particles in the cascade could be investigated.

The following are discrepancies observed for which there are no explanations readily available: (a) a lack of consistency in the predictions of spallation product yields for high-energy reactions. For example, the theoretical cross sections for producing ^{22}Na from 0.5- to 3-GeV protons on aluminum are in excellent agreement with the experimental

data, while the predictions for producing ^{24}Na from the same reactions are about a factor of 2 smaller than the data. (b) The shape of the $(p,p\pi^+)$ reaction cross sections for ^{65}Cu is not properly reproduced by the theory; and finally, (c) the ratio of the π^+ to π^- cross sections for reactions of the type $\pi^{\pm} + {}^{12}C \rightarrow {}^{11}C + \chi$ at 180 MeV do not correspond to the experimental values.

All of the discrepancies can be subjects for further theoretical investigation.

PROGRAM INFORMATION

The calculation is programmed in FORTRAN with a few of the subroutines in assembly language. It operates on the IBM 360/75 and /91 computers. The running times on the 360/91 per 1000 incident particles are about 15 sec for oxygen to 3 min for lead at reaction energies of 1 GeV. At 3 GeV, the running time is approximately doubled. The minumum number of histories run for this paper was 2000 in calculating the inelastic cross sections, and the maximum number was 100,000 in calculating some of the secondary pion spectra at reaction energies of 660 MeV. A large quantity of data that was generated using this code is available, and its description and the method for obtaining it was given elsewhere.[51] The present cascade code, MECC-7, is now available from RSIC.[52] It replaces the earlier version, MECC-3, described in ref. 51 and ref. 5.

ACKNOWLEDGMENTS

The authors are greatly indebted to Mrs. Elsie Pickell, Miss Barbara Bishop, and Mrs. Jackie Gillen for the endless hand calculations that were required in preparing the input data and in checking out the program.

REFERENCES

1. N. Metropolis *et al.*, Phys. Rev. 110, 185 and 204 (1958).

2. Hugo W. Bertini, Phys. Rev. 131, 1801 (1963); 138, AB2 (1965).

3. K. Chen *et al.*, Phys. Rev. 166, 949 (1968).

4. K. Chen *et al.*, Phys. Rev. C 4, 2234 (1971).

5. Hugo W. Bertini, Phys. Rev. 188, 1711 (1969).

6. V. S. Barashenkov *et al.*, "Classification of Inelastic Interactions of High Energy Protons and Nuclei. II. Characteristics of Low-Energy Particles," JINR-P2-5549 (1970).

7. R. J. Gauber, "Lectures in Theoretical Physics," Vol. I, p. 315 (Wiley Interscience, N.Y., 1959).

8. L. I. Schiff, Phys. Rev. 176, 1390 (1968).

9. D. K. Ross, Phys. Rev. 173, 1695 (1968).

10. K. Chen, G. Friedlander, and J. M. Miller, Phys. Rev. 176, 1208 (1968).

11. J. S. Trefil, Phys. Rev. 180, 1366 (1969).

12. Paul M. Fishbane and J. S. Trefil, Phys. Rev. D 3, 238 (1971).

13. J. S. Trefil, private communication.

14. R. M. Sternheimer and S. J. Lindenbaum, Phys. Rev. 123, 333 (1961); 109, 1723 (1958); 105, 1874 (1957).

15. D. V. Bugg *et al.*, Phys. Rev. 146, 980 (1966).

16. V. S. Barashenkov and V. M. Maltsev, Forschritte der Physik 9, 549 (1961).

17. H.-W. Bertini, "Monte Carlo Calculations on Intranuclear Cascades," ORNL-3383 (1963).

18. L. W. Smith, A. W. McReynolds, and G. Snow, Phys. Rev. 97, 1186 (1955); T. W. Morris, E. C. Fowler, and J. D. Garrison, Phys. Rev. 103, 1472 (1956); L. O. Roelling and D. A. Glaser, Phys. Rev. 116, 1001 (1959); P. J. Duke *et al.*, Phil Mag. Ser. 8, 2, 204 (1957); W. K. McFarlane *et al.*, Nuovo Cimento 28, 943 (1963); J. D. Dowell *et al.*, Nuovo Cimento 18, 818 (1960); V. M. Guzhavin *et al.*, Soviet Phys.-JETP, 20, 830 (1965).

19. L. W. Smith, A. W. McReynolds, and G. Snow, Phys. Rev. 97, 1186 (1955); Bruce Cork, W. E. Wenzel, and C. W. Causey, Jr., Phys. Rev. 107, 859 (1957); M. M. Block *et al.*, Phys. Rev. 103, 1484 (1956); T. Fujii *et al.*, Phys. Rev. 128, 1836 (1962); S. P. Kruchinin *et al.*, Sov. J. Nuc. Phys. 1, 225 (1965); S. A. Azimov *et al.*, Soviet Phys.-JETP 15, 299 (1962).

20. H. Palevsky *et al.*, Phys. Rev. Letters 9, 509 (1962); J. L. Friedes *et al.*, Phys. Rev. Letters 15, 38 (1965); M. N. Kreisler, F. Martin, and M. L. Perl, Phys. Rev. Letters 16, 1217 (1966); A. P. Batson *et al.*, Proc. Roy. Soc. (London) A251, 233 (1959); N. S. Amaglobeli *et al.*, Proc. of the Annual Int. Conf. on High En. Physics at Rochester, p. 64 (1960).

21. A. Donnachie, R. G. Kirsopp, and C. Lovelace, "Evidence from πp Phase Shift Analysis for Nine More Possible Nucleon Resonances," CERN report No. TH-838 (1967).

22. A. D. Brody *et al.*, Phys. Rev. Letters 22, 1401 (1969).

23. Hugo W. Bertini, "Pion-Nucleon Differential Cross Sections in the 0- to 700-MeV Energy Region in Terms of the Coulomb Phase Shifts and Nuclear Phase Shifts up to $\ell = 4$," ORNL-4197 (1968).

24. H. W. Bertini, M. P. Guthrie, and A. H. Culkowski, "Phenomenologically Determined Isobar Angular Distributions for Nucleon-Nucleon and Pion-Nucleon Reactions Below 3 GeV," ORNL-TM-3132 (1970).

25. Ya. Ya. Shalamov and A. F. Grashin, Soviet Phys.-JETP 15, 770 (1962); J. P. Baton *et al.*, Nuovo Cimento 35, 713 (1965); J. Alitti *et al.*, Nuovo Cimento 29, 515 (1963); Data quoted by M. Olsson and G. B. Yodh, University of Maryland, Dept. of Physics and Astronomy Technical Report No. 358 (Feb. 1964).

26. See Appendix.

27. R. L. Hahn and H. W. Bertini, "Calculation of Spallation Fission Competition in the Reaction of Protons with ^{238}U at Energies < 3 GeV," to be published in Phys. Rev.

28. R. S. Vasilkov *et al.*, Soviet J. Nucl. Phys. 7, 64 (1968).

29. V. S. Barashenkov and O. B. Abdinov, "Intranuclear Cascades with Allowances for α-Clusters," JINR-P2-4568 (1969).

30. Miriam P. Guthrie, "EVAP-4: Another Modification of a Code to Calculate Particle Evaporation from Excited Compound Nuclei," ORNL-TM-3119. The basis of this model is still that of I. Dostrovsky, Z. Fraenkel, and G. Friedlander, Phys. Rev. 116, 683 (1959). It is a modification of the program by L. Dresner, "EVAP - A FORTRAN Program for Calculating the Evaporation of Various Particles from Excited Compound Nuclei," ORNL-CF-61-12-30 (1961).

31. Jacob Gilat and J. Robb Grover, Phys. Rev. C 3, 734 (1971).

32. Endre Lillethun, Phys. Rev. 125, 665 (1962).

33. W. Hirt *et al.*, "Etude Experimentale de la Production de Pions Charges

dans le Collisions Proton-Noyau a 600 MeV," CERN-69-24 (1969).

34. Robert Burman, LASL, Los Alamos, N. M., private communication.

35. R. P. Haddock, M. Zeller, and K. M. Crowe, "Production of Charged Pions from Complex Nuclei in the Forward Direction," University of California at Los Angeles, Dept. of Physics, Technical Report MEG 64-2, UCLA-34P106.

36. R. Hofstadter, Rev. Mod. Phys. 28, 214 (1956).

37. Garimella V. S. Rayudu, J. Inorg, Nucl. Chem. 30, 2311 (1968); A. F. Stehney and E. P. Steinberg, Nucl. Phys. B5, 188 (1968).

38. Hugo W. Bertini, Phys. Rev. 171, 1261 (1968).

39. A. M. Poskanzer, J. B. Cumming, and L. P. Remsberg, Phys. Rev. 168, 1331 (1968).

40. G. Friedlander, J. Hudis, and R. L. Wolfgang, Phys. Rev. 99, 263 (1955).

41. I. Dostrovsky, Z. Fraenkel, and J. Hudis, Phys. Rev. 123, 1452 (1961); I. Dostrovsky, Z. Fraenkel, and P. Rabinowitz, Phys. Rev. 118, 791 (1960); J. Hudis and J. M. Miller, Phys. Rev. 112, 1322 (1958).

42. Sheldon Kaufman, Phys. Rev. 126, 1189 (1962).

43. G. Friedlander and L. Yaffe, Phys. Rev. 117, 578 (1960).

44. Inge-Maria Ladenbauer and Lester Winsberg, Phys. Rev. 119, 1368 (1960).

45. M. Ia. Kuznetsova, V. N. Mekhedov, and V. A. Khalkin, Soviet Phys.-JETP 34, 759 (1958).

46. Samuel S. Markowitz, F. S. Rowland, and G. Friedlander, Phys. Rev. 112, 1295 (1958).

47. L. P. Remsberg, Phys. Rev. 138, B572 (1965).

48. D. T. Chivers *et al.*, Nucl. Phys. A126, 129 (1969).

49. F. Ajzenberg-Selove and T. Lauritsen, Nucl. Phys. A114, 1 (1968).

50. V. P. Crespo, J. M. Alexander, E. K. Hyde, Phys. Rev. 131, 1765 (1963); I. Dostrovsky, Z. Fraenkel, and J. Hudis, Phys. Rev. 123, 1452 (1961).

51. Hugo W. Bertini and Miriam P. Guthrie, Nucl. Phys. A169, 670 (1971).

52. Radiation Shielding Information Center, Oak Ridge National Laboratory, P. O. Box X, Oak Ridge, Tenn. 37830 USA

Table I

Low-Energy Elastic p-p and
p-n Cross Sections

Energy (MeV)	Cross Section (mb)	
	p-p	p-n
0	675	1965 ~~196.5~~
20	155	475
40	67.5	220
60	44.2	130

Table II

Composite Isobar Angular Distribution in the Center-of-Mass System for Nucleon-Nucleon Single and Double π-Meson Production Reactions

Laboratory Kinetic Energy Range (MeV)	% of Each Distribution Contributing to Composite		
	Isotropic	Forward	Backward
Single Production			
$E < 500$	100	0	0
$500 \leq E < 1000$	75	12.5	12.5
$1000 \leq E < 1300$	50	25	25
$1300 \leq E < 2500$	25	37.5	37.5
$2500 \leq E \leq 3500$	0	50	50
Double Production			
All Energies	0	50	50

Table III

Composite Isobar Angular Distribution in the Center-of-Mass System for Pion-Nucleon Single π-Meson Production Reactions

Laboratory Kinetic Energy Range (MeV)	% of Each Distribution Contributing to Composite		
	Isotropic	Forward	Backward
	$\pi^+ + p$ and $\pi^- + n$		
All energies	75	0	25
	$\pi^- + p$ and $\pi^+ + n$		
$E < 500$	80	20	0
$E \geq 500$	80	0	20
	$\pi^o + p$ and $\pi^o + n$		
	(Assumed to be the same as $\pi^- + p$)		

Table IV

Total Nonelastic Cross Sections for Incident π^- Mesons

Target	π^- Energy (MeV)	Nonelastic Cross Section (mb) Theory	Exp.[a]
Be	485	165 ± 7	184 ± 6[b]
	598	182 ± 7	179 ± 6[b]
	894	217 ± 7	189 ± 5[b]
	1256	218 ± 7	200 ± 6[b]
C	216	414 ± 9	350 ± 24
	256	360 ± 7	326 ± 31
	350	239 ± 5	166 ± 21
	485	217 ± 8	231 ± 7[b]
	598		226 ± 7[b]
	600	233 ± 5	216 ± 10
	894		233 ± 6[b]
	970	271 ± 5	252 ± 13
	1200	262 ± 5	246 ± 14
	1256		239 ± 5[b]
	1510	258 ± 5	240 ± 14
Al	970	477 ± 13	442 ± 20
Cu	970	819 ± 12	806 ± 35
Sn	970	1194 ± 17	1199 ± 52
Pb	216	2022 ± 21	2356 ± 152
	256	1906 ± 20	2430 ± 183
	970	1712 ± 18	1690 ± 100
	1510	1700 ± 18	1600 ± 95

[a]Unless otherwise indicated the data are from the compilation of V. S. Barashenkov, K. K. Gudima, and V. D. Toneev, JINR-P2-4068 (1968).

[b]M. Crozon *et al.*, Congrès International de Physique Nucléaire, Paris, 1964, Vol. II, p. 222, Ed. Mme. P. Gugenberger (Centre National de la Recherche Scientifique, Paris 1964).

Table V

Total Nonelastic Cross Sections for Incident π^+ Mesons

Target	π^+ Energy (MeV)	Nonelastic Cross Section (mb) Theory	Exp.[a]
Be	442	162 ± 7	238 ± 20
	2500	190 ± 7	
	2860		192 ± 8
C	442	220 ± 5	238 ± 20
	2500	241 ± 8	
	2860		213 ± 8
Al	442	388 ± 11	410 ± 25
	2500	434 ± 11	
	2860		$428 {}^{+15}_{-12}$
Cu	442	756 ± 16	686 ± 106
	2500	778 ± 16	
	2860		$790 {}^{+41}_{-26}$
Cd	442	1074 ± 20	754 ± 200

[a]From the compilation of V. S. Barashenkov, K. K. Gudima, and V. D. Toneev, JINR-P2-4068 (1968).

Table VI

Experimental[a] and Theoretical Average Number of Neutrons Emitted Per Inelastic Event for Incident Protons on Various Elements

	Proton Energy											
	400 MeV				500 MeV				660 MeV			
	Theoretical				Theoretical				Theoretical			
Target	Cas.[b]	Evap.[c]	Total	Exp.	Cas.	Evap.	Total	Exp.	Cas.	Evap.	Total	Exp.
C	0.82	0.36	1.18		0.98	0.45	1.43	1.4 ± 0.2	1.05	0.57	1.62	1.5 ± 0.2
Al	1.2	0.7	1.9	2.1 ± 0.3	1.3	0.8	2.1	2.3 ± 0.3	1.45	0.96	2.41	2.8 ± 0.3
Cu	1.6	2.7	4.3	3.7 ± 0.4	1.8	3.0	4.8	3.9 ± 0.4	2.1	3.3	5.4	4.4 ± 0.4
Pb	2.2	9.3	11.5	9.4 ± 1.0	2.1	10.4	12.5	11.2 ± 1.0	3.1	12.1	15.2	11.9 ± 1.0
U	2.2	11.7	13.9	14.1 ± 1.4	2.7	12.9	15.6	14.7 ± 1.3	3.3	14.5	17.8	16.8 ± 1.2

[a] R. G. Vasilkov *et al.*, Sov. J. Nucl. Phys. 7, 64 (1968).

[b] All cascade neutrons emitted with angles greater than 20° to the incident beam.

[c] Evaporation neutrons emitted in all directions.

Table VII

Average Number of Cascade Particles per Star Whose Charge Is One From Protons on Heavy Emulsion Nuclei

Incident Proton Energy (MeV)	Theoretical[a] Average No. of Cascade Particles				Exp[b]
	p	π^+	π^-	Total	
130	0.78	0	0	0.78	0.74 ± 0.15
460					1.52 ± 0.30
500	1.62	0.06	0.03	1.71	
660	1.83	0.12	0.05	2.00	1.87 ± 0.37

[a]The statistical error is less than 3%. The target is $^{100}_{44}Ru$.

[b]V. I. Ostroumov, Soviet Phys.-JETP 5, 12 (1957).

Table VIII

Average Number of Singly Charged Particles per Star from 950-MeV Protons on Heavy Emulsion Nuclei

Theoretical[a]									Ratio of Alphas to Protons	
Evaporation			Cascade							
p	Deut.	Trit.	P	π^+	π^-	Total	Exp.		Theor.	Exp.[b]
2.96	0.47	0.08	0.23	0.21	0.17	4.12	4.26[b] ±0.18	5.54[c] ±0.78	0.11	0.36

[a]The statistical error is about 3%. The case calculated was 1 GeV P on $^{100}_{44}$Ru.

[b]W. O. Lock, P. V. March, and R. McKeague, Proc. Roy Soc. A(London) 231, 368 (1955).

[c]George Philbert, Comp. Rend. 241, 944 (1955).

Table IX

Average Number of Charged Pions per Star from π^- on Heavy Emulsion Nuclei

π^- Energy (GeV)	Theoretical[a]			Exp.[b]
	π^+	π^-	Total	
1	0.24	0.80	1.04	
1.3				1.85
1.5	0.32	0.90	1.22	

[a]Target, $^{100}_{44}$Ru. Statistical Error $\leq$ 2%.

[b]G. D. Gordon *et al.*, Phys. Rev. 108, 1315 (1957).

Table X

The Cross Section for the Emission of π^o's From 660-MeV Protons on Several Elements

Target	Cross Section (mb)	
	Exp.[a]	Theor.
Al	45.9 ± 2.6	60 ± 4
Cu	73.4 ± 4.2	109 ± 6
Pb	143 ± 8	200 ± 12

[a]A. F. Dunaitsev and Yu. D. Prokoshkin, Nucl. Phys. 56, 300 (1964).

Table XI

Table XI. Comparison of Theoretical and Experimental Cross Sections (mb) for the Production of Various Spallation Products from Protons on Aluminum

Incident Proton Energy (GeV)	$^{27}_{12}Mg$		$^{17}_{7}N$		$^{13}_{7}N$		$^{16}_{6}C$		$^{11}_{6}C$		$^{9}_{3}Li$	
	Th.[a]	Ex.[b]	Th.	Ex.[c]	Th.	Ex.[d]	Th.	Ex.[c]	Th.	Ex.[d]	Th.	Ex.[c]
0.5	0.09 ±.09 [0.6]		0.09 ±.09		0		0.34 ±.17		0.34		0	
0.6		0.103 ±.005				0.88 ±.06				3.4 ±1.5		
1.0	0.43 ±.19 [1.6]	0.138 ±.006	0	0.66 ±.07	0.17 ±.12		0.69 ±.24	0.05 ±.005	0.86 ±.27	5.1 ±2.2	0.17 ±.12	0.13 ±.01
1.4						1.4 ±0.9				5.0 ±2.2		
1.5	1.5 ±.3 [3.6]		0.17 ±.12		0.17 ±.12		0.86 ±.27		1.7 ±.4		0.60 ±.23	
1.7		0.138 ±.005										
2.0	1.4 ±.3 [3.4]		0.13 ±.13		0.26 ±.18		0.77 ±.31		1.3 ±.4		0.26 ±.18	
2.2						1.5 ±0.9				5.0 ±2.2		
2.5	1.4 ±.3 [3.4]		0.13 ±.13		0.26 ±.18		0.13 ±.13		1.8 ±.5		0.90 ±.34	
2.8				0.72 ±.07				0.07 ±.007				0.24 ±.02
2.9		0.111 ±.005										
3.0	1.4 ±.3 [3.3]		0.13 ±.13		0	0.89 ±0.6	0.26 ±.18		1.9 ±.5	5.0 ±2.2	0.26 ±.18	

[a] The numbers in brackets are the cross sections for the direct $(p,p\pi^+)$ reaction from the cascade.

[b] A. M. Poskanzer, J. B. Cumming, and L. P. Remsberg, Phys. Rev. 168, 1331 (1968).

[c] I. Dostrovsky *et al.*, Phys. Rev. 139, 1513 (1965).

[d] G. Friedlander, J. Hudis, and R. L. Wolfgang, Phys. Rev. 99, 263 (1955).

Table XII

Comparison of Theoretical and Experimental Average Forward Momentum Transfer from the $^{27}Al(p,p\pi^{+})^{27}Mg$ Reaction

Incident Proton Energy (GeV)	Average Forward Momentum Transfer ($m_o c$)[a]	
	Theor.	Exp.[b]
0.5	0.37	
0.6		0.37
1.0	0.24	0.27
1.5	0.19	
1.7		0.22
2.0	0.15	
2.5	0.15	
2.9		0.19
3.0	0.12	

[a] m_o is the proton rest mass.

[b] A. M. Poskanzer, J. B. Cumming, and L. P. Remsberg, Phys. Rev. 168, 1331 (1968).

Table XIII

Theoretical and Experimental Cross Sections for the Production of Various Radionuclides from 2.9-GeV Protons on $^{75}_{33}As$

Nuclide	Cross Sections (mb)	
	Theoretical	Experimental[a]
$^{72}_{30}Zn$	0.4 ± 0.4	0.025 ± 0.003
$^{66}_{31}Ga$	4.3 ± 1.3	5.1 ± 0.5
$^{67}_{31}Ga$	7.8 ± 1.7	8.0 ± 0.8
$^{72}_{31}Ga$	2.7 ± 1.0	2.28 ± 0.19
$^{73}_{31}Ga$	3.1 ± 1.1	0.62 ± 0.07
$^{72}_{32}Ge$	17 ± 3	
$^{71}_{33}As$	6.2 ± 1.6	7.0 ± 0.6
$^{72}_{33}As$	11 ± 2	14.3 ± 0.9
$^{73}_{33}As$	24 ± 3	17 ± 2
$^{74}_{33}As$	58 ± 5	47 ± 3
$^{72}_{34}Se$	1.6 ± 0.8	0.45 ± 0.08

[a]Sheldon Kaufman, Phys. Rev. 126, 1189 (1962).

Table XIV

Calculated Cross Sections for the Total Production of Nuclides of a Given Mass from 2.9-GeV Protons on ^{75}As

Mass (A)	Cross Section (mb)
73	39 ± 4
72	32 ± 4
71	21 ± 3
70	23 ± 3
69	17 ± 3
68	21 ± 3
67	10 ± 2
66	13 ± 2

Table XV

Effect of Nucleon Density Distribution on Theoretical "(p,pxn)" Reactions for I

Proton Energy (GeV)	"(p,pn)"		"(p,p3n)"		"(p,p6n)"	
	Un.[a]	Non-Un.[b]	Un.	Non-Un	Un.	Non-Un
0.25	5	68	9	38	19	51
2.0	0.23	69	1.6	11	2.3	15

[a]A uniform nucleon density distribution whose radius is the root mean square value of the continuous distribution given by R. Hofstader, Rev. Mod. Phys. 28, 214 (1956).

[b]Diffuse nuclear edge included.

Table XVI

Cross Sections for Producing Isotopes of

$_{52}$Te from Protons on $^{127}_{53}$I

Proton Energy (GeV)	Cross Sections (mb)					
	$^{116+117}_{52}$Te		$^{118}_{52}$Te		$^{127}_{52}$Te	
	Theor.	Exp.[a]	Theor.	Exp.[a]	Theor.	Exp.[a]
0.25	82 ± 6	40.2 ± 7.8	51 ± 4	64.5 ± 6.6	0	< 1.5 ± 0.5
0.50	55 ± 6	30.6 ± 2.8	26 ± 4	38.7 ± 1.4	0	< 1.7 ± 0.3
1.0	27 ± 4	20.2 ± 3.0	19 ± 3	28.5 ± 1.0	0	< 1.2 ± 0.7
2.0	20 ± 4	7.0 ± 1.5	13 ± 3	18.1	2.6 ± 1.3	< 2.6 ± 1.1

[a]Inge-Maria Ladenbauer and Lester Winsberg, Phys. Rev. 119, 1368 (1960).

Table XVII

Theoretical Cross Sections for the "$(p,p\pi^+)$" Reactions on Copper-65 Following the Cascade and Following the Cascade and Evaporation

Incident Proton Energy (GeV)	Theoretical	
	After Cascade	After Cascade and Evaporation
0.5	0.61	0.12 ± 0.12
1.0	1.3	0.49 ± 0.24
1.5	3.2	0.73 ± 0.30
2.0	4.6	1.1 ± 0.5
2.5	3.1	1.5 ± 0.5
3.0	3.7	1.6 ± 0.4

Table XVIII

Theoretical Cross Sections for Several Specific Cascade Reactions for Protons on ^{65}Cu

	Cascade Cross Section (mb)[a]			
	Proton Energy (GeV)			
Reaction	1.5	2.0	2.5	3.0
$(p,p\pi^{+}\pi^{o})$	0.12	0.18	0.18	0.19
$(p,n2\pi^{+})$	0	0	0	0

[a]Cross sections for all other reactions that could lead to a nickel-65 final state were calculated to be zero.

Table XIX

Average Value of the Forward Projection of the Recoil Kinetic Energy (MeV) for the $^{65}Cu(p,p\pi^{+})^{65}Ni$ Reaction

Incident Proton Energy (GeV)	Cascade Calculation[a]	OPE[b]
0.5	1.6	1.29
1.0	0.44	0.75
1.5	0.25	0.55
2.0	0.18	0.49
2.5	0.15	0.48
3.0	0.19	0.50

[a]Method of calculation described in text.

[b]L. P. Remsberg, Phys. Rev. 138, B572 (1965).

Table XX

Knockout Reactions for Light Elements from Incident π^+- and π^--Mesons at 180 MeV

Incident Pion	Target	Product Nuclei	Cross Section (mb) Theor.	Cross Section (mb) Exp.[a]	Ratio (π^+/π^-) Theor.	Ratio (π^+/π^-) Exp.[a]
π^+	^{12}C	^{11}C	37 ± 2	75 ± 4	0.41	1.03
π^-	^{12}C	^{11}C	91 ± 4	72 ± 6		
π^+	^{14}N	^{13}N	24 ± 2	56 ± 6	0.49	1.05
π^-	^{14}N	^{13}N	49 ± 3	53 ± 6		
π^+	^{16}O	^{15}O	31 ± 2	41 ± 4	0.37	0.98
π^-	^{16}O	^{15}O	83 ± 3	42 ± 4		

[a]D. T. Chivers *et al.*, Nucl. Phys. A126, 129 (1969).

Table XXI

Cross Sections for the Production of
^{11}C and ^{18}F from π^- on $^{27}_{13}Al$

π^- Energy (GeV)	Cross Sections (mb)			
	$^{11}_{6}C$		$^{18}_{9}F$	
	Theor.	Exp.[a]	Theor.	Exp.[a]
0.45		2.2 ± 0.3		6.2 ± 0.8
0.5	0.5 ± 0.2		4 ± 1	
0.7		3.8 ± 0.4		6.2 ± 0.6
0.9		4.2 ± 0.4		6.8 ± 0.5
1.0	0.9 ± 0.3		5 ± 1	
1.46		5.8 ± 0.9		6.0 ± 1.0
1.5	0.7 ± 0.2		4 ± 1	
1.76		4.9 ± 1.0		6.6 ± 1.0

[a]A. M. Poskanzer and L. P. Remsberg, Phys. Rev. 134, B779 (1964).

Table XXII

Calculated Cross Sections for Reactions from the Cascade That Could Lead to ^{11}C Final States from π^- on ^{12}C

π^- Energy (GeV)	Cross Sections from Cascade (mb)[a]						
	(π^-,π^-)	$(\pi^-,2\pi^-)$	$(\pi^-,\pi^0\pi^-)$	(π^-,π^-n)	$(\pi^-,\pi^-\pi^0n)$	$(\pi^-,2\pi^-p)$	$(\pi^-,2\pi^0\pi^-n)$
0.9	7.5	0.13	0.39	20.0	13.3	2.3	0
1.4	5.7	0.06	0.45	24.6	19.6	3.4	0.13

[a]The cross section for all other reactions that could lead to a carbon-11 final state were calculated to be zero.

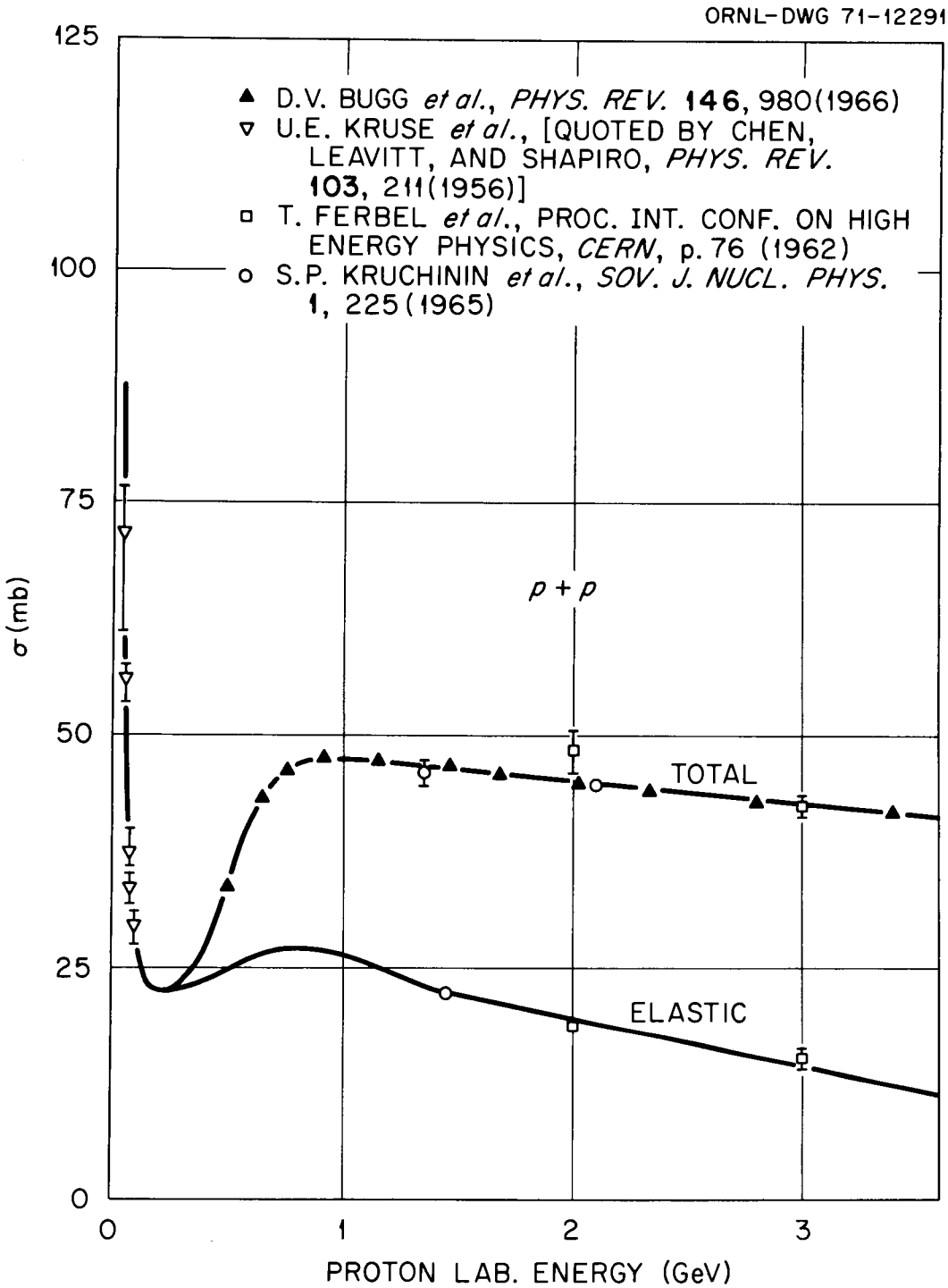

Fig. 1. Proton-proton total and elastic cross sections.

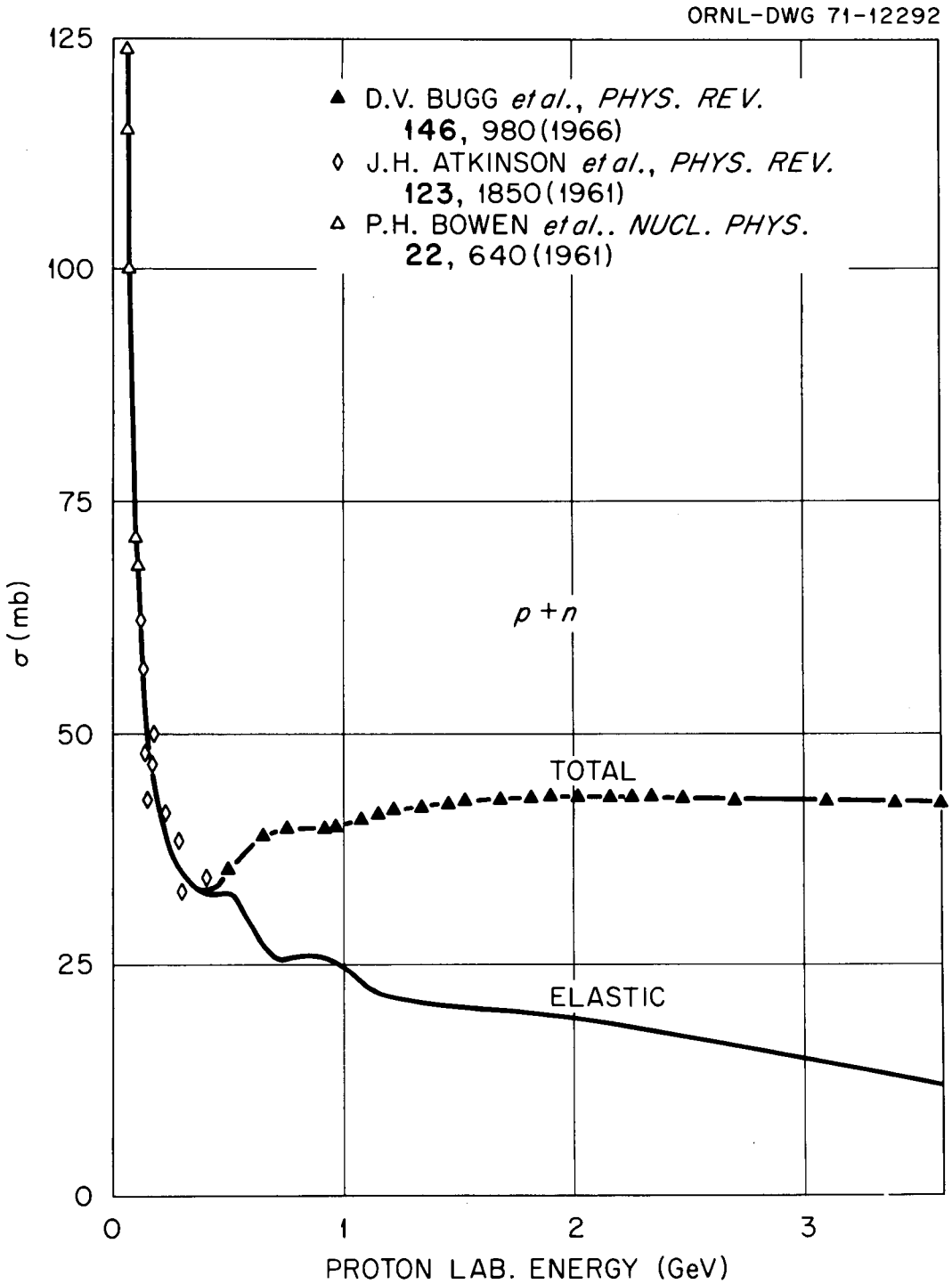

Fig. 2. Proton-neutron total and elastic cross sections.

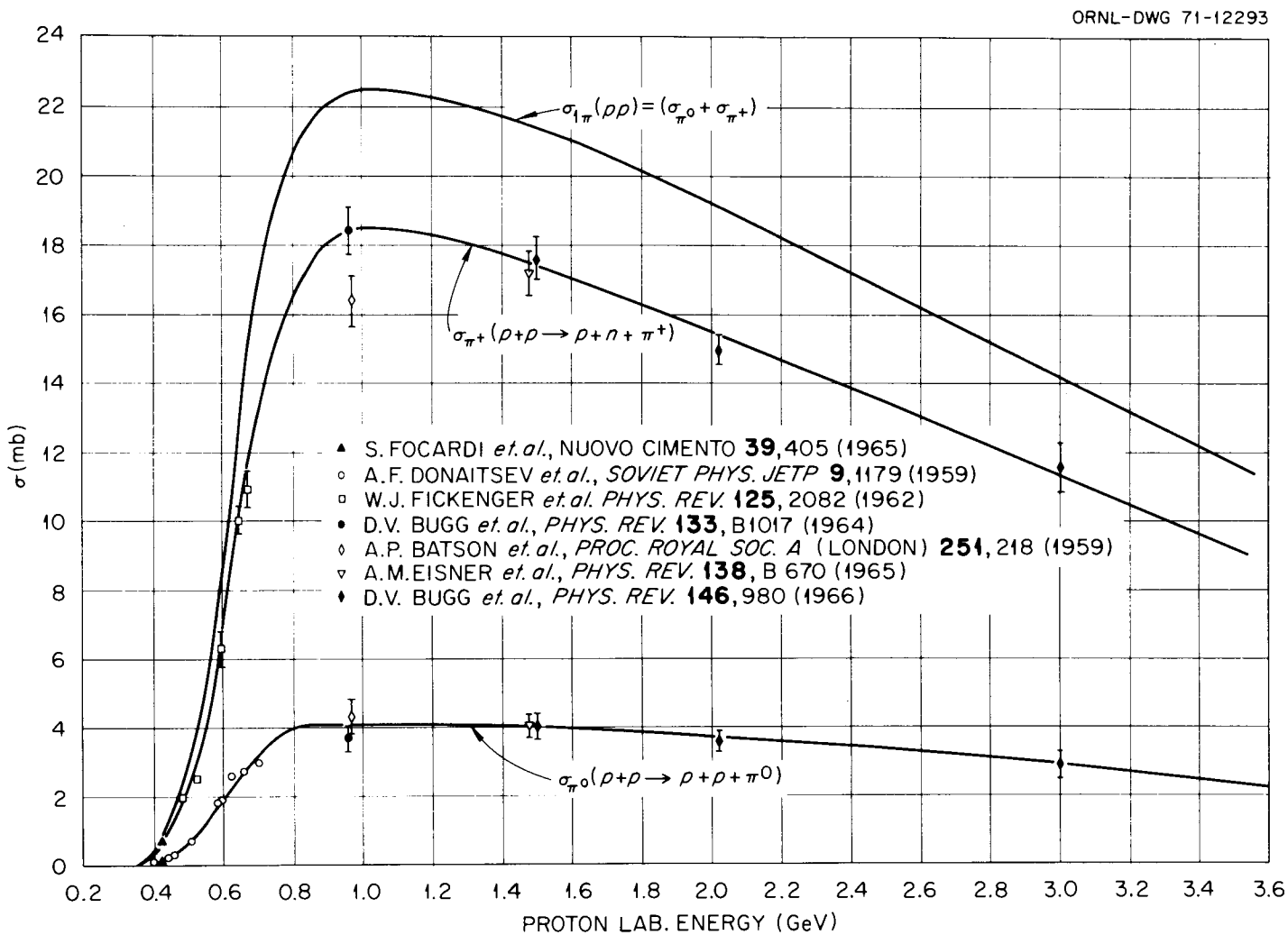

Fig. 3. Cross sections for producing single π-mesons in p-p collisions.

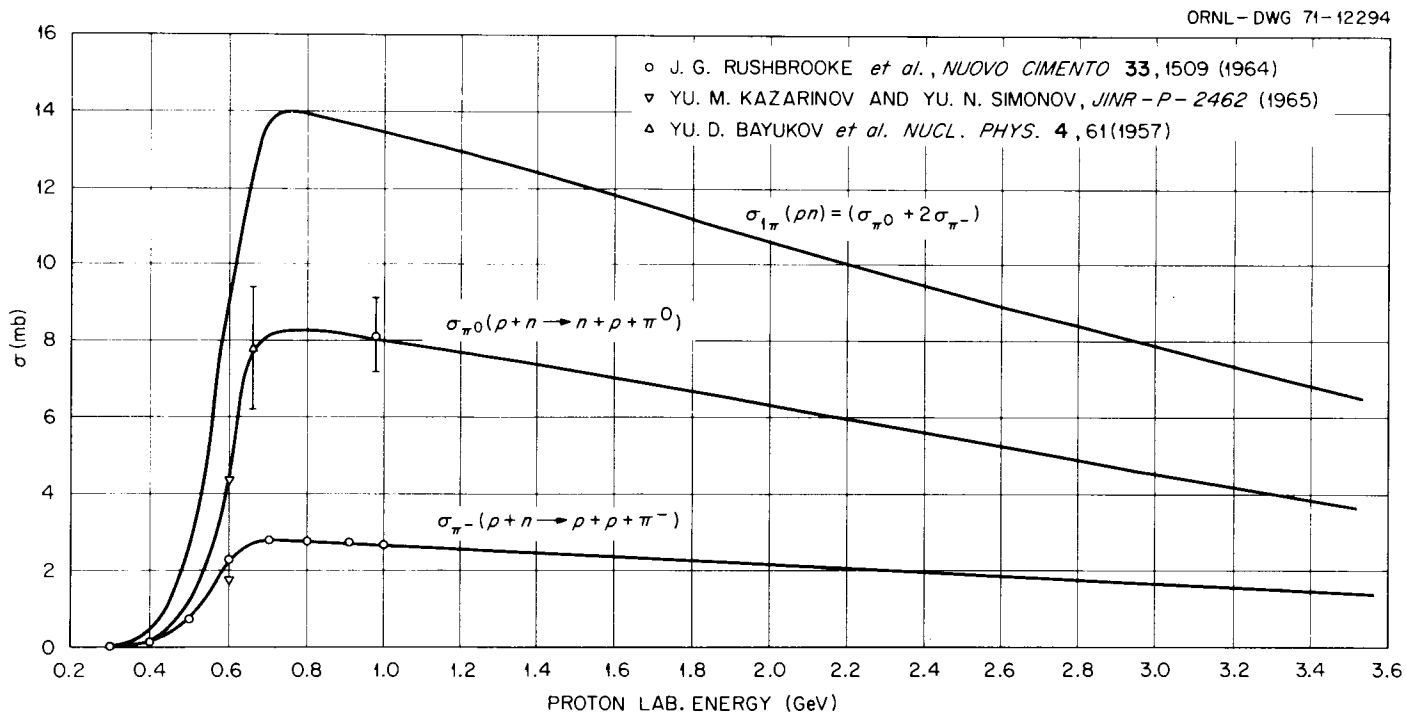

Fig. 4. Cross sections for producing single π-mesons in p-n collisions.

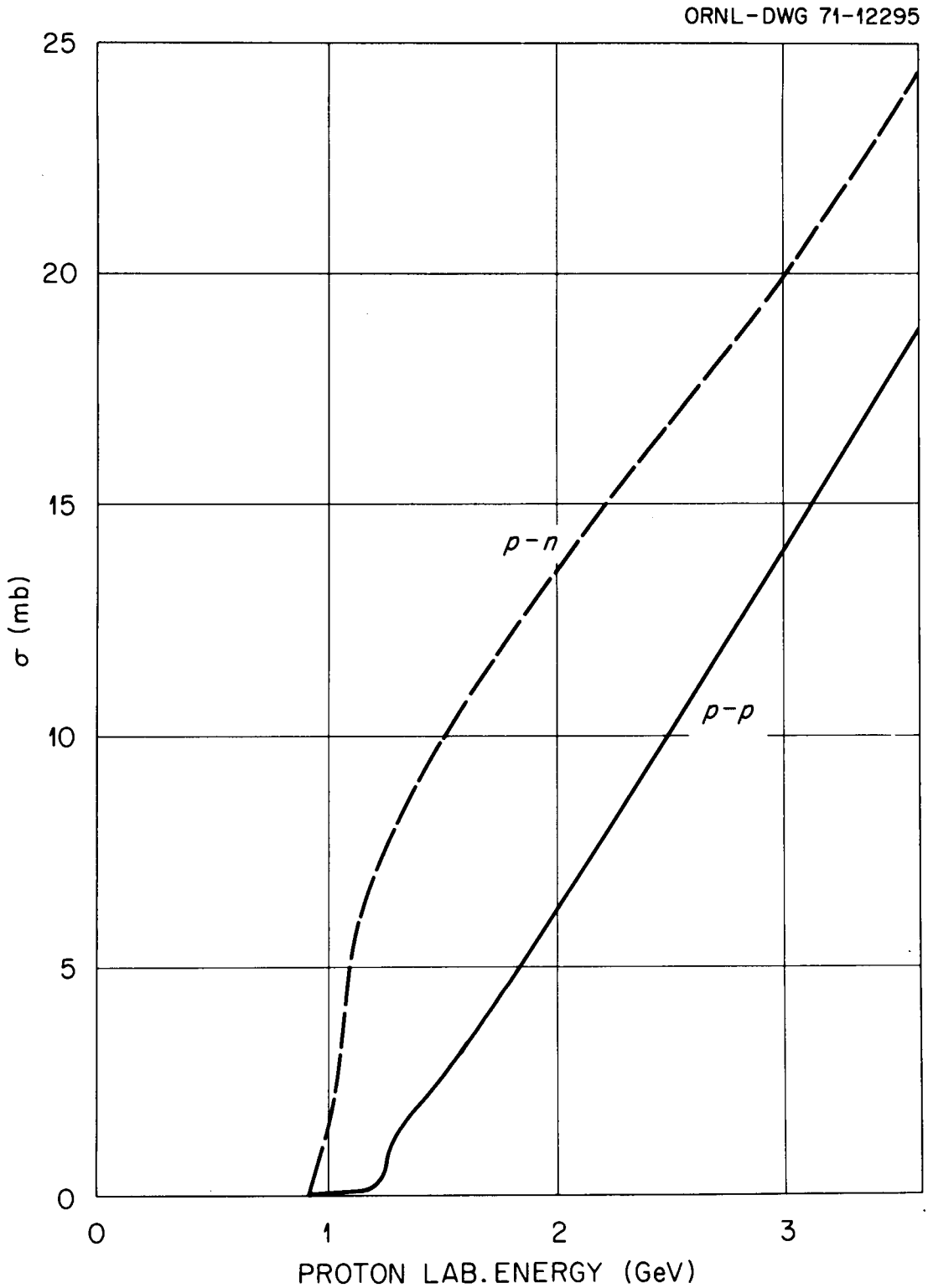

Fig. 5. Cross sections for producing two π-mesons in p-p and p-n collisions.

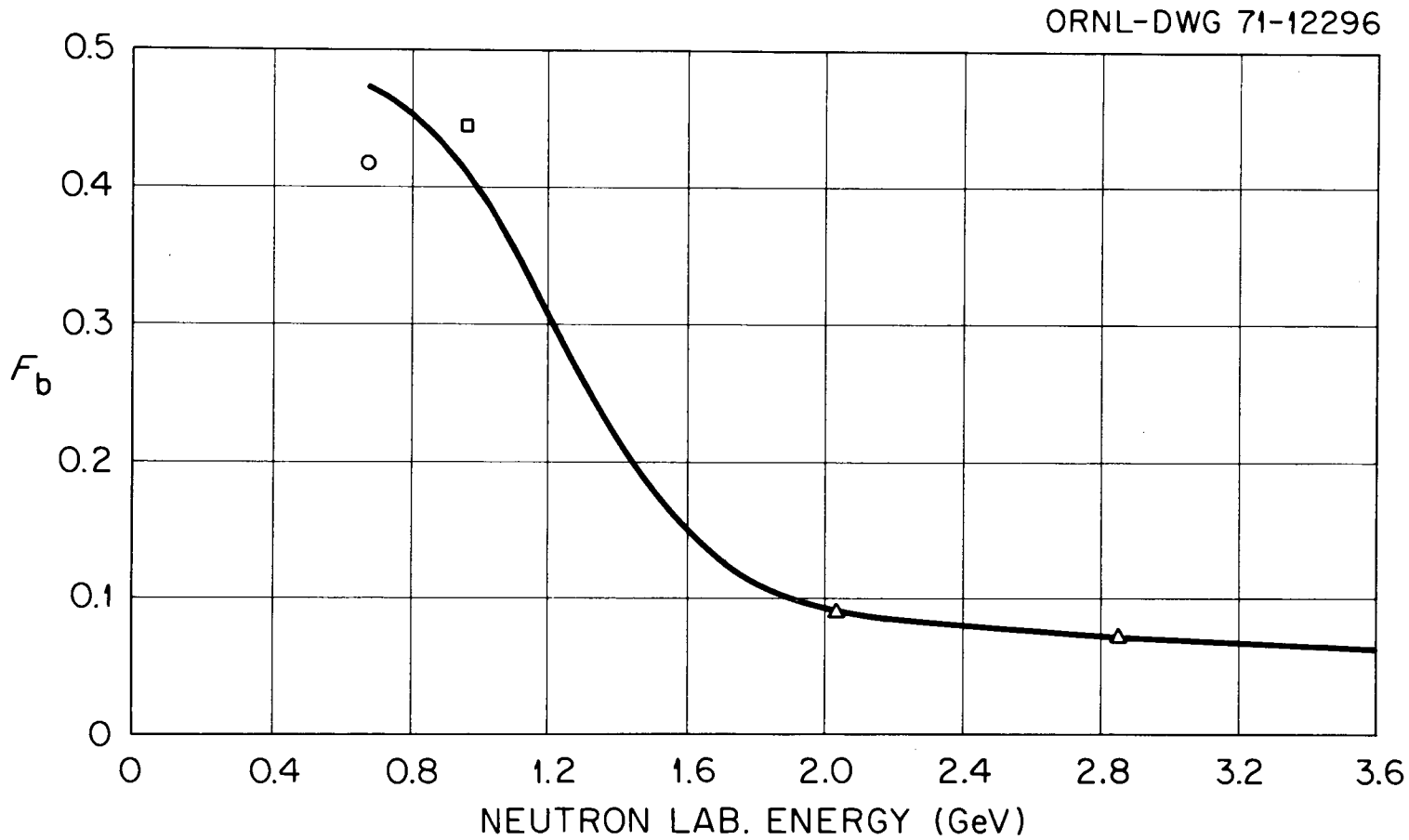

Fig. 6. Fraction of the n-p elastic scattering in the backward direction. The symbols represent results of integrations of the following data:

○ N. S. Amaglobeli *et al.*, Proc. Ann. Int. Conf. on High Energy Physics, Rochester, N. Y. (1960), p. 64;

□ A. P. Batson *et al.*, Proc. Roy. Soc. (London) A251, 233 (1959);

△ J. L. Freides *et al.*, Phys. Rev. Letters 15, 38 (1965), who estimated the illustrated fraction.

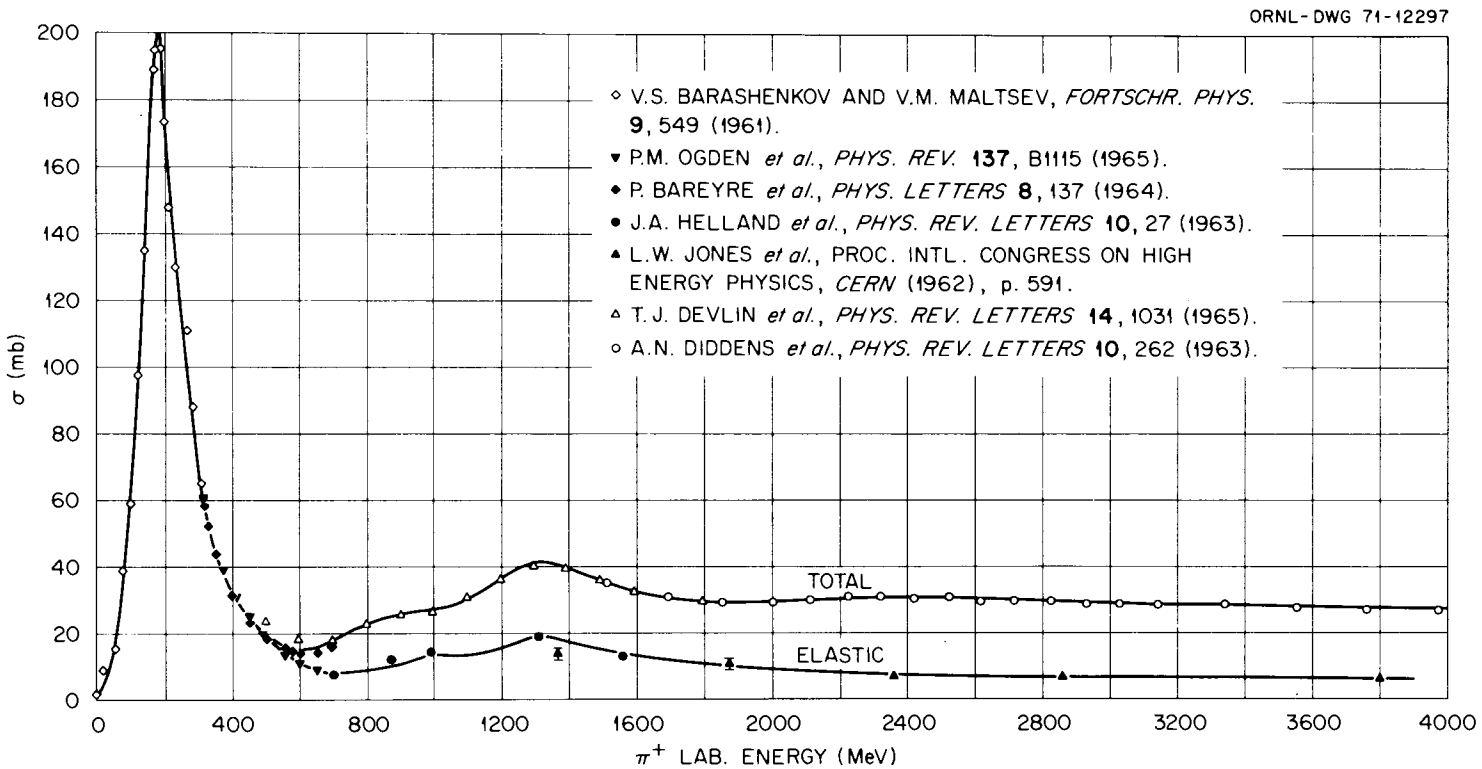

Fig. 7. The $\pi^+ + p$ total and elastic cross sections.

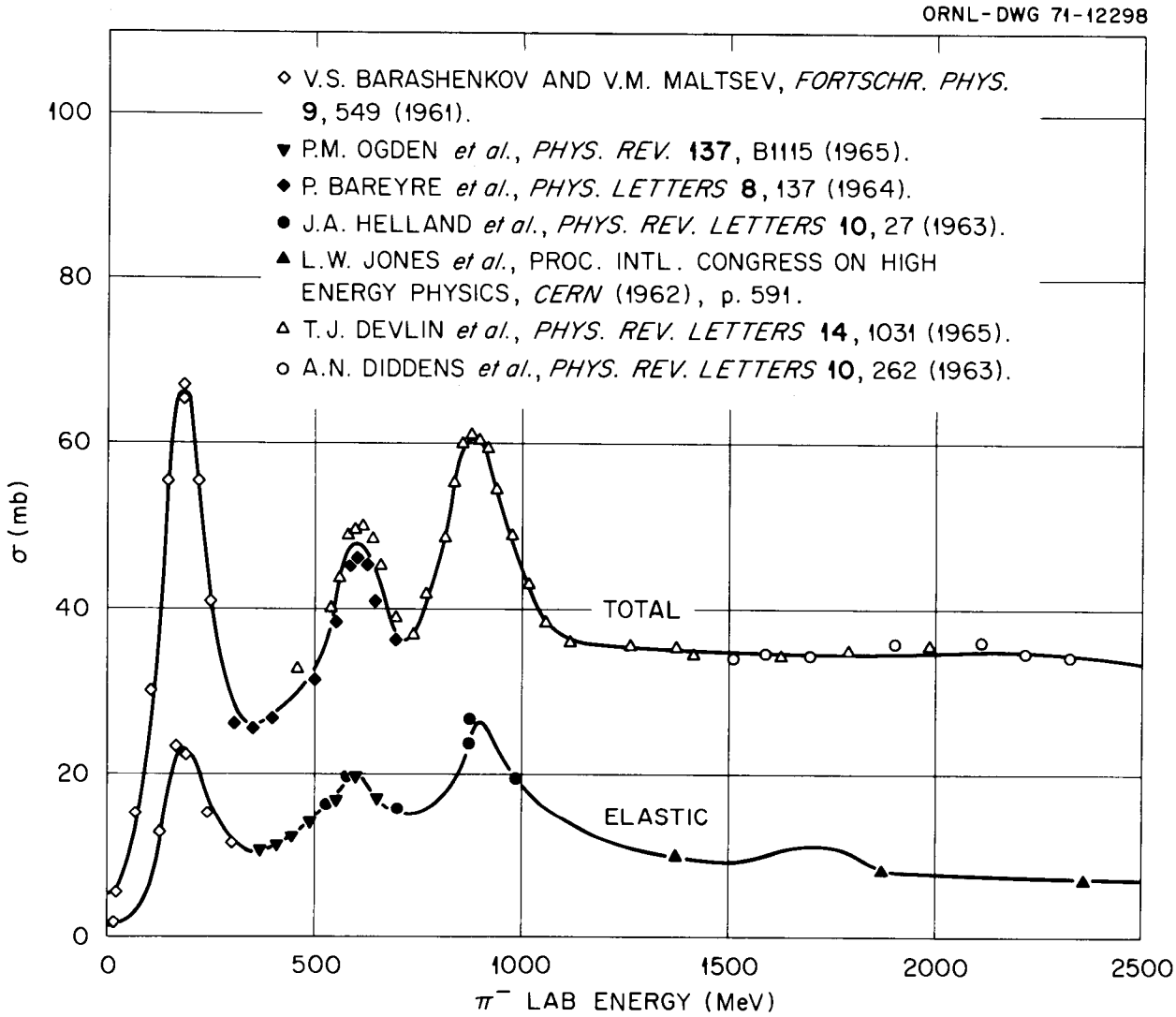

Fig. 8. The $\pi^- + p$ total and elastic cross sections.

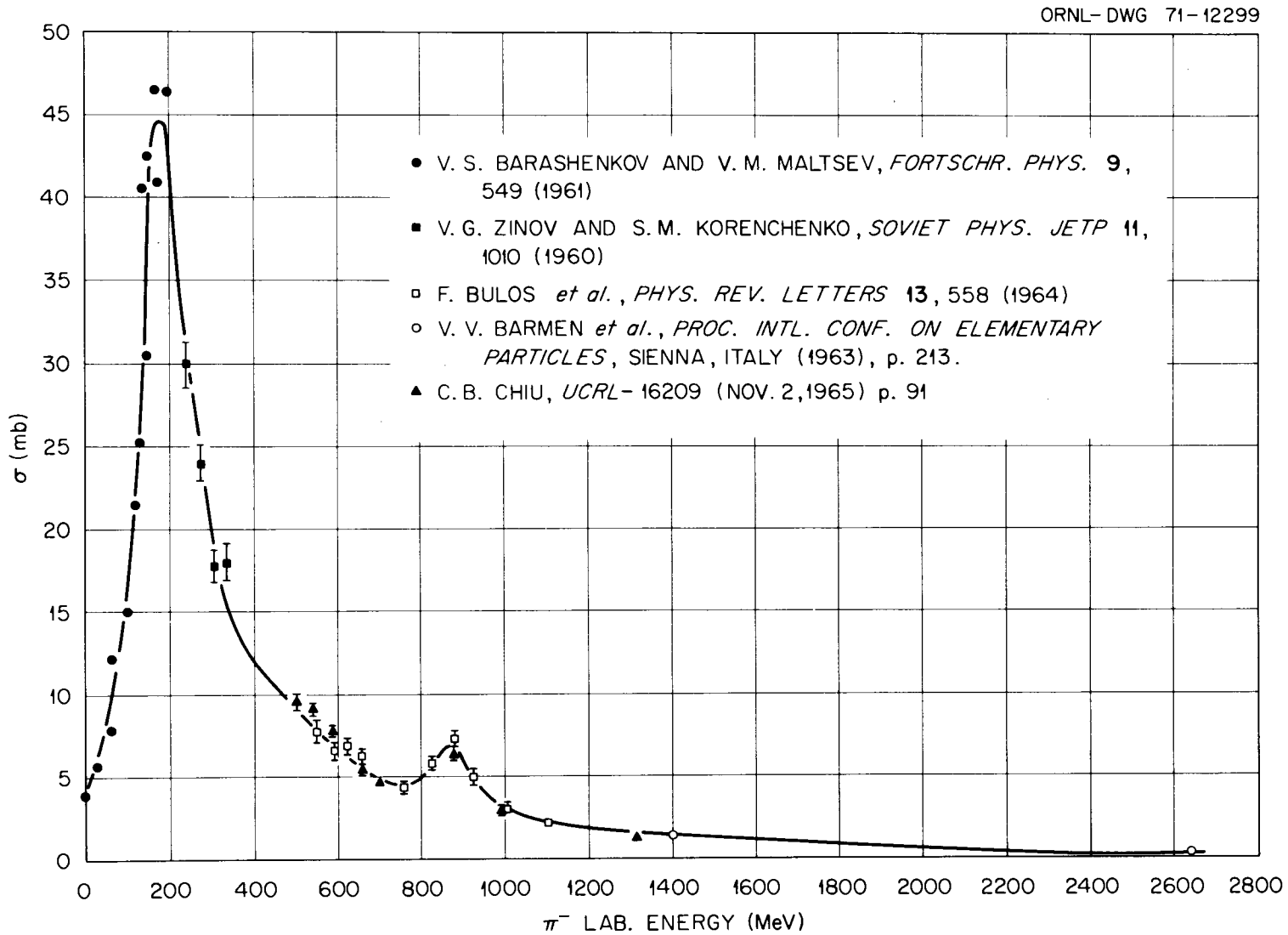

Fig. 9. The $\pi^- + p$ charge-exchange scattering cross section.

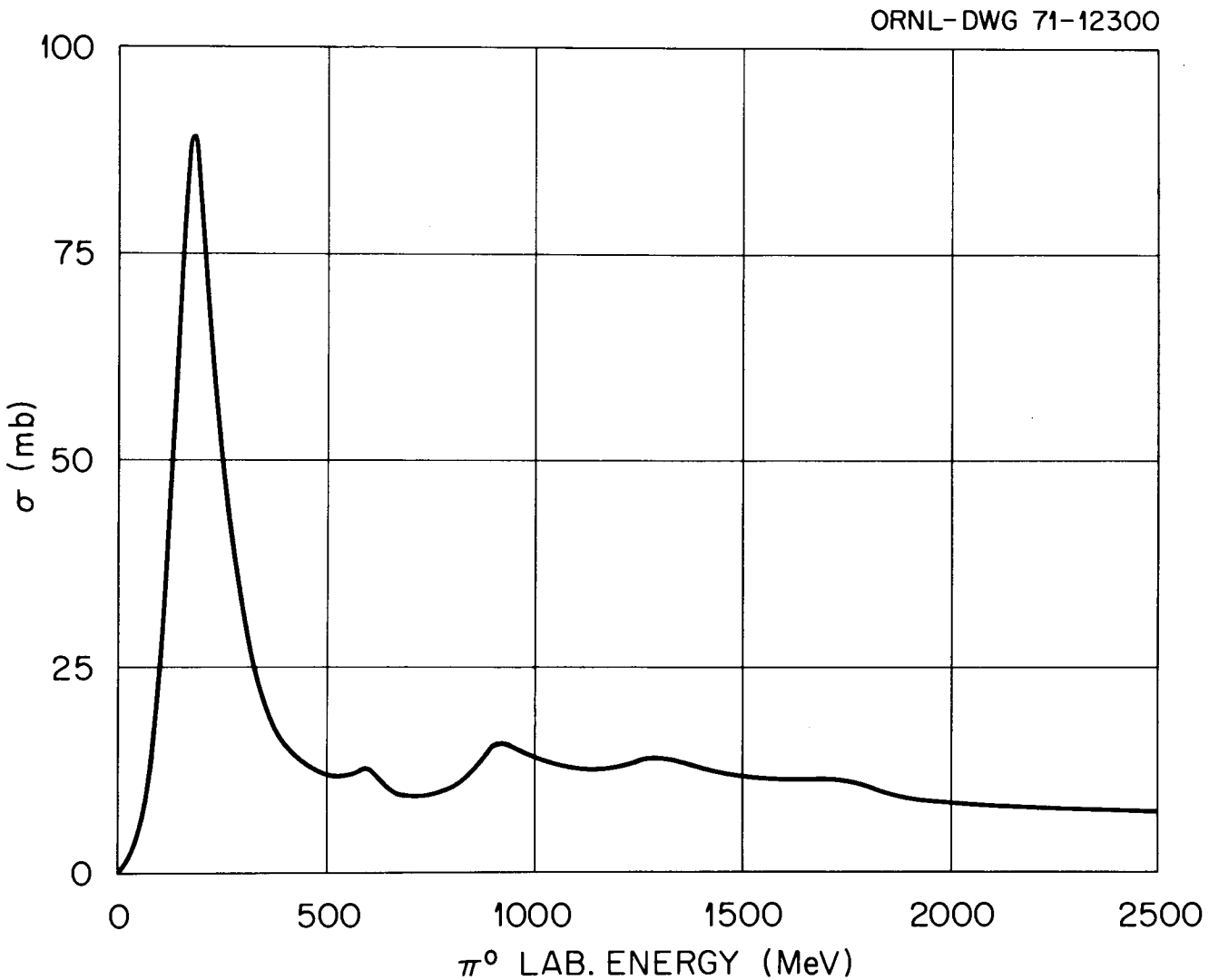

Fig. 10. The π^{o} + p elastic scattering cross section.

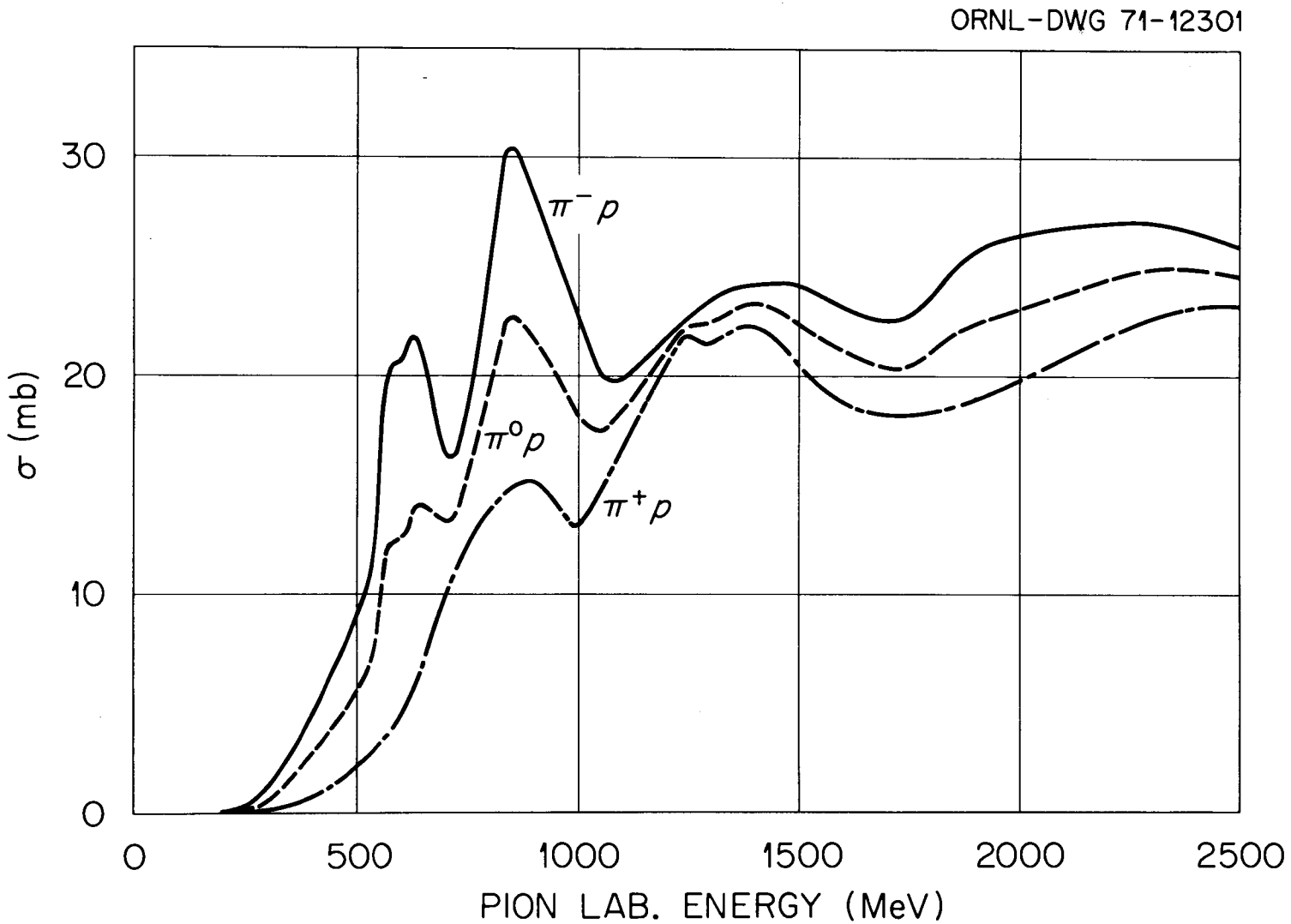

Fig. 11. The pion proton cross section for producing one π meson.

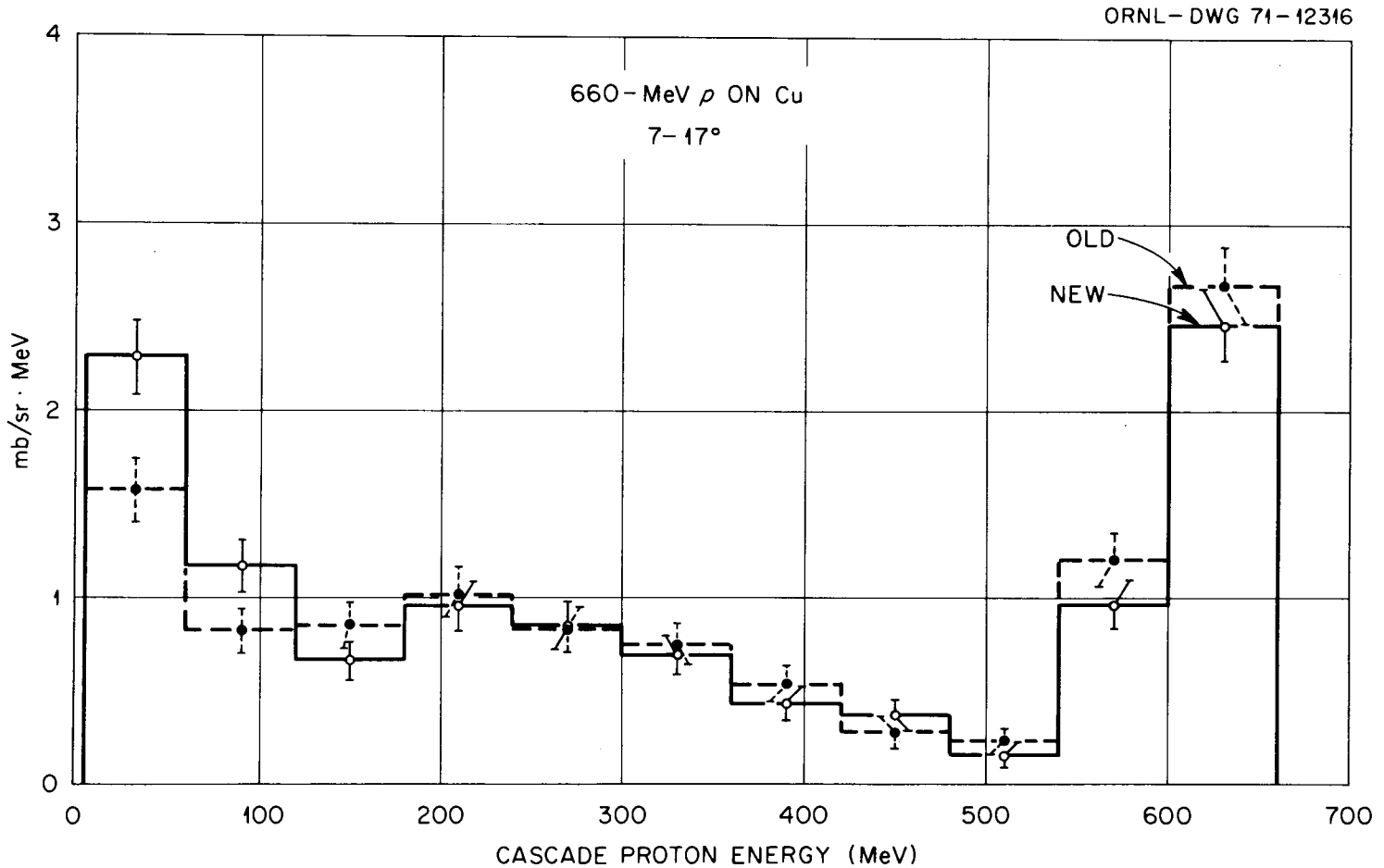

Fig. 12. Energy spectra of cascade protons emitted into the laboratory angular interval 7 to 17° from 660-MeV protons on Cu. The solid-line histogram represents the results of the calculation described in this report and the dashed-line histogram is from ref. 5. The error bars are due to the statistical nature of the calculation and represent one standard deviation.

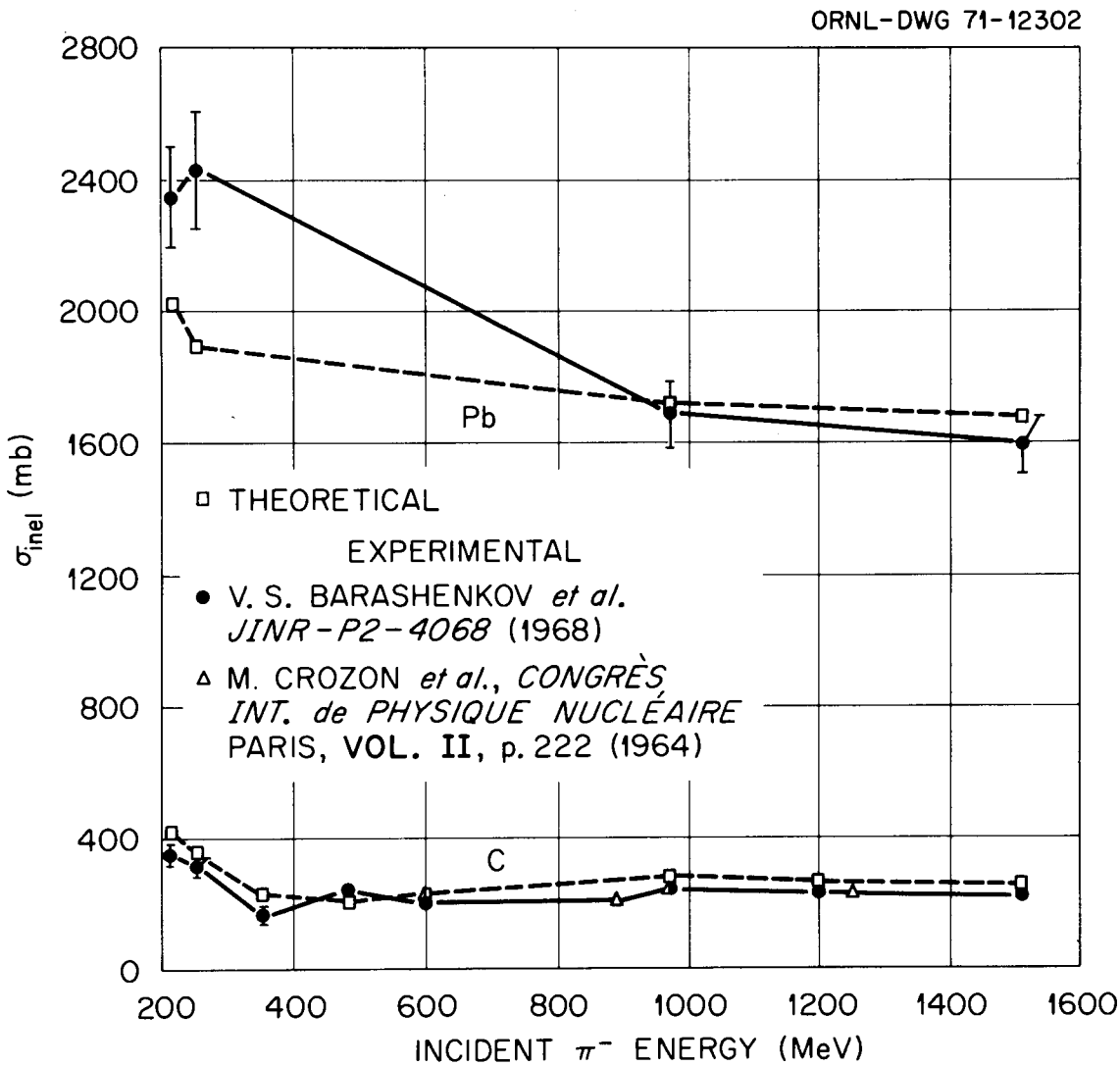

Fig. 13. Nonelastic cross section vs incident π^- energy for C and Pb targets. Solid lines connect the experimental data points. Dashed lines connect the theoretical values. When error bars are not shown, they are smaller than the symbols.

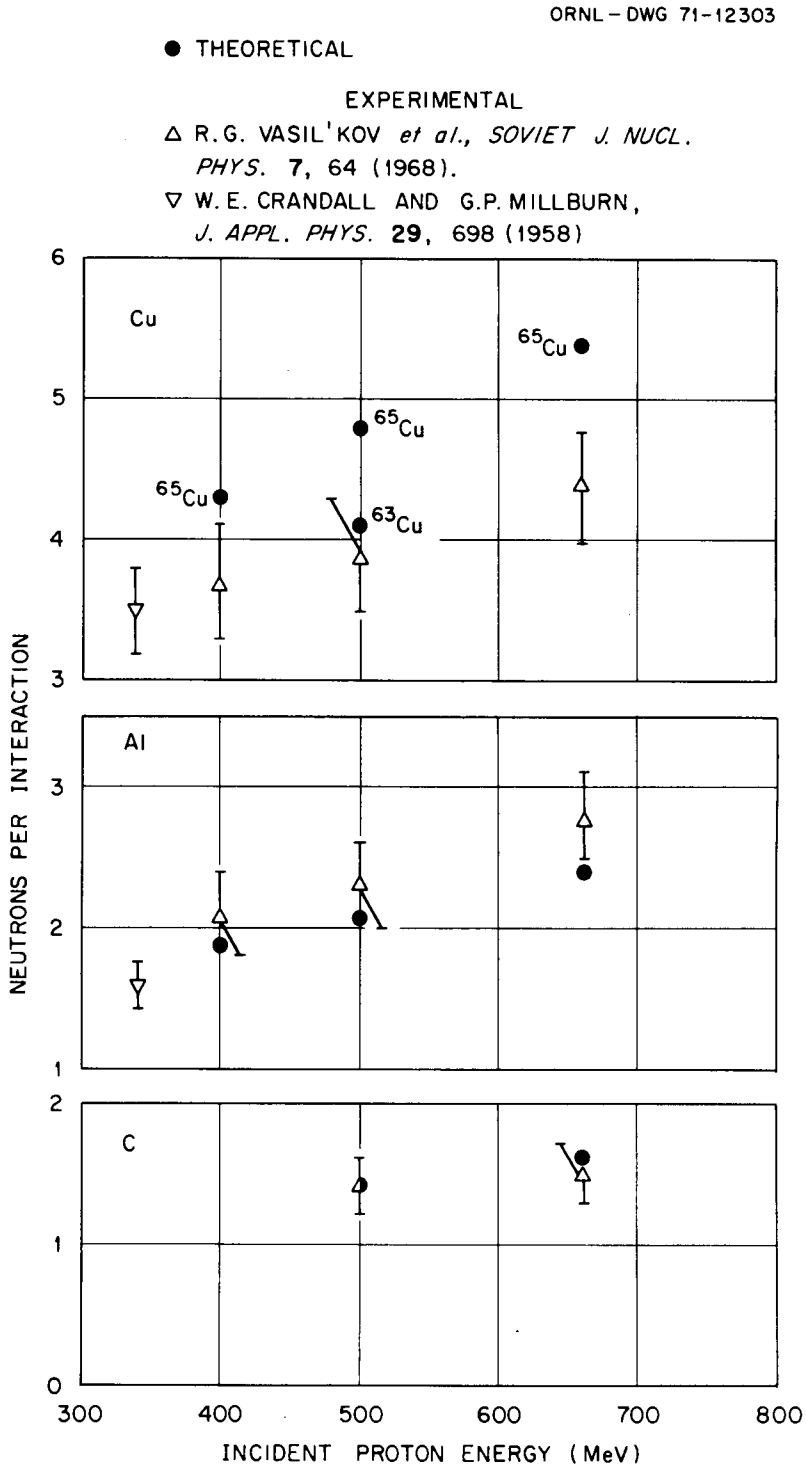

Fig. 14. The average number of neutrons emitted per interaction of protons with carbon, aluminum, and copper. Where error bars are not indicated, they are smaller than the symbols.

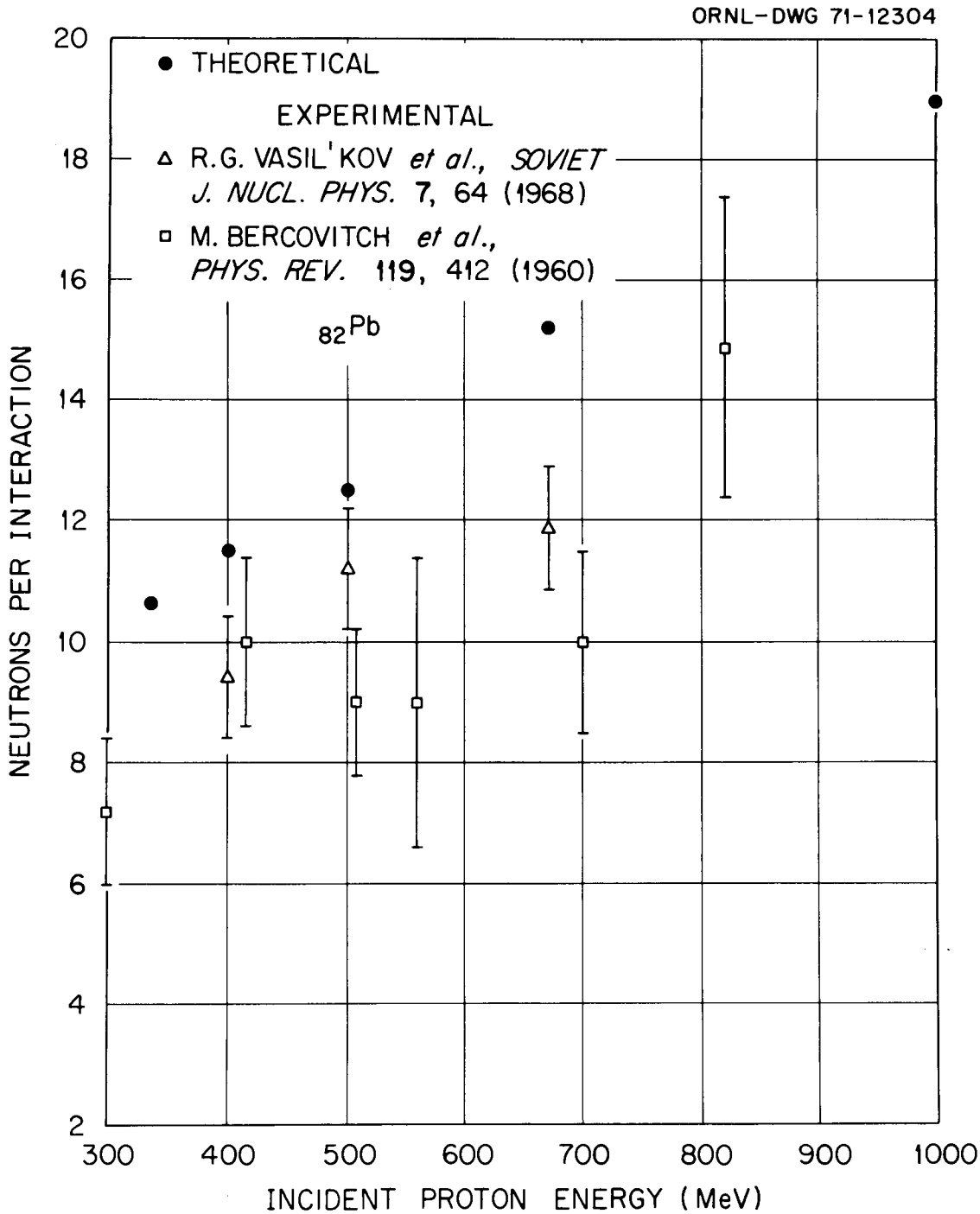

Fig. 15. The average number of neutrons emitted per interaction of protons with lead. Where error bars are not indicated, they are smaller than the symbols.

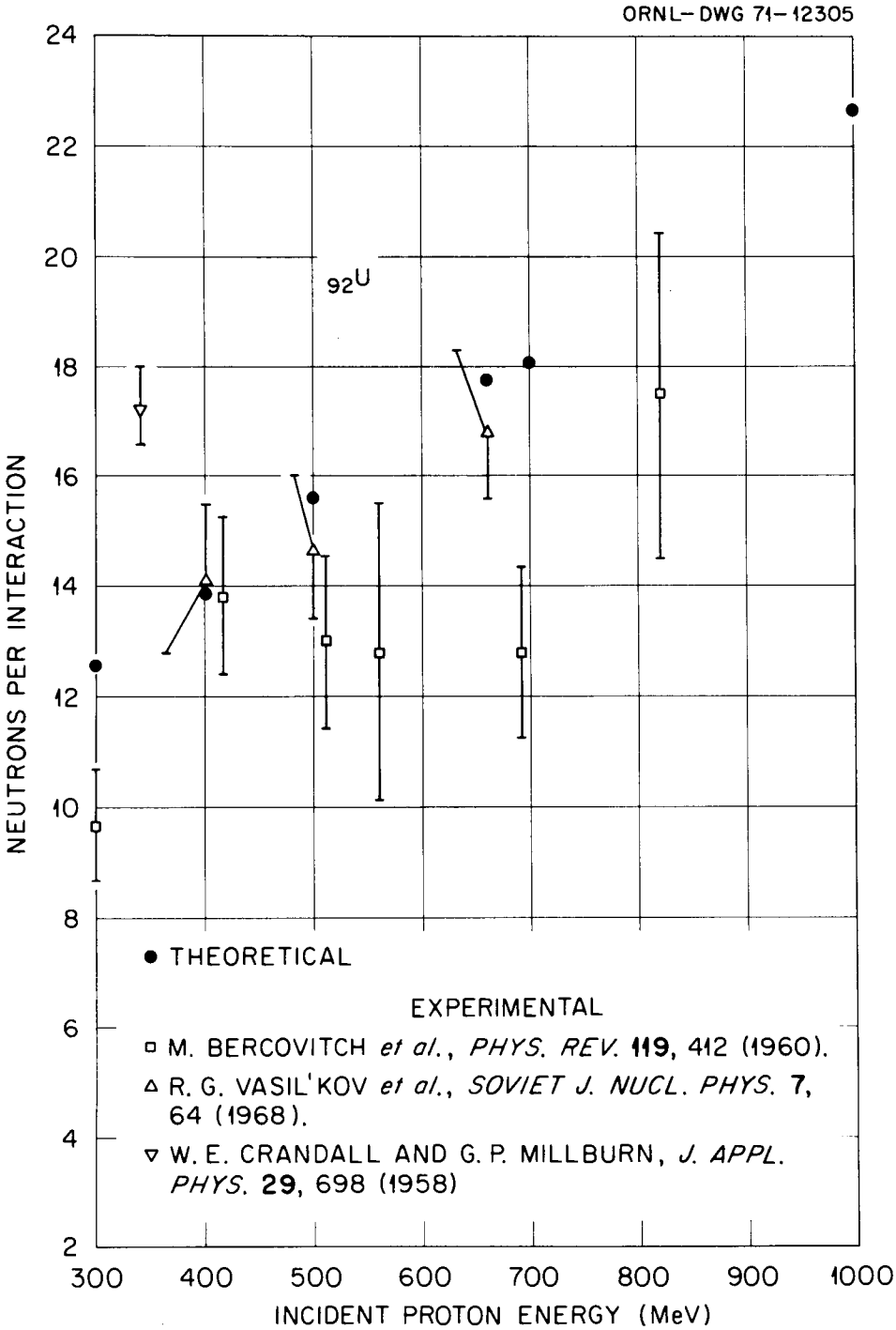

Fig. 16. The average number of neutrons emitted per interaction of protons with uranium. Where error bars are not indicated, they are smaller than the symbols.

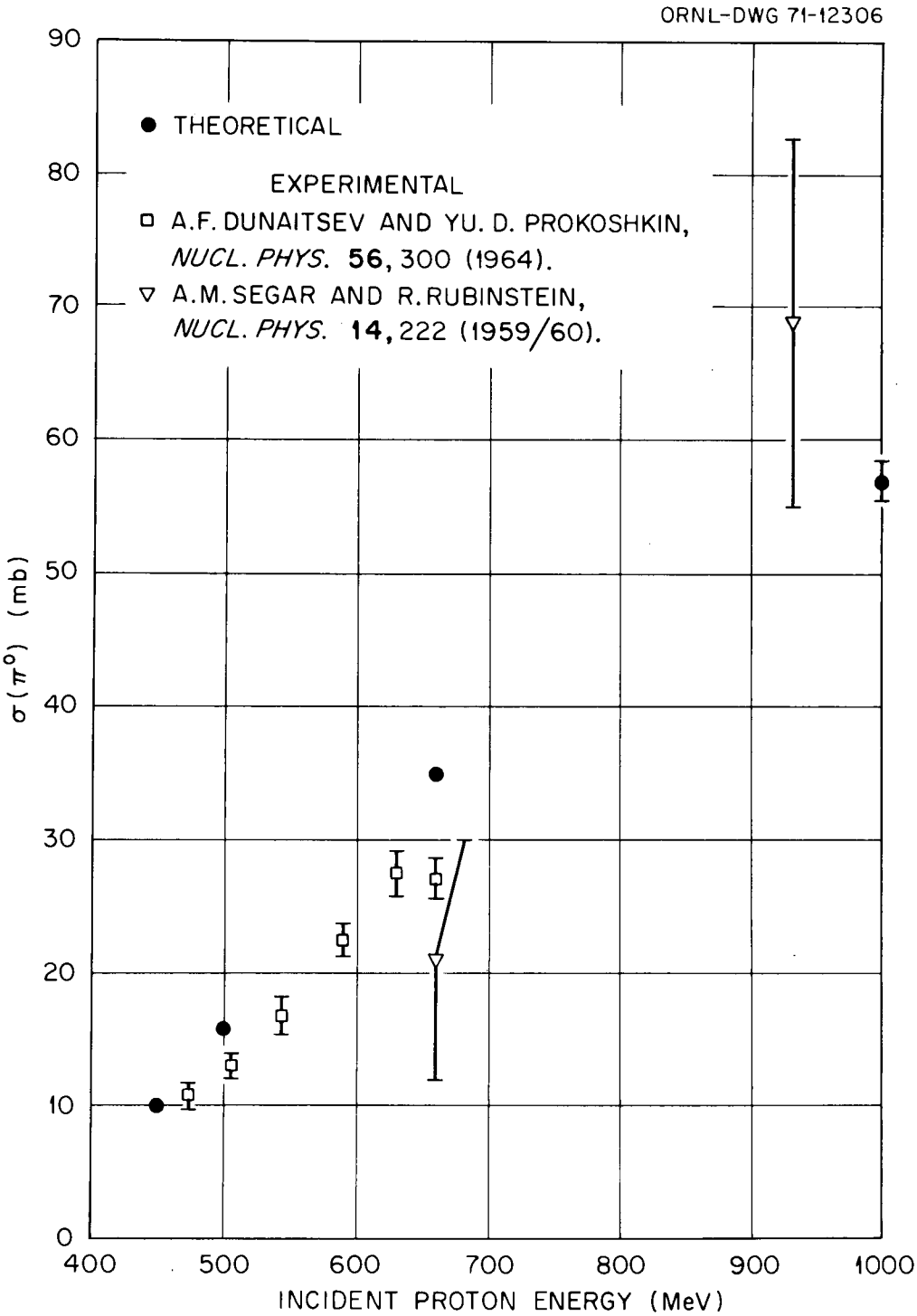

Fig. 17. The π^0 production cross section for protons on carbon. Where not illustrated, the error bars are smaller than the symbols.

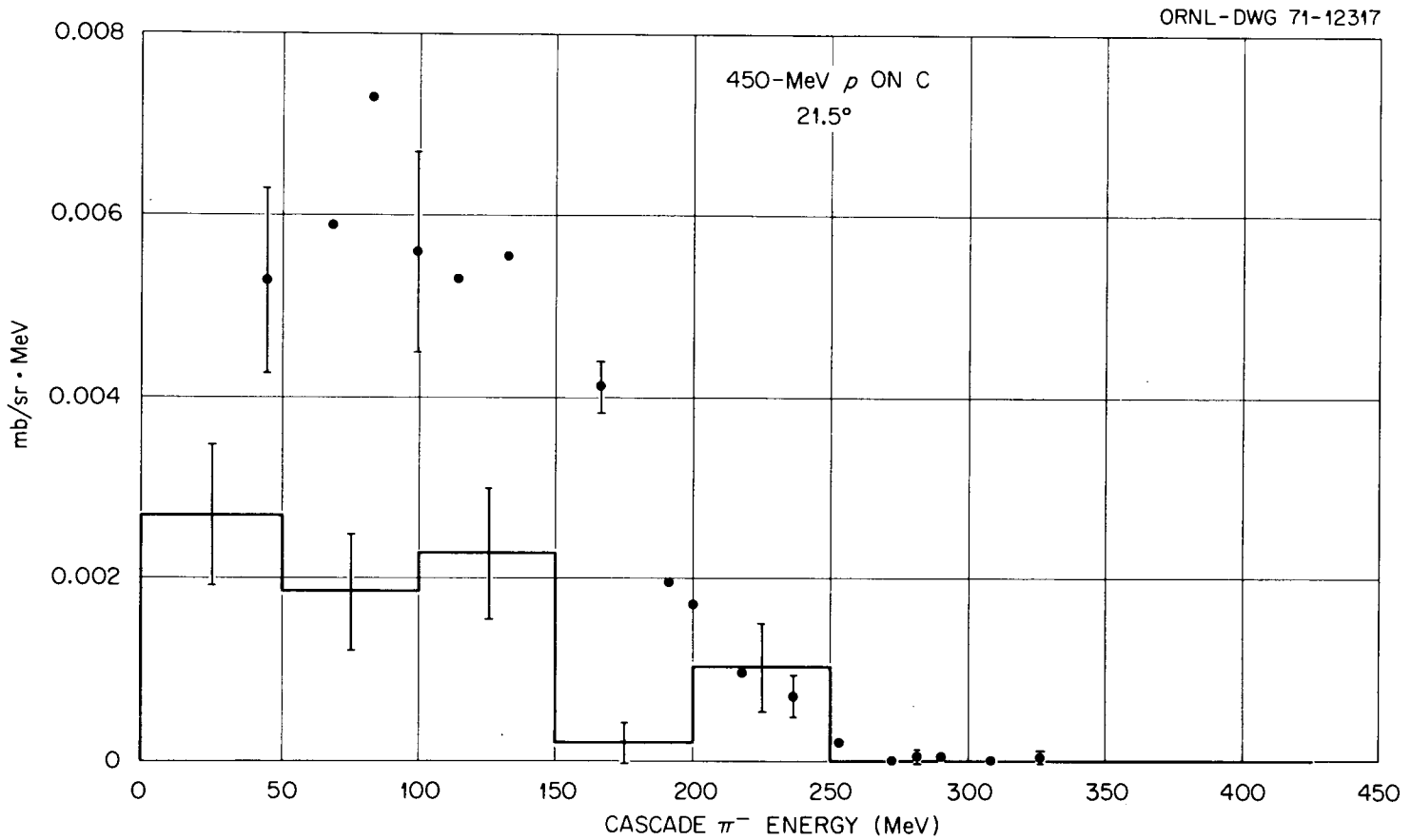

Fig. 18. Energy spectrum of π^- emitted at 21.5° from 450-MeV protons on carbon. ●: experimental data of Endre Lillethun, Phys. Rev. 125, 665 (1962); histogram: theoretical results for the angular interval 10-30°.

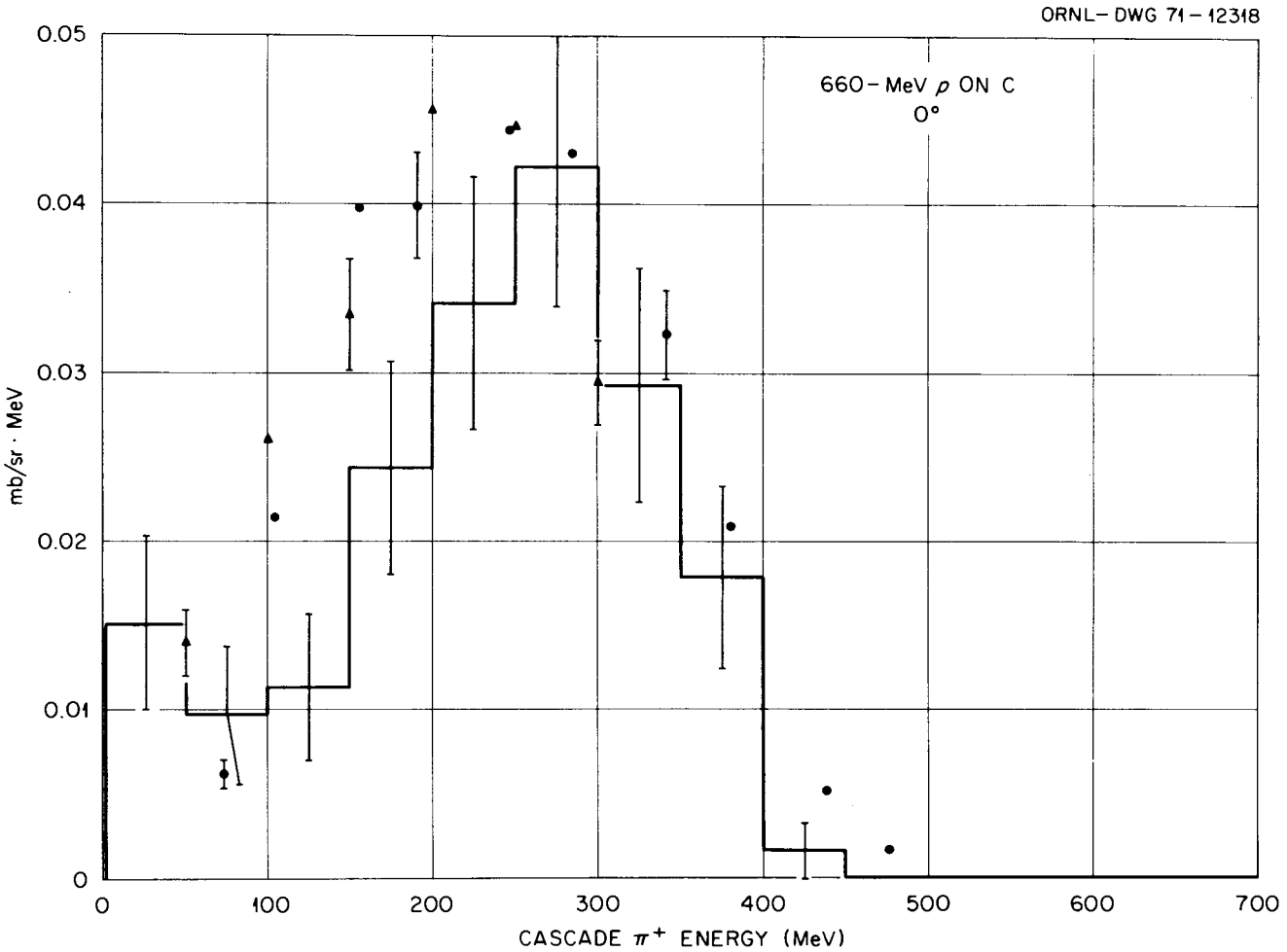

Fig. 19. Energy spectra of π^+ emitted at 0° from 660-MeV protons on carbon. Experimental data: ●: R. P. Haddock, M. Zeller, and K. M. Crowe, University of California at Los Angeles Technical Report MPG-64-2, UCLA-34P106, Dept. of Physics (incident proton energy, 725 MeV); ▲: W. Hirt *et al.*, CERN report No. 69-24 (1969), incident proton energy 600 MeV; histogram: theoretical results for the angular interval $0\text{-}10^o$.

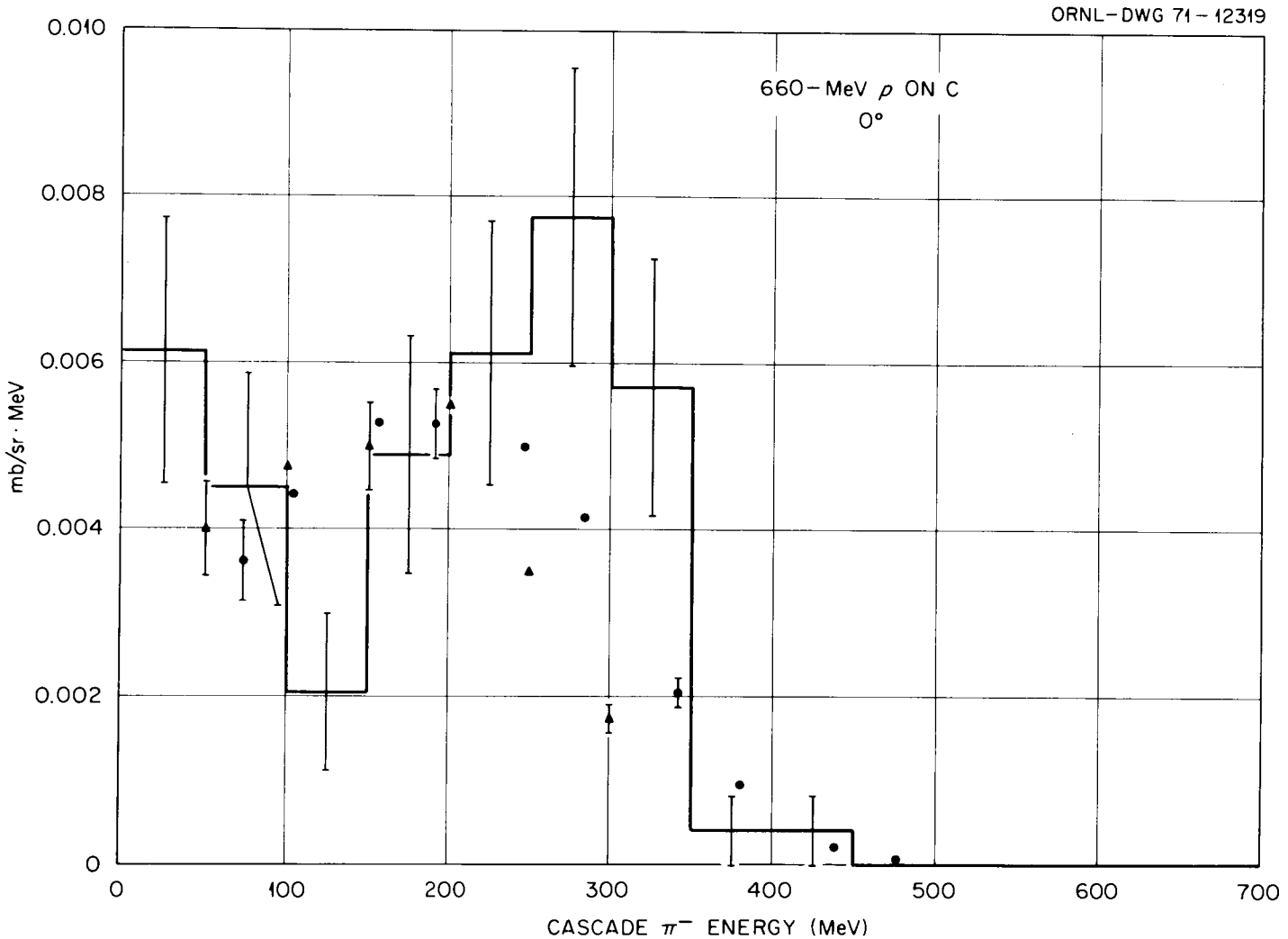

Fig. 20. Energy spectra of π^- emitted at 0° from 660-MeV protons on carbon. Experimental data of Haddock *et al.* and Hirt *et al.* (see Fig. 19 for references and symbols) and an angular interval of $0\text{-}20^\circ$ used for the theoretical results.

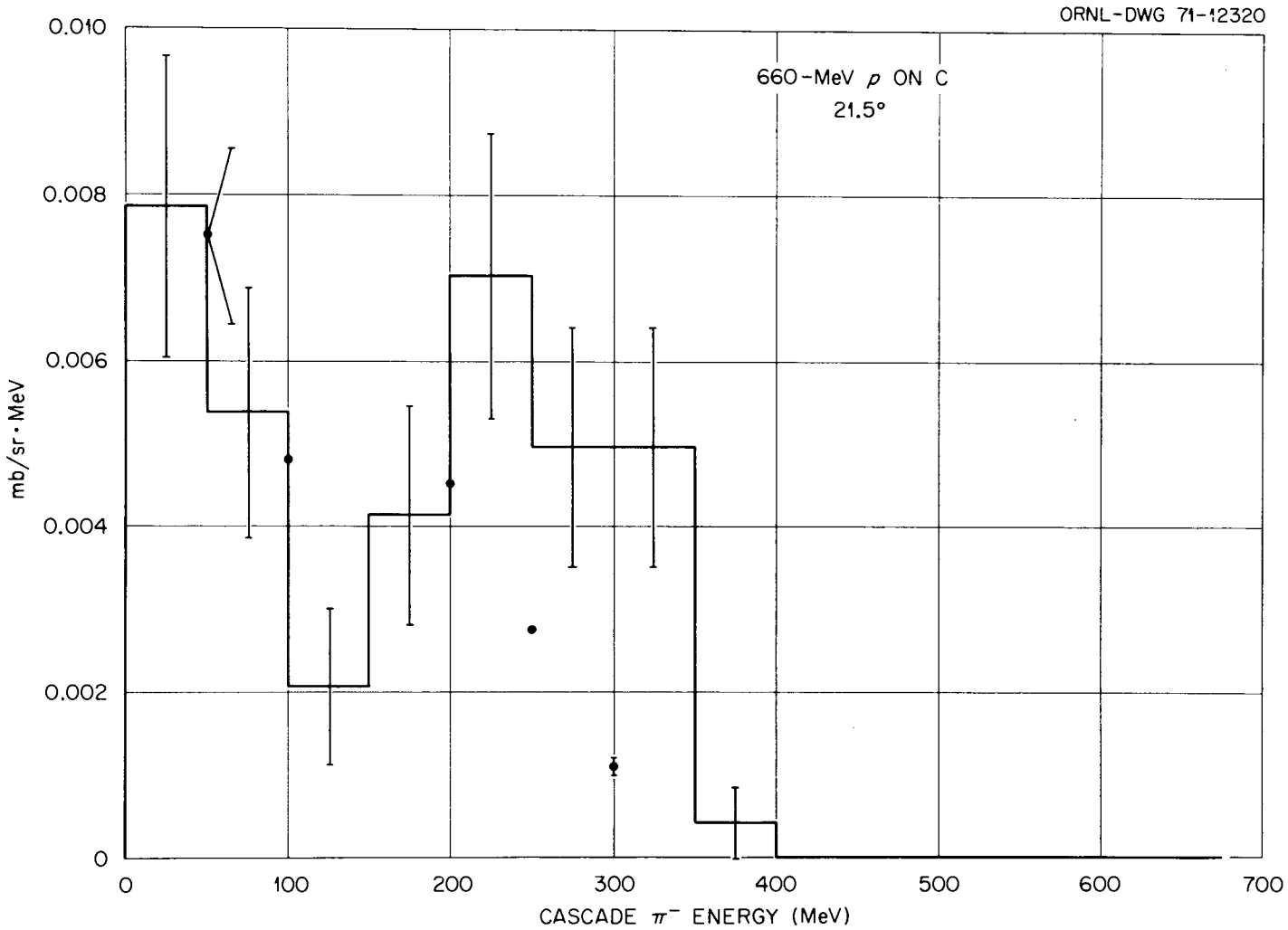

Fig. 21. Energy spectra of π^- emitted at 21.5° from 660-MeV protons on carbon. ●: experimental data of Hirt *et al.* (see Fig. 19 for reference); histogram: theoretical results for the angular interval 15-25°.

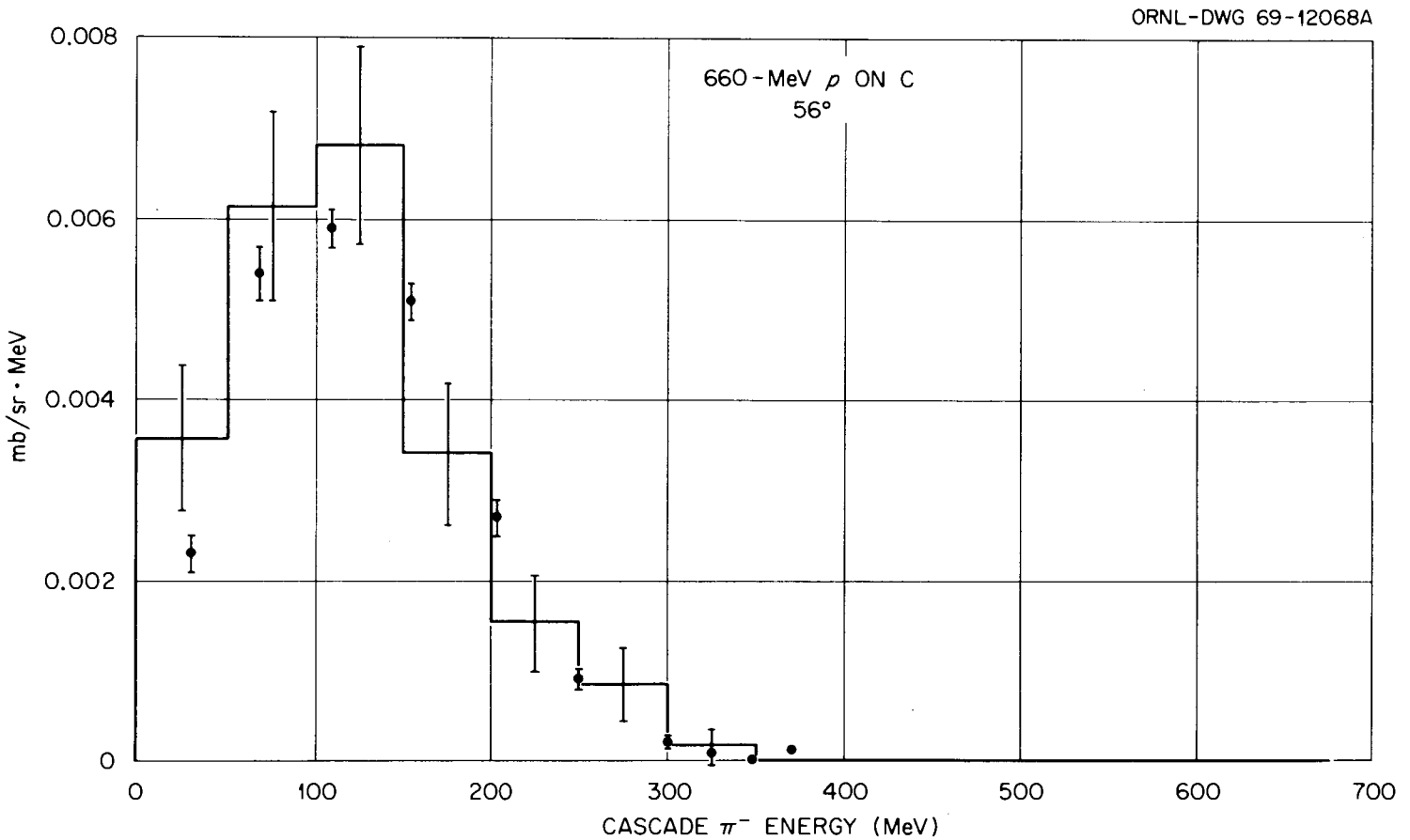

Fig. 22. Energy spectra of π^- emitted at 56° from 660-MeV protons on carbon. ●: experimental data of L. S. Azhgirei *et al.*, Soviet Phys. JETP 34, 939 (1958); histogram: theoretical results for the angular interval $51\text{-}61^\circ$.

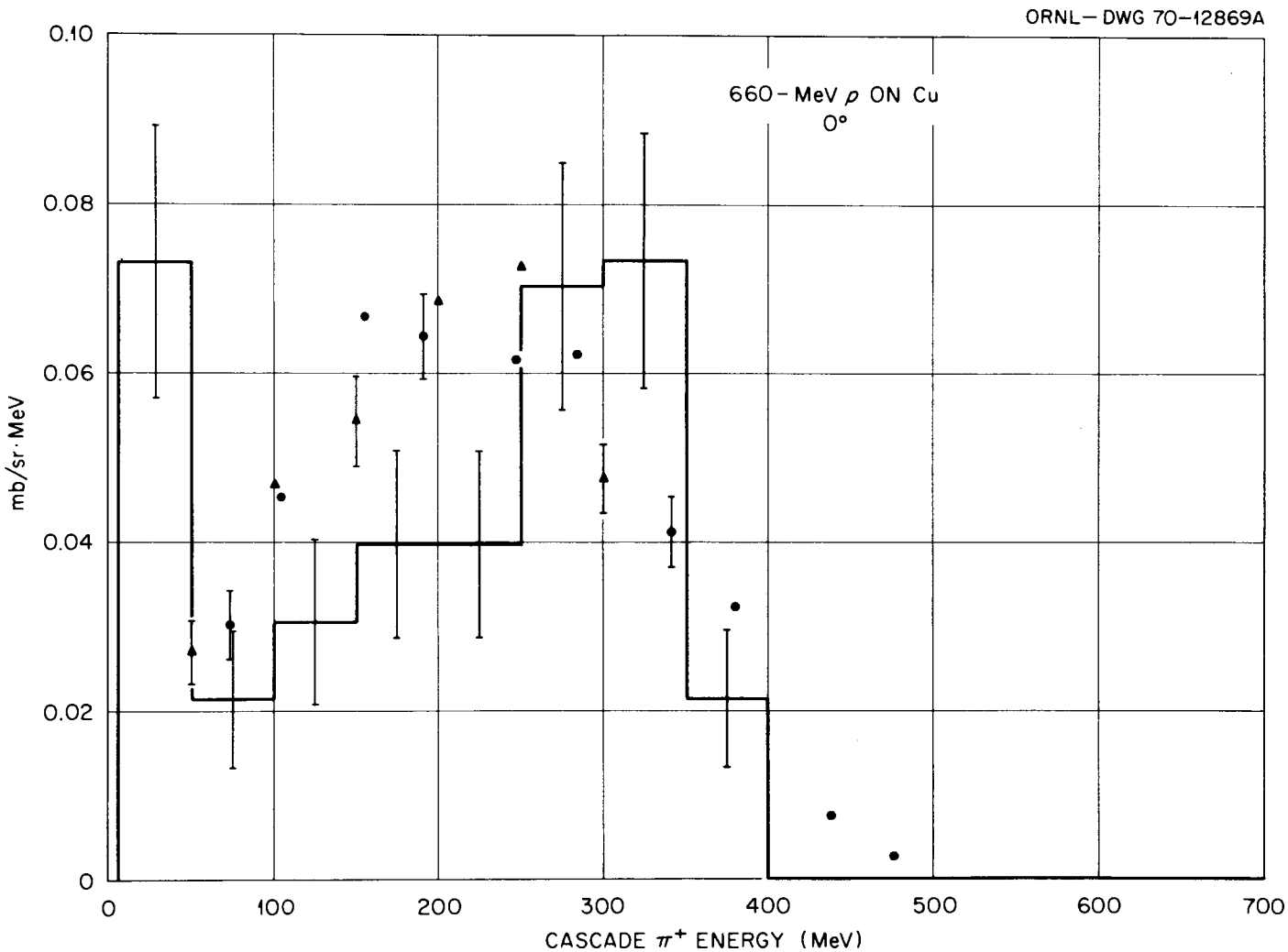

Fig. 23. Energy spectra of π^+ emitted at 0° from 660-MeV protons on copper. Experimental data: same as shown in Fig. 19; histogram: same as in Fig. 19.

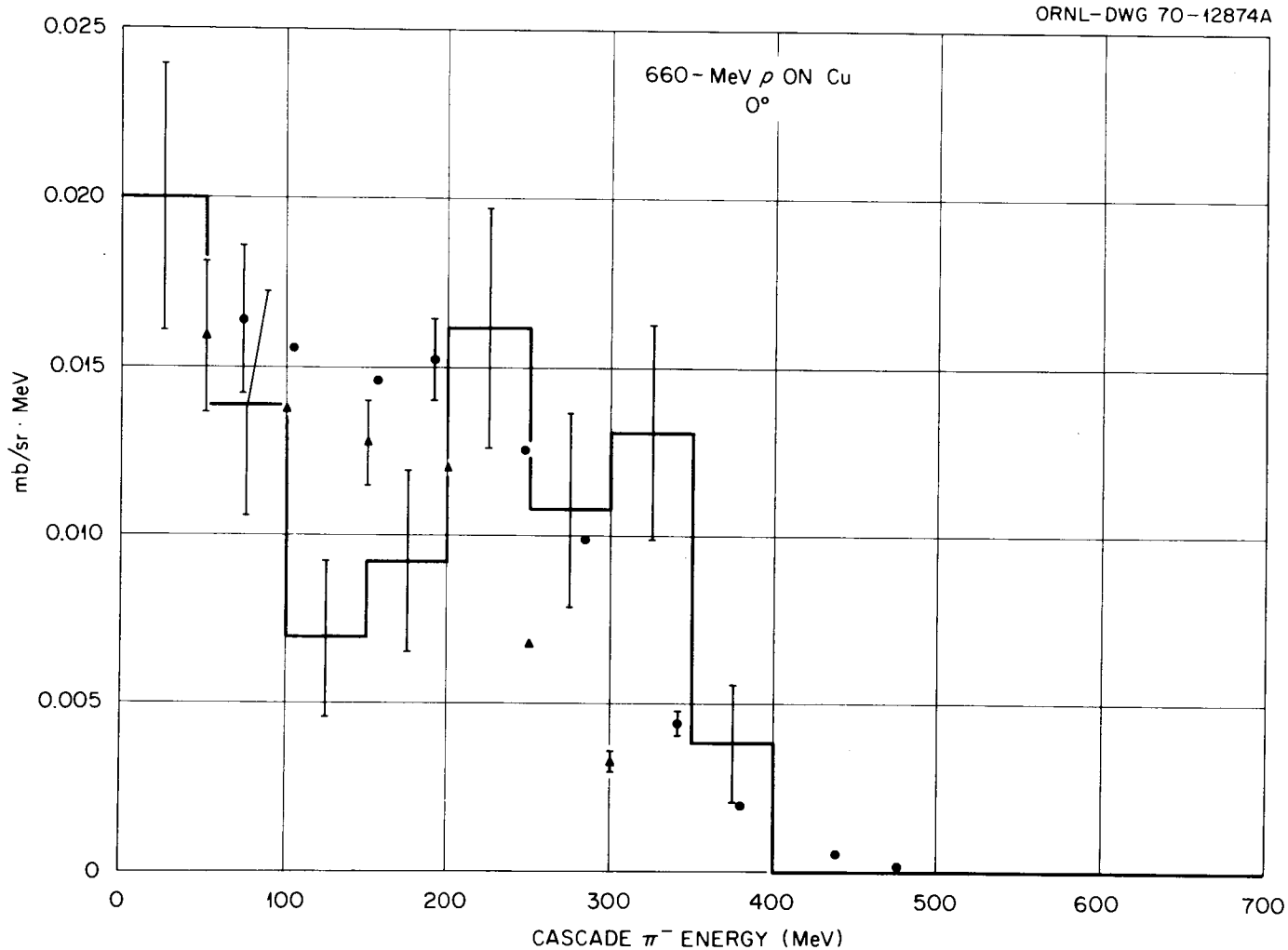

Fig. 24. Energy spectra of π^- emitted at 0° from 660-MeV protons on copper. Experimental data of Haddock *et al.* and Hirt *et al.* (see Fig. 19 for references and symbols) and an angular interval of $0\text{-}20^\circ$ used for the theoretical results.

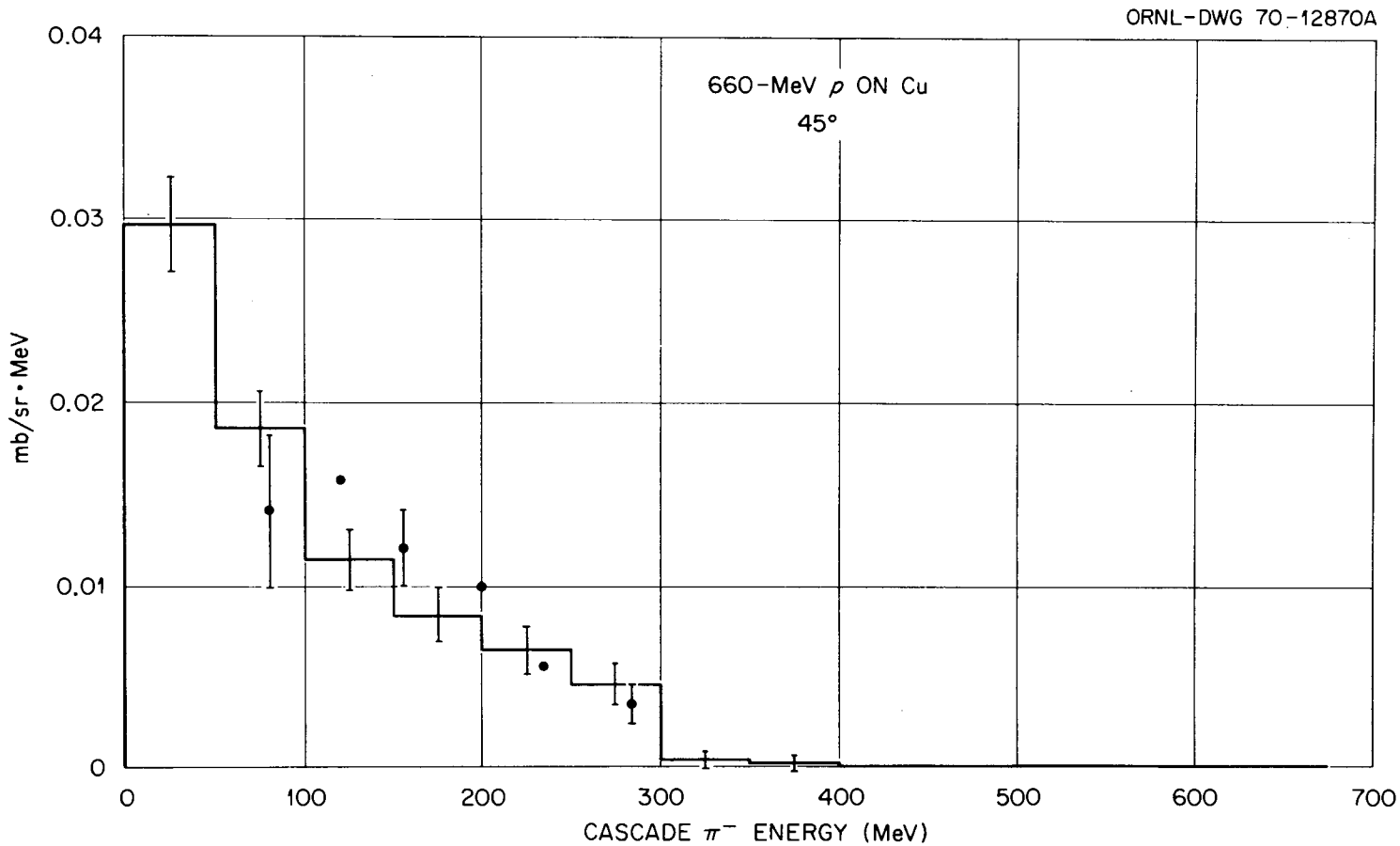

Fig. 25. Energy spectrum of π^- emitted at 45° from 660-MeV protons on copper. •: experimental data of A. G. Meshkovskii, Ia. Ia. Shalamov, and V. A. Shebanov, Soviet Phys. JETP 6, 463 (1958); histogram: theoretical results for the angular interval $35-55^\circ$.

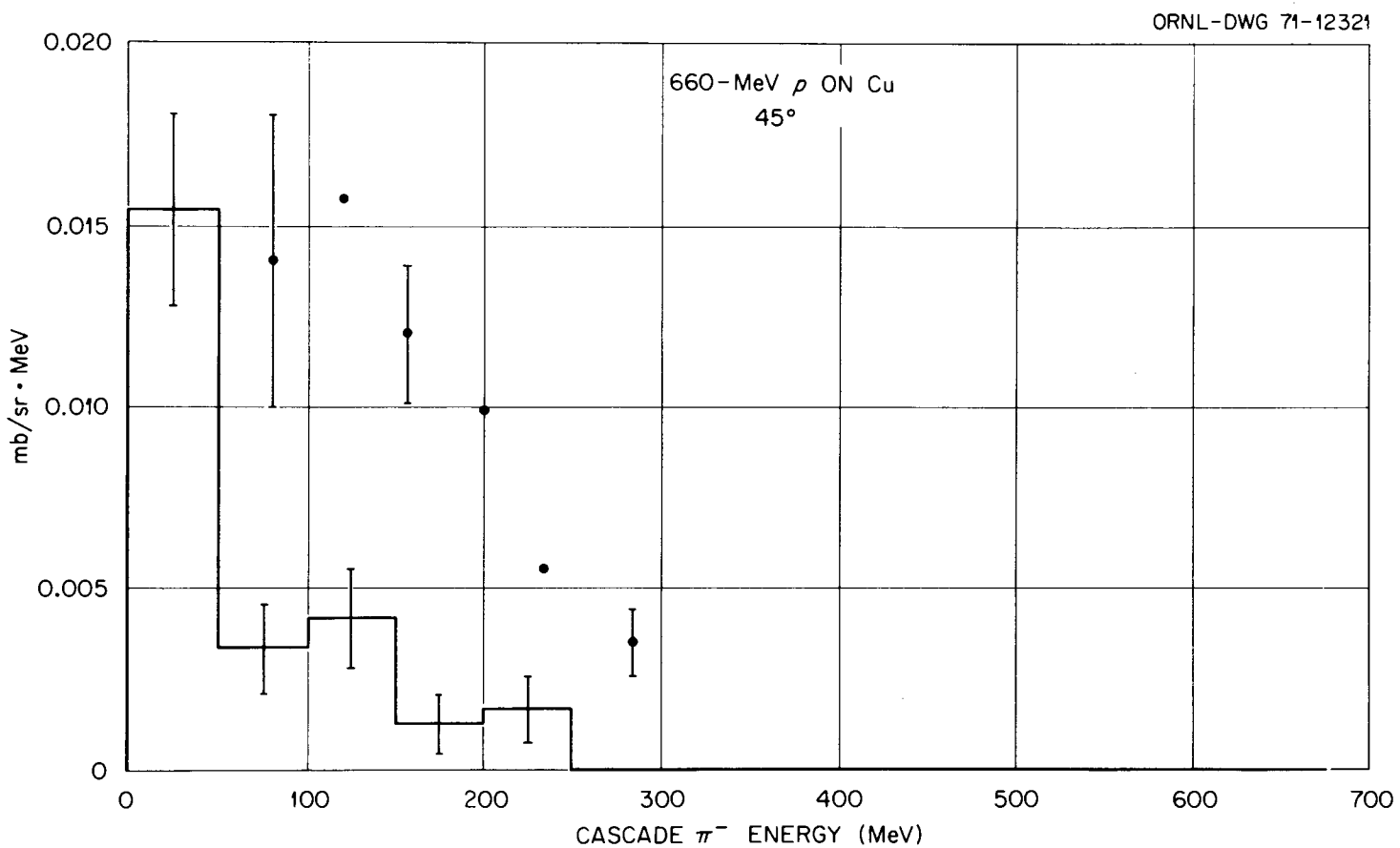

Fig. 26. Same as Fig. 25 with an rms radius used for the target in the theoretical calculations (described in the text).

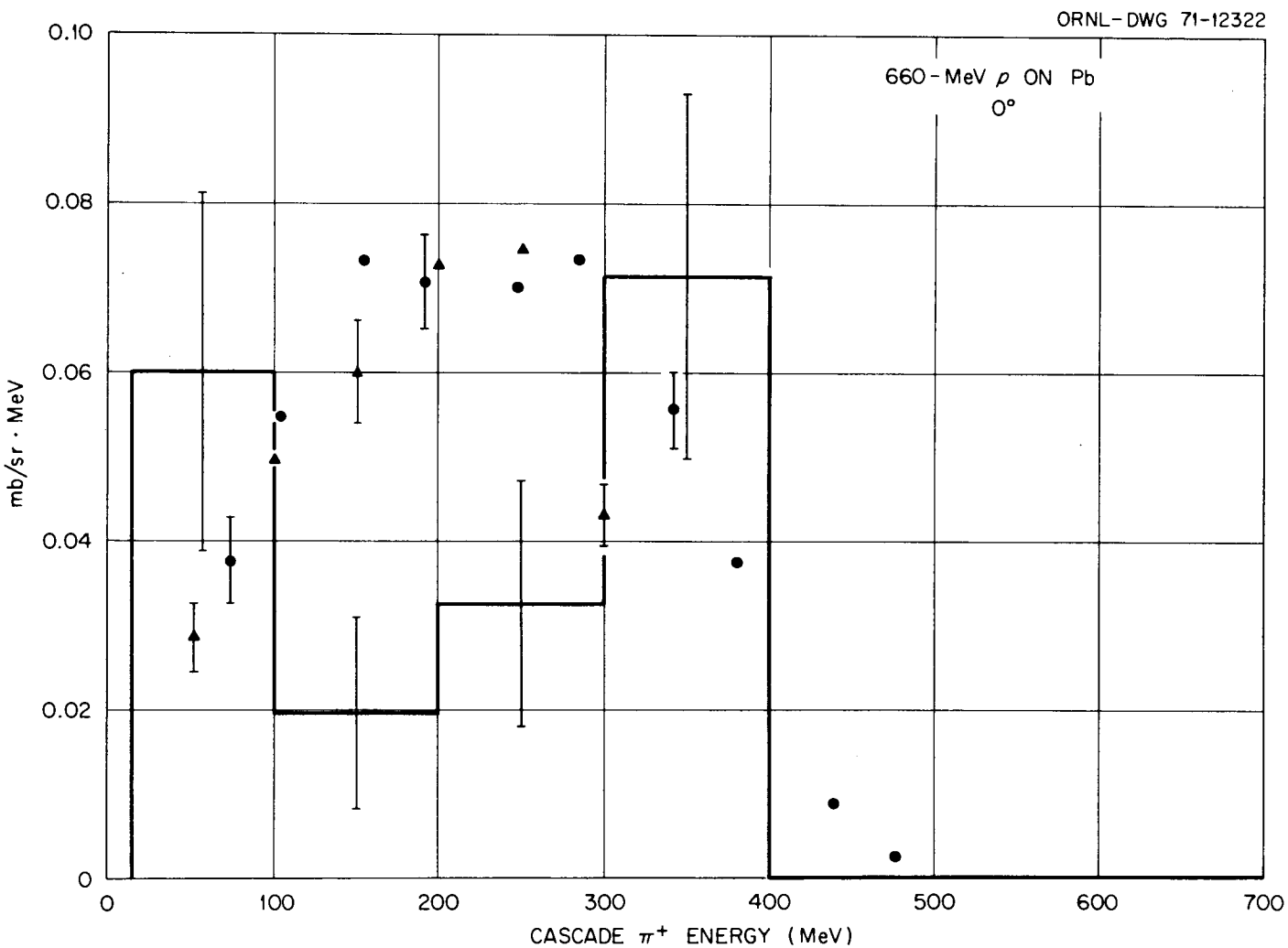

Fig. 27. Energy spectra of π^+ emitted at 0° from 660-MeV protons on lead. Experimental data of Haddock *et al.* and Hirt *et al.* (see Fig. 19 for references and symbols) and an angular interval of $0\text{-}20^\circ$ used for the theoretical results.

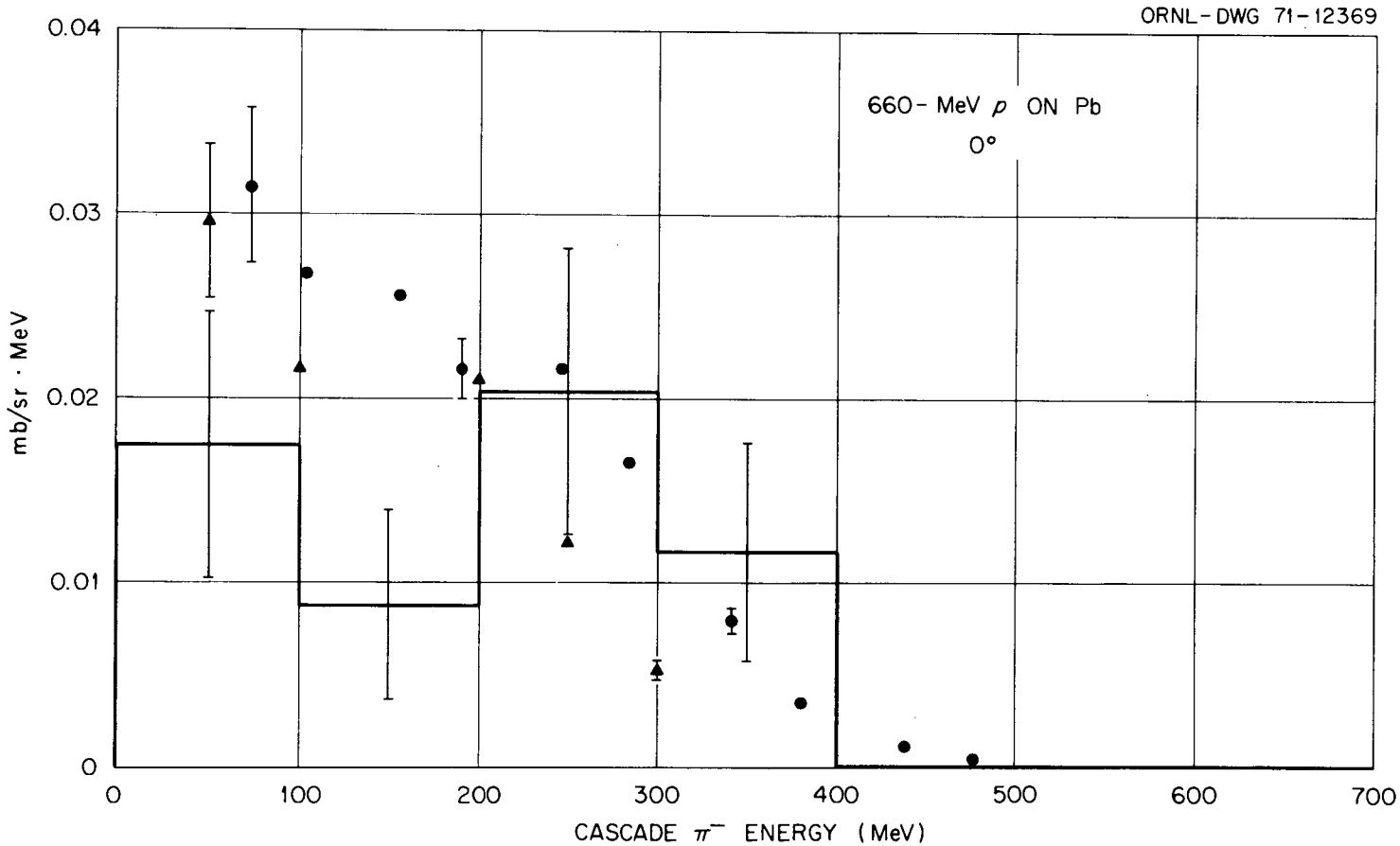

Fig. 28. Energy spectra of π^- emitted at 0° from 660-MeV protons on lead. Experimental data of Haddock *et al.* and Hirt *et al.* (see Fig. 19 for references and symbols) and an angular interval of $0\text{-}30^\circ$ used for the theoretical results.

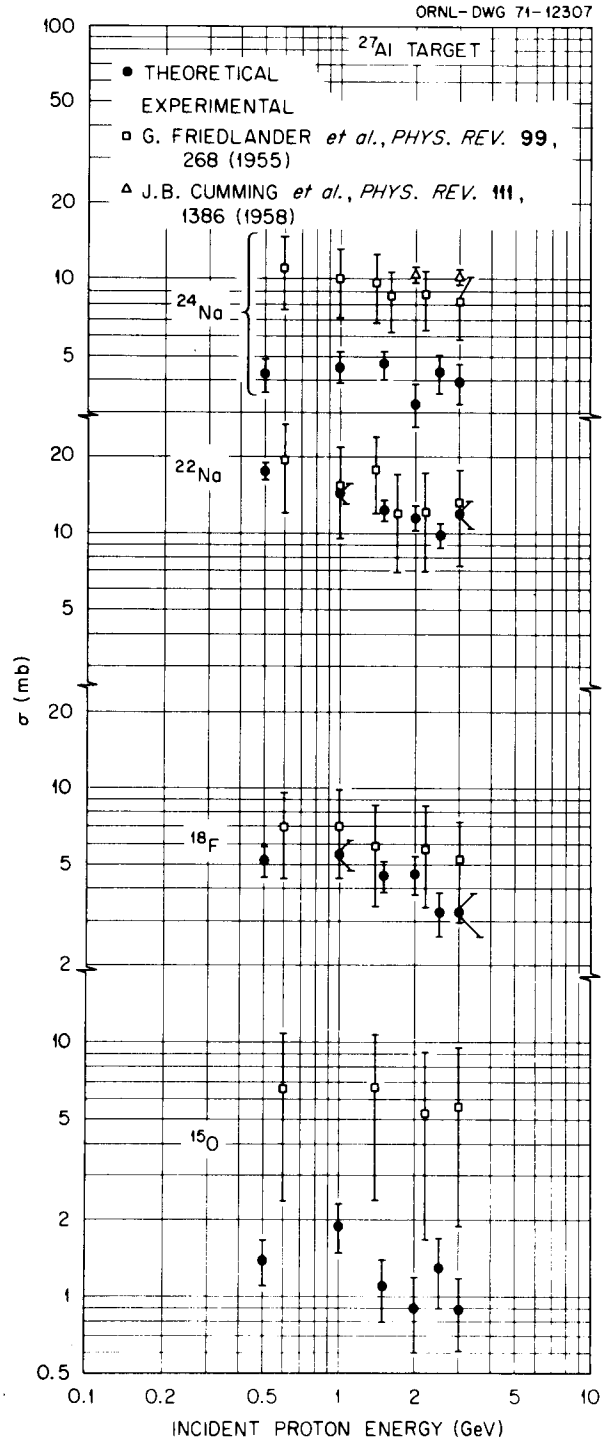

Fig. 29. Spallation cross sections for protons on aluminum.

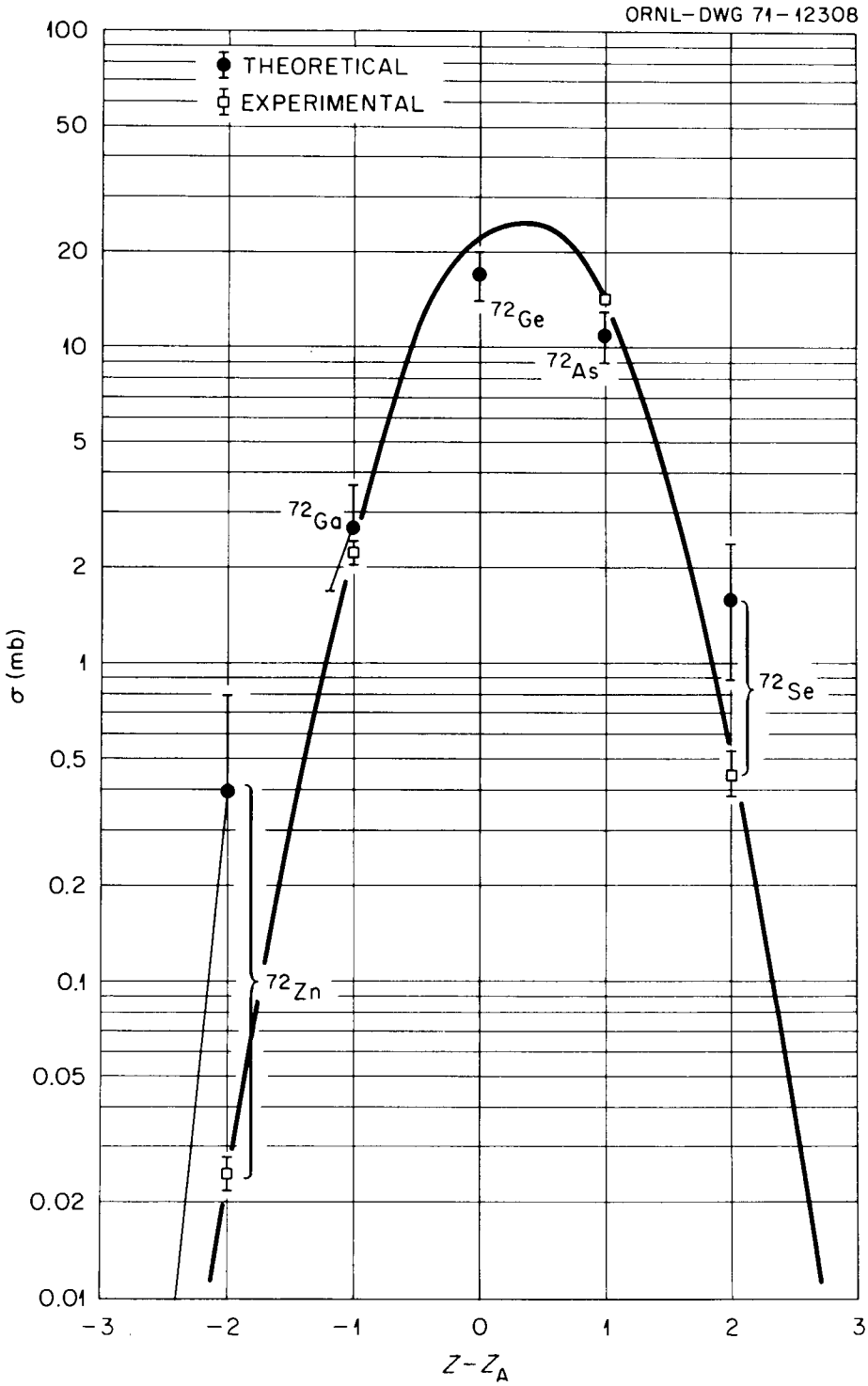

Fig. 30. Spallation cross sections for the isotopes of mass 72 from 2.9-GeV protons on arsenic. Experimental data are from Sheldon Kaufman, Phys. Rev. 126, 1189 (1962). The solid line, from Kaufman, is the Gaussian curve that best fits the experimental points. He takes $Z_A = 32$.

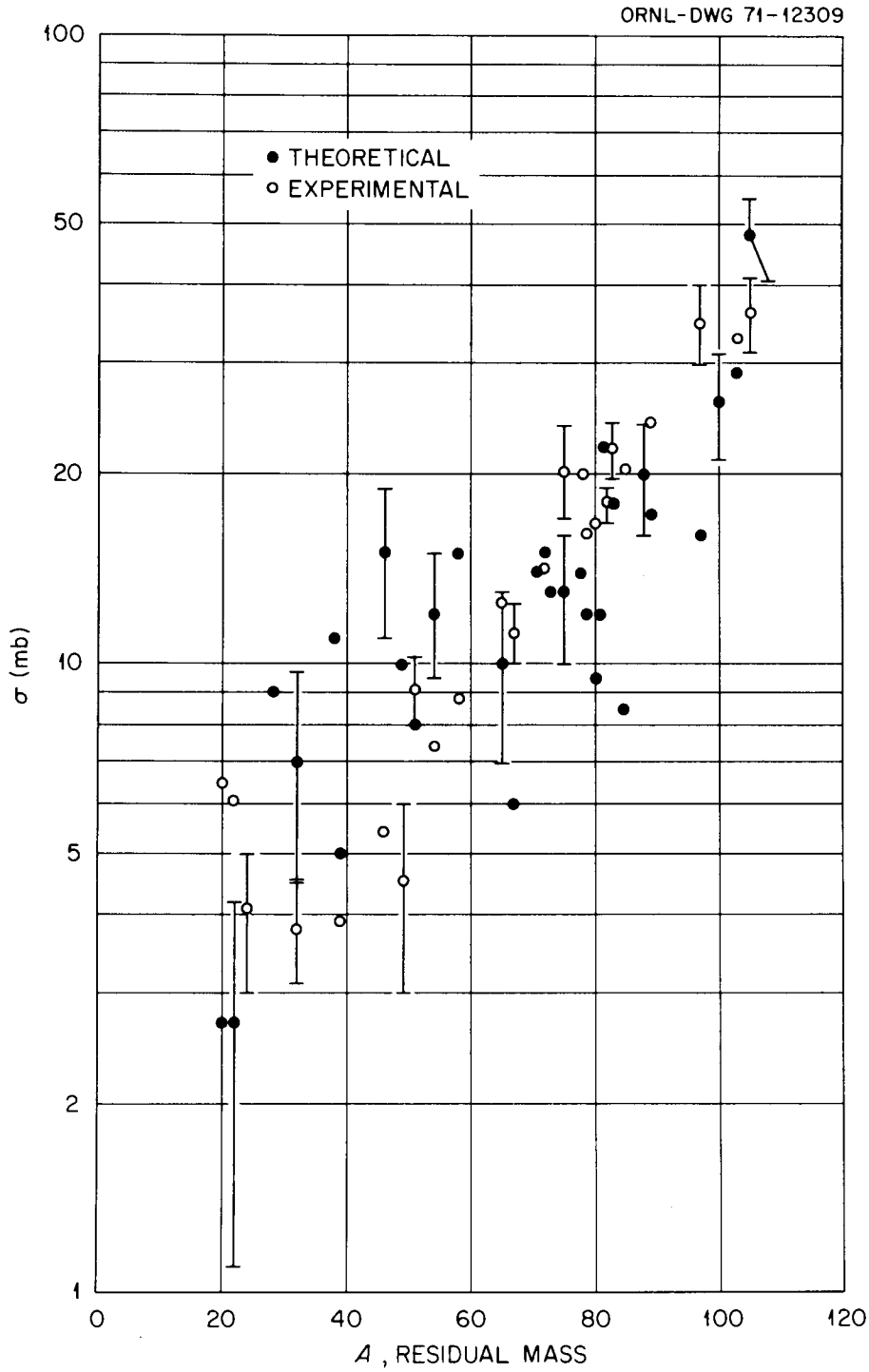

Fig. 31. Total mass yield from 3-GeV protons on silver. Experimental data are from S. Katcoff, H. R. Fickel, and A. Wyttenbach, Phys. Rev. 166, 1147 (1968), which include measured plus estimated yields. Only representative error bars are illustrated.

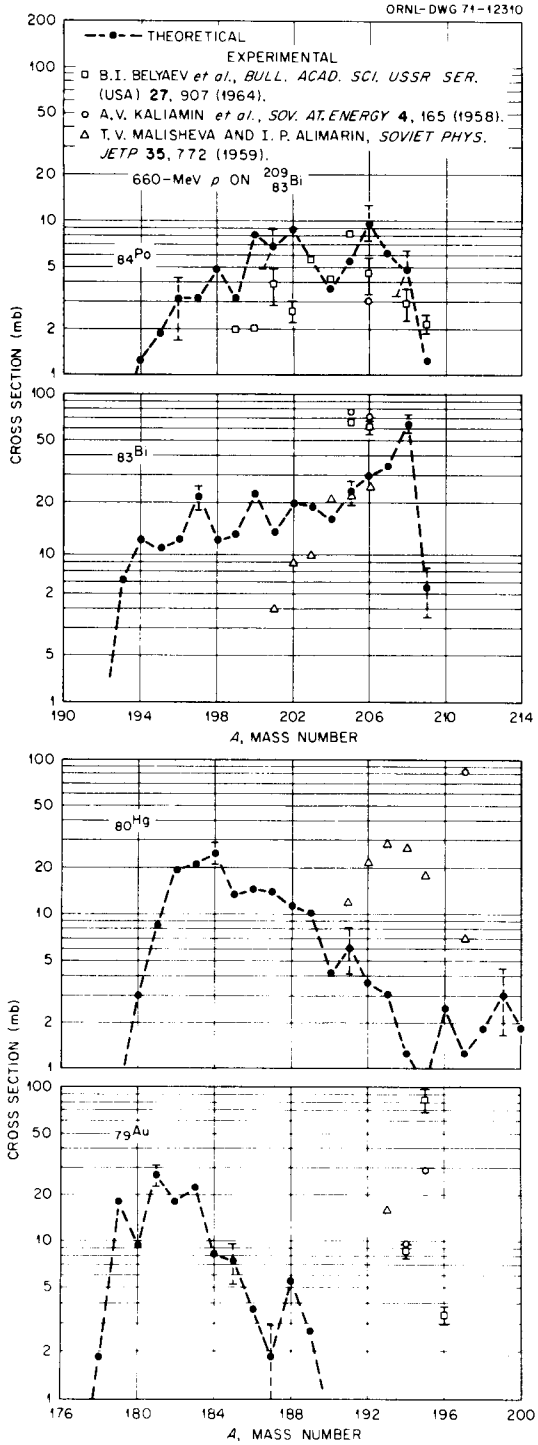

Fig. 32. Mass yield from 660-MeV protons on bismuth. The dashed lines connect the theoretical values where typical error bars are shown.

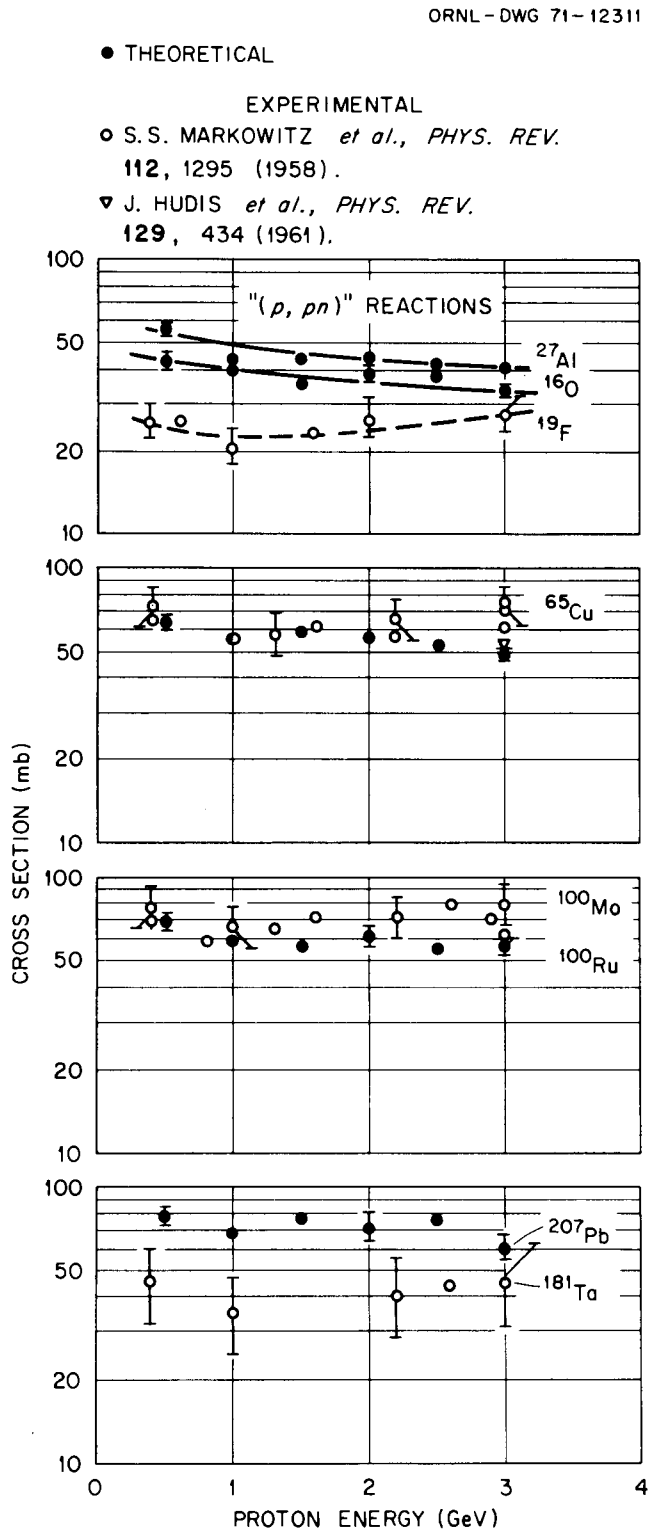

Fig. 33. Reactions of the type (p,pn) for protons on the targets illustrated. The solid and dashed curves are drawn through the data merely to guide the eye.

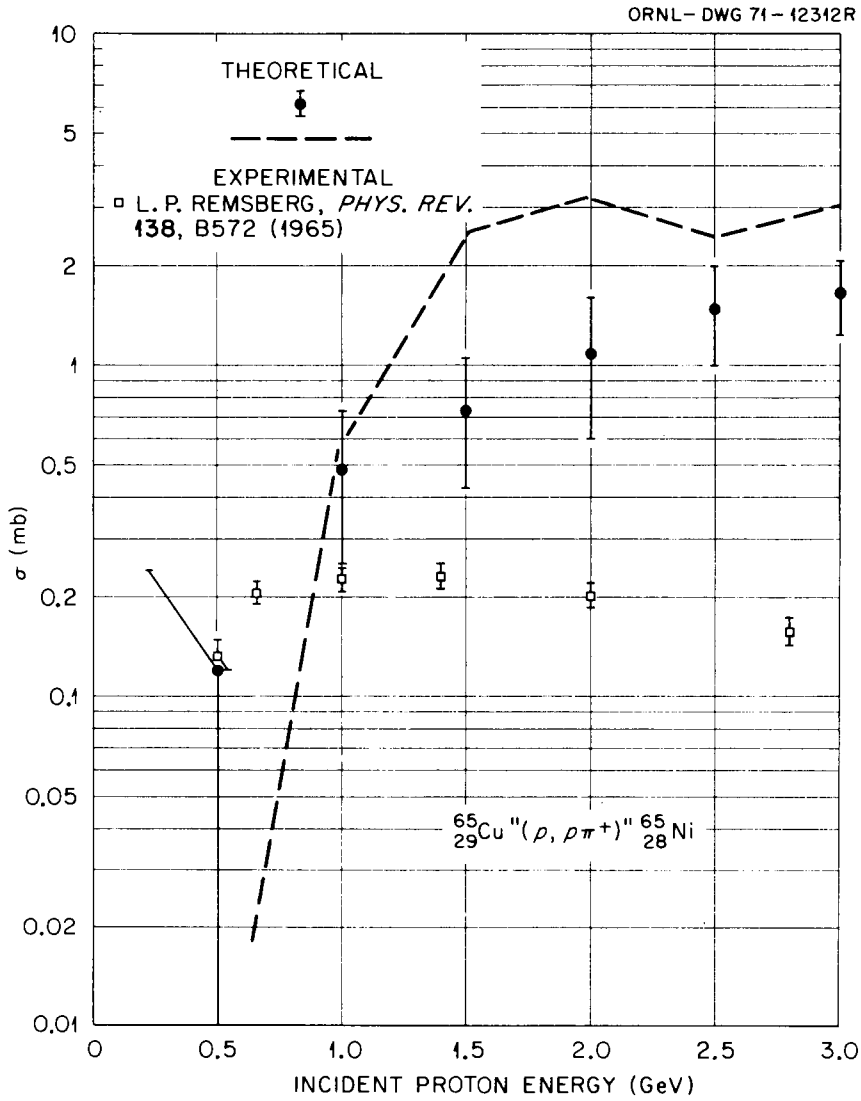

Fig. 34. Reaction of the type $(p,p\pi^+)$ for protons on ^{65}Cu. The dashed line connects theoretical values calculated with an exclusion principle bypass, as described in the text. The solid circles are the theoretical values for the unmodified calculation.

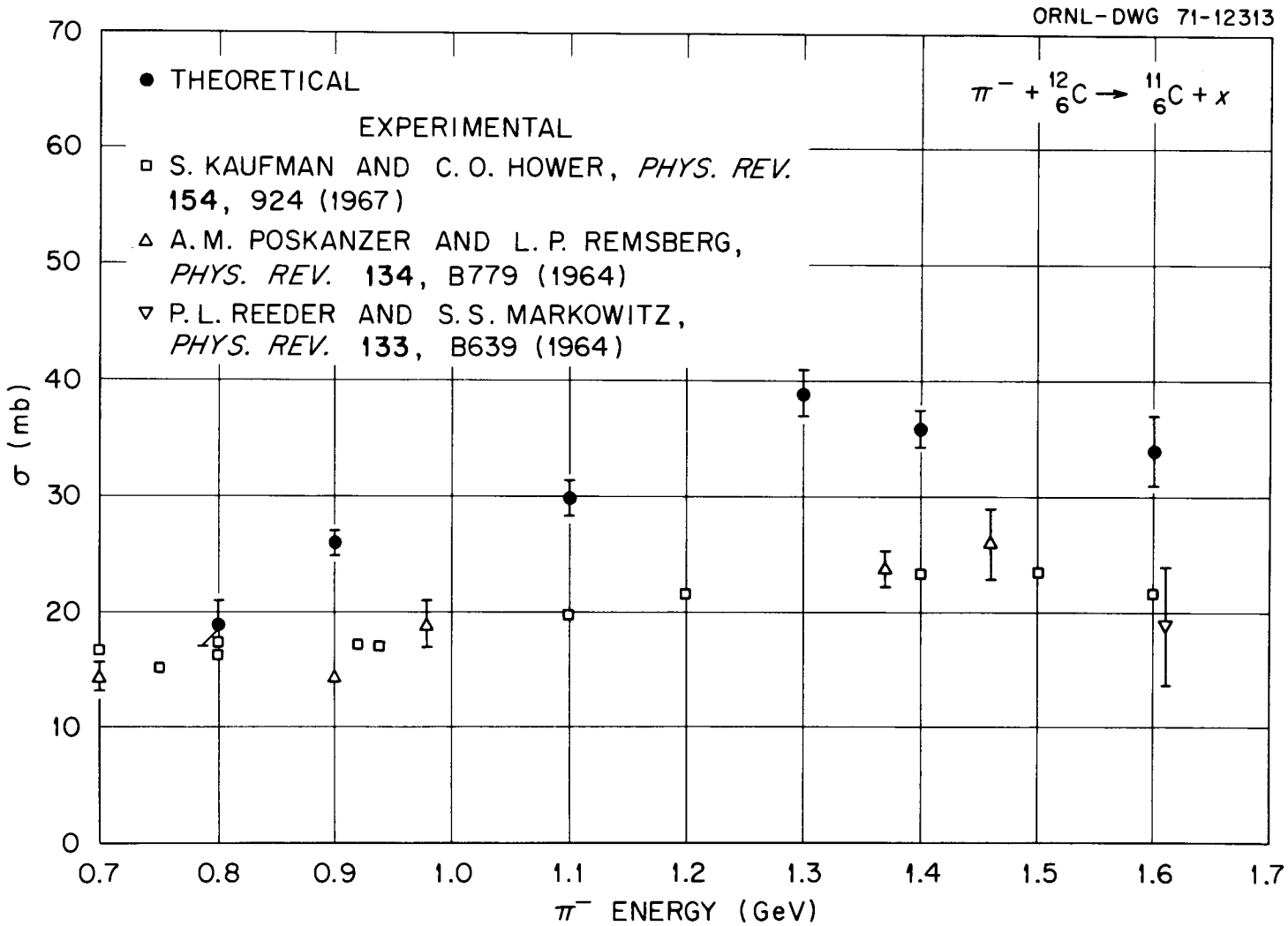

Fig. 35. Cross sections for the production of ^{11}C from incident π^--mesons. The experimental error in the data of Kaufman and Hower is about the size of the symbols.

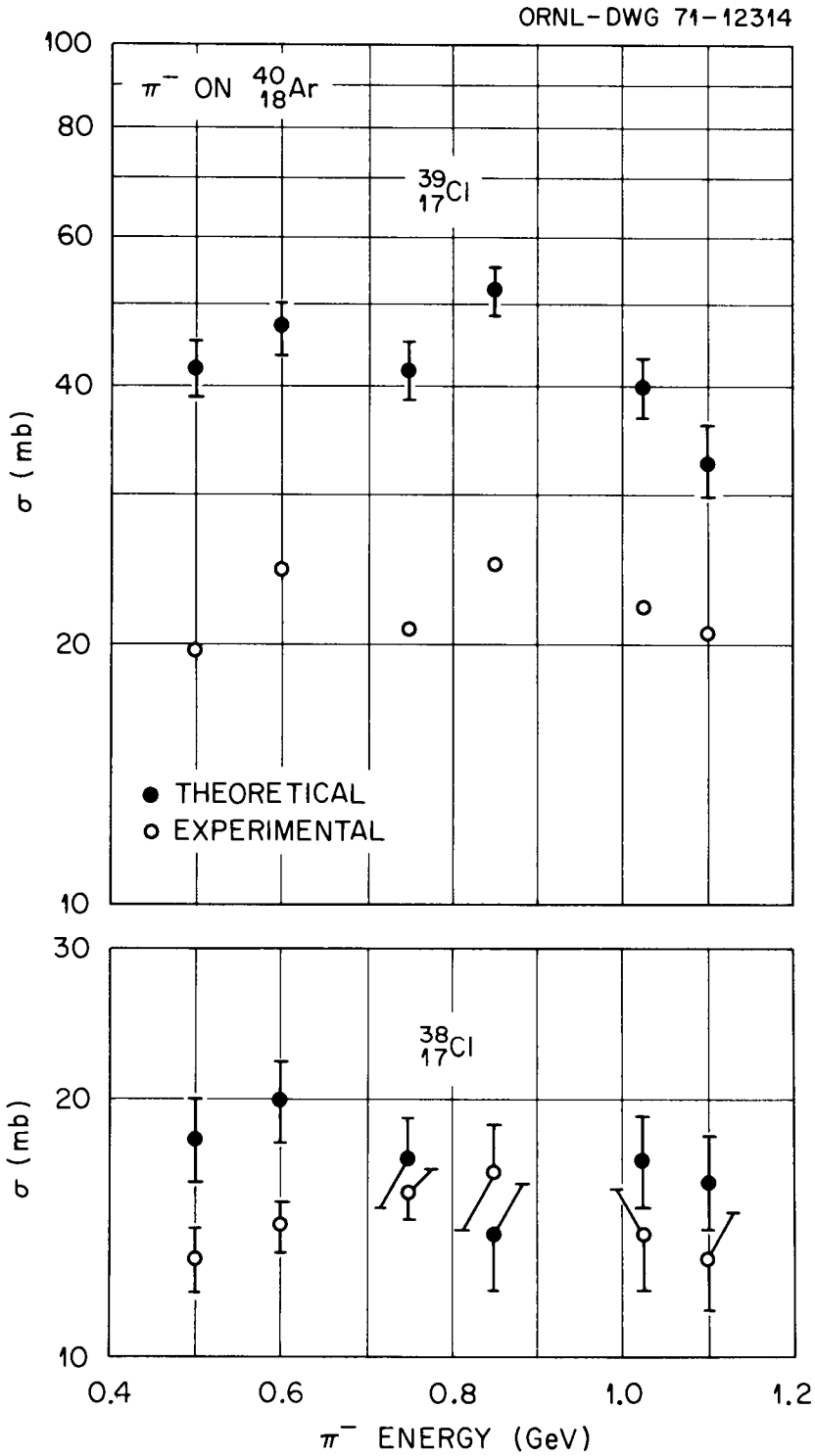

Fig. 36. Cross sections for producing ^{39}Cl and ^{38}Cl from π^- reactions with argon. The experimental data are from C. O. Hower and S. Kaufman, Phys. Rev. 144, 917 (1966). The experimental error, where not illustrated, is smaller than the symbols.

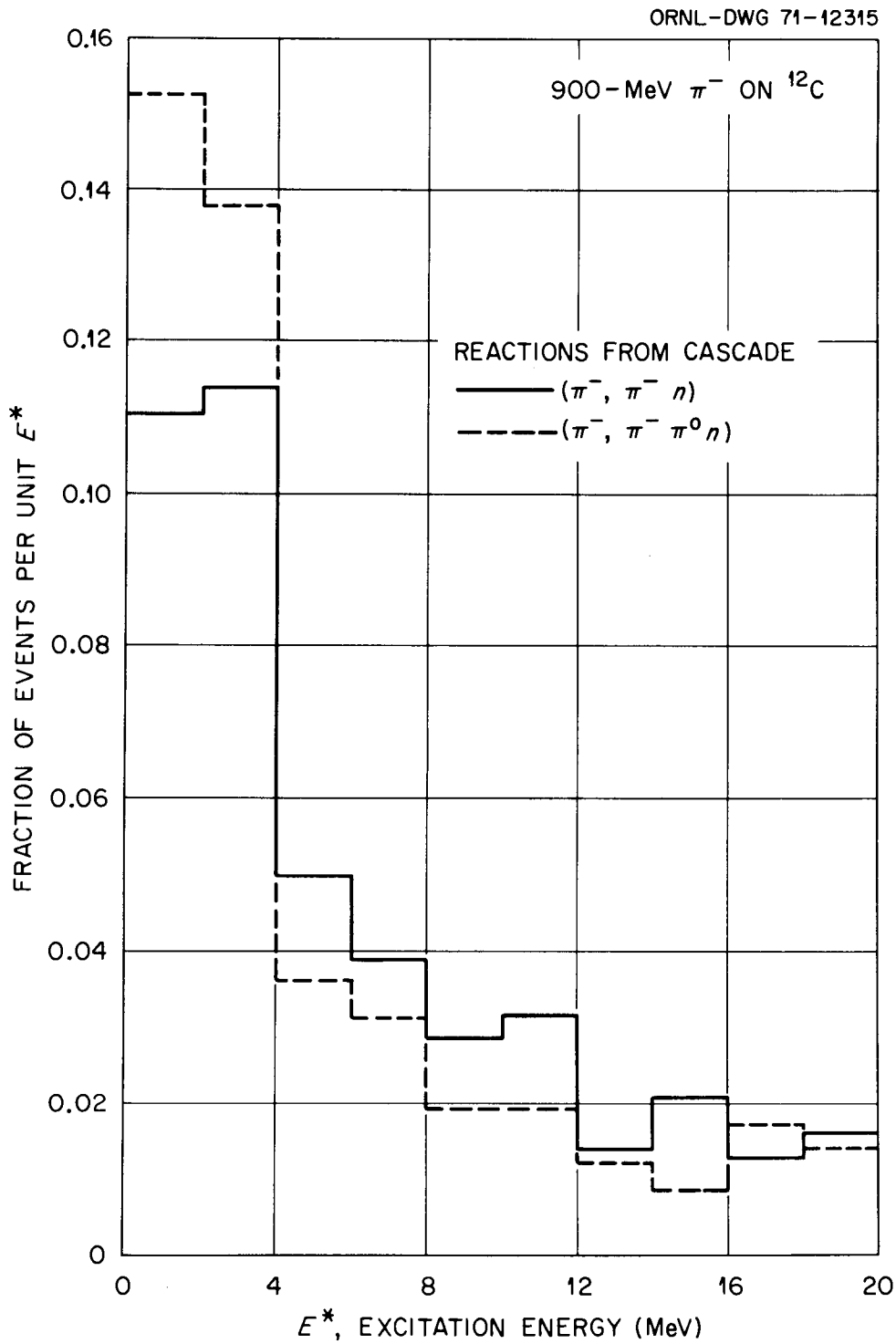

Fig. 37. Calculated excitation energy distributions following the cascade for the reactions indicated from 900-MeV π^- on ^{12}C.

APPENDIX

The Appendix contains the figures discussed, but not illustrated, in the text. To facilititate the reader's locating specific graphs, a brief table of contents is given here.

Fig. Nos.	Contents	Page Nos.
38 - 41	The quantities k_o, ρ, $\sigma(\pi^- + p \rightarrow \pi^- + p + \pi^o)$, and a vs energy.	95 - 98
42 - 46	Comparisons of the proton spectra from the calculation described in Ref. 5 (MECC-3) with those from the calculation described in this paper (MECC-7).	99 - 103
47 - 56	π^+, π^-, and neutron spectra from protons at various energies on beryllium.	104 - 113
57 - 65	π^+ and π^- spectra from protons on carbon.	114 - 122
66 - 68	π^+ and π^- spectra from protons on copper.	123 - 125
69 - 73	π^+ and π^- spectra from protons on lead.	126 - 130
74	Spallation yields from protons on carbon.	131
75a-c	Spallation yields from protons on iodine.	132 - 134

ORNL DWG. 72-4379

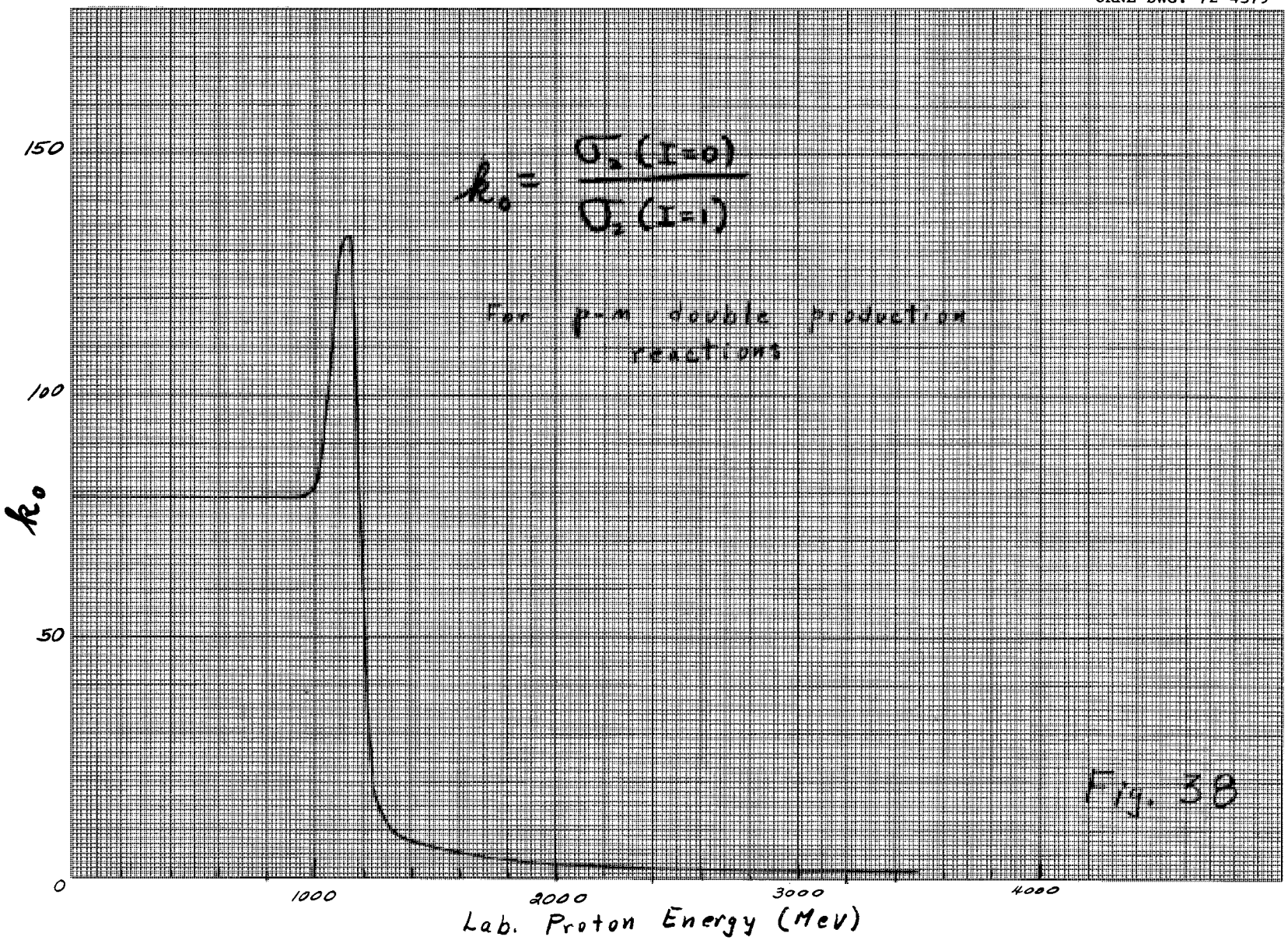

Fig. 38

ORNL DWG. 72-4380

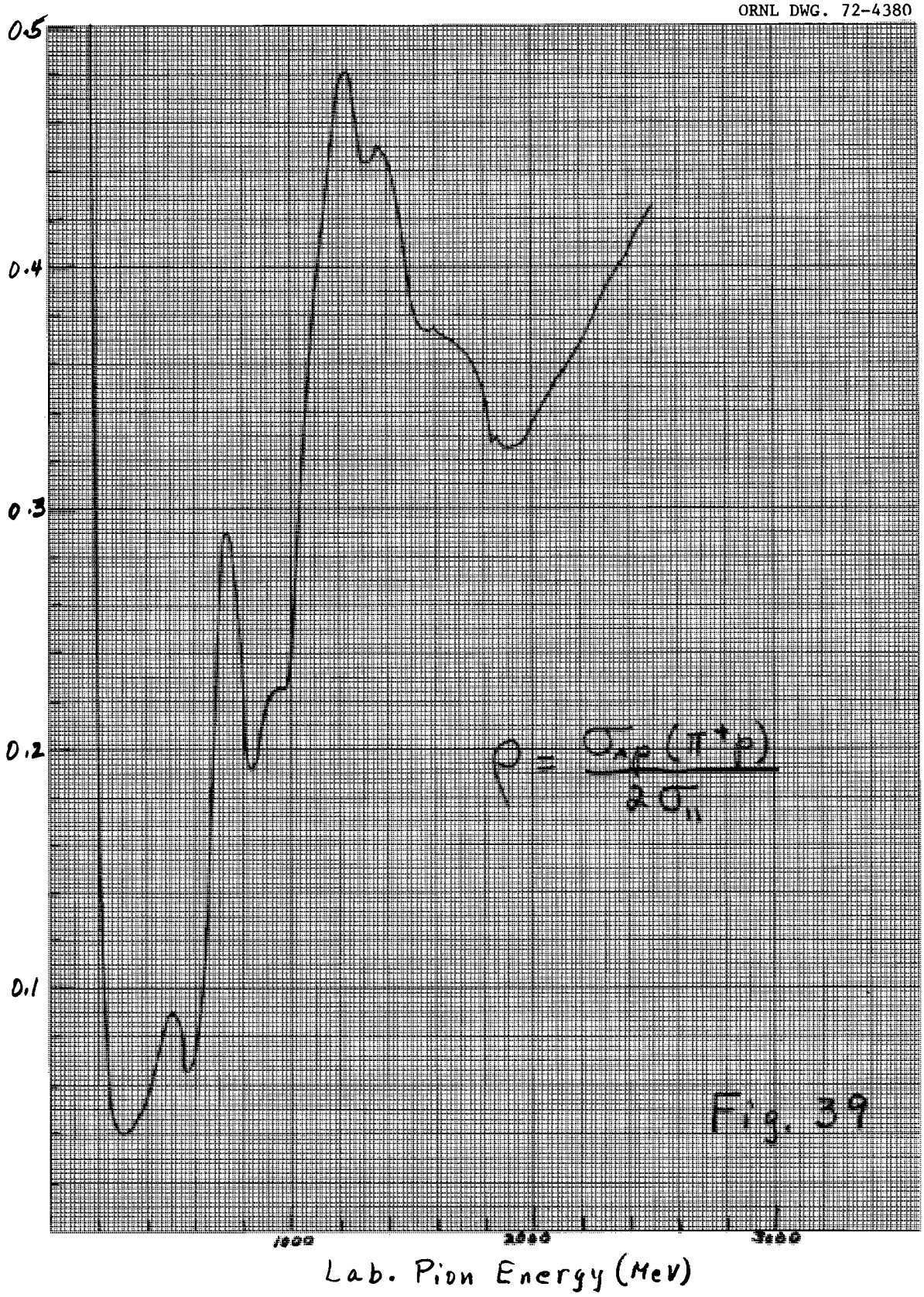

ORNL DWG. 72-4381

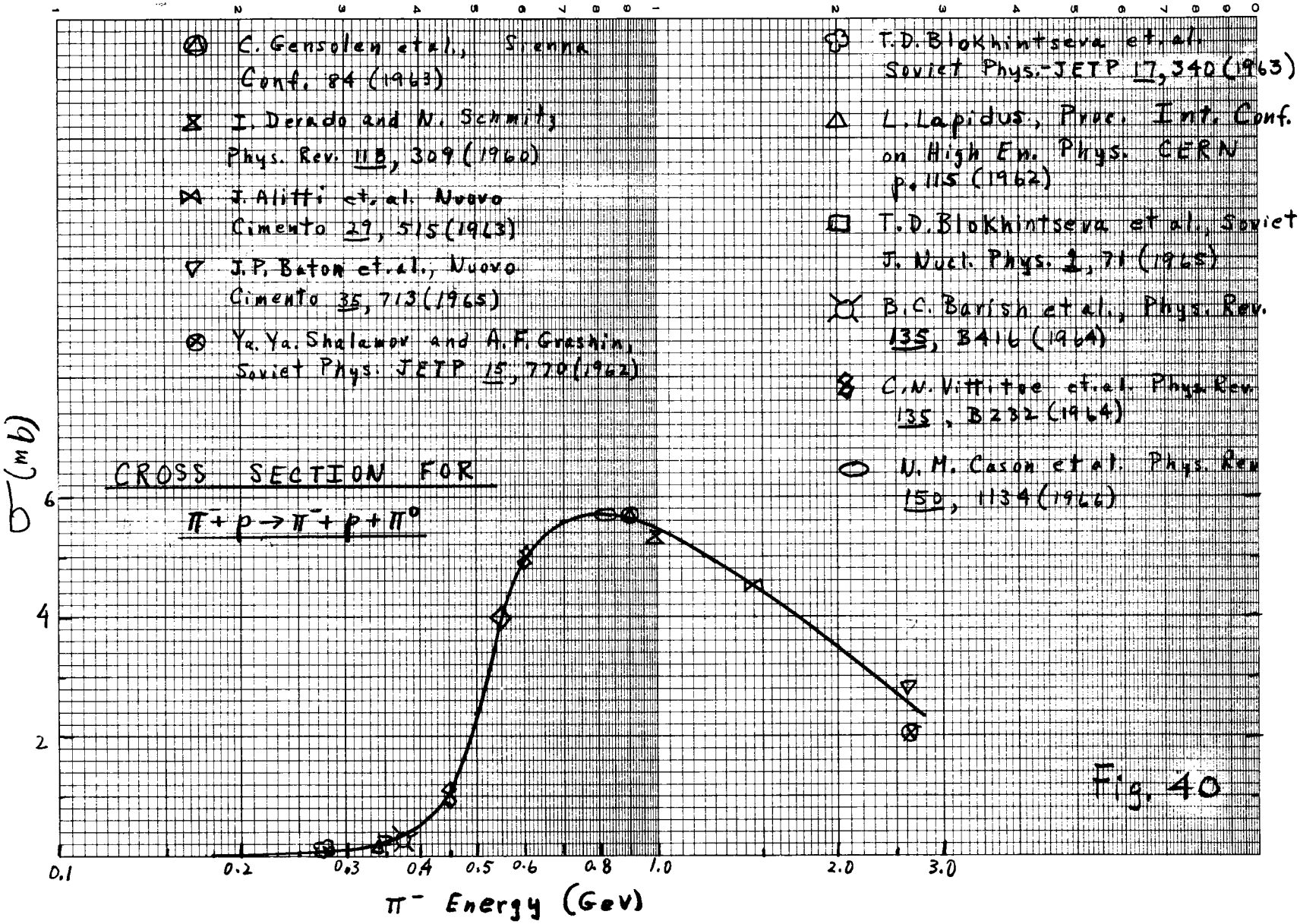

Fig. 40

ORNL DWG. 72-4382

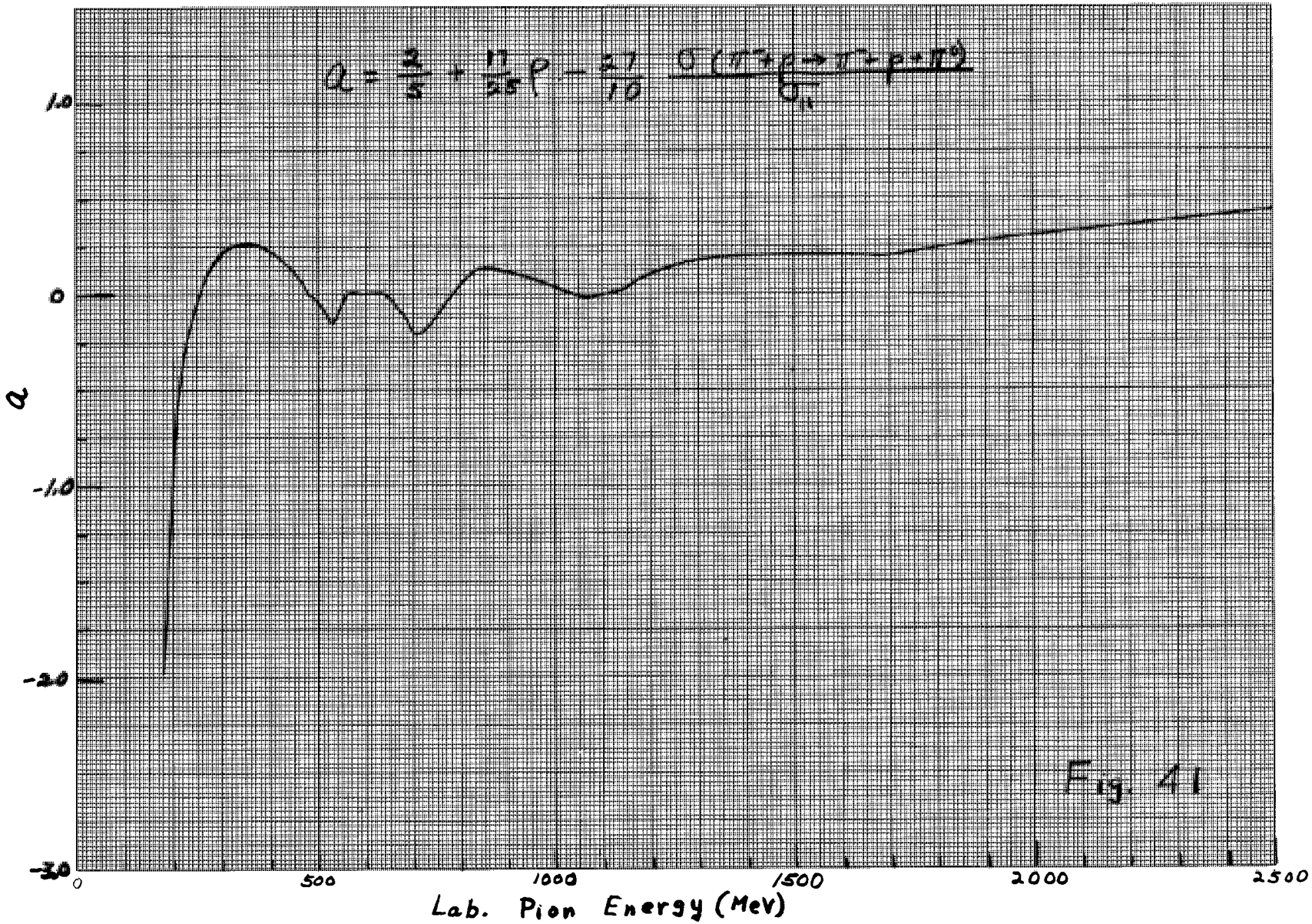

Fig. 41

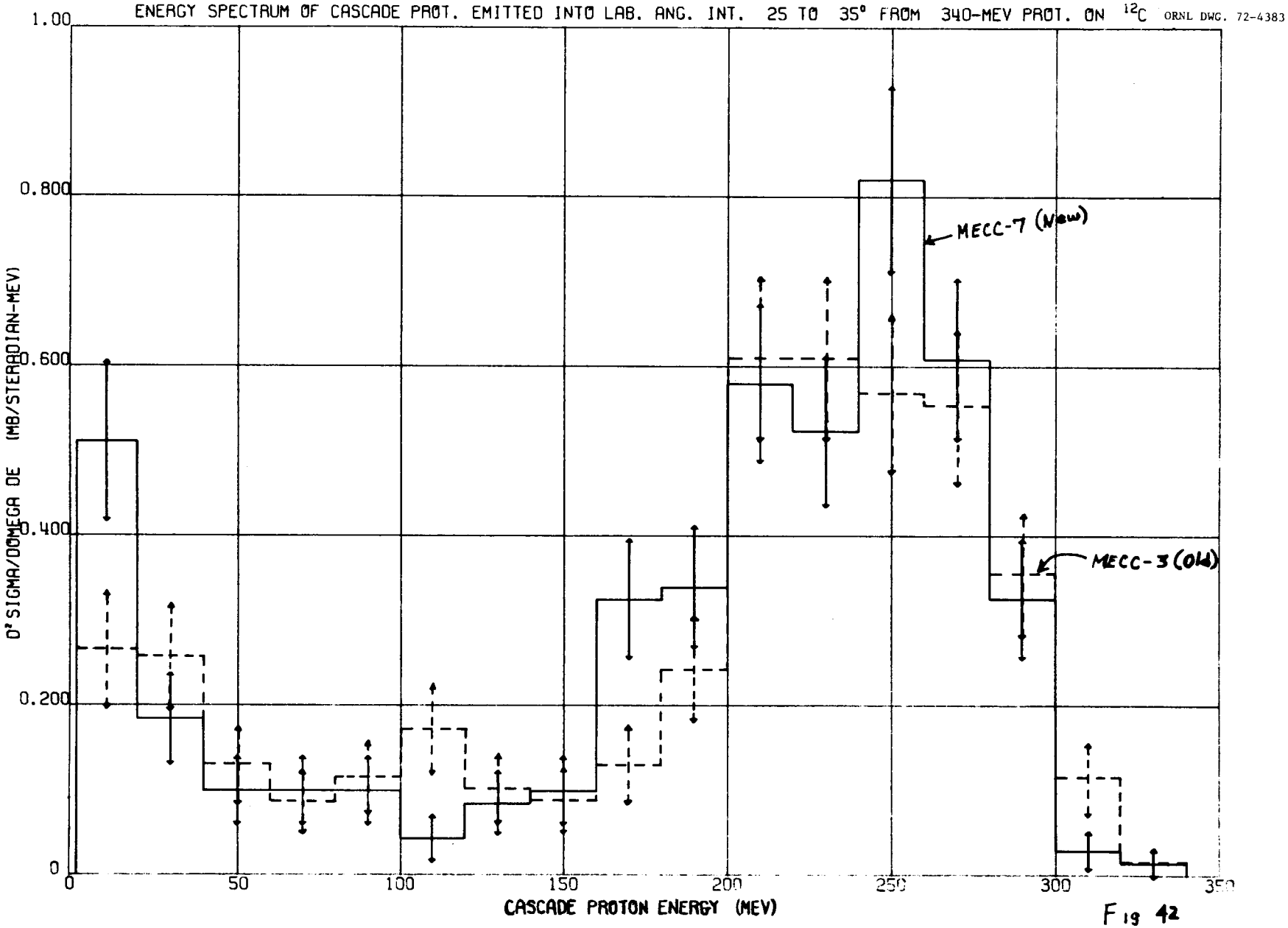
ENERGY SPECTRUM OF CASCADE PROT. EMITTED INTO LAB. ANG. INT. 25 TO 35° FROM 340-MEV PROT. ON ^{12}C
ORNL DWG. 72-4383
D²SIGMA/DOMEGA DE (MB/STERADIAN-MEV)
1.00
0.800
0.600
0.400
0.200
0
0
50
100
150
200
250
300
350
CASCADE PROTON ENERGY (MEV)
MECC-7 (New)
MECC-3 (Old)

Fig 42

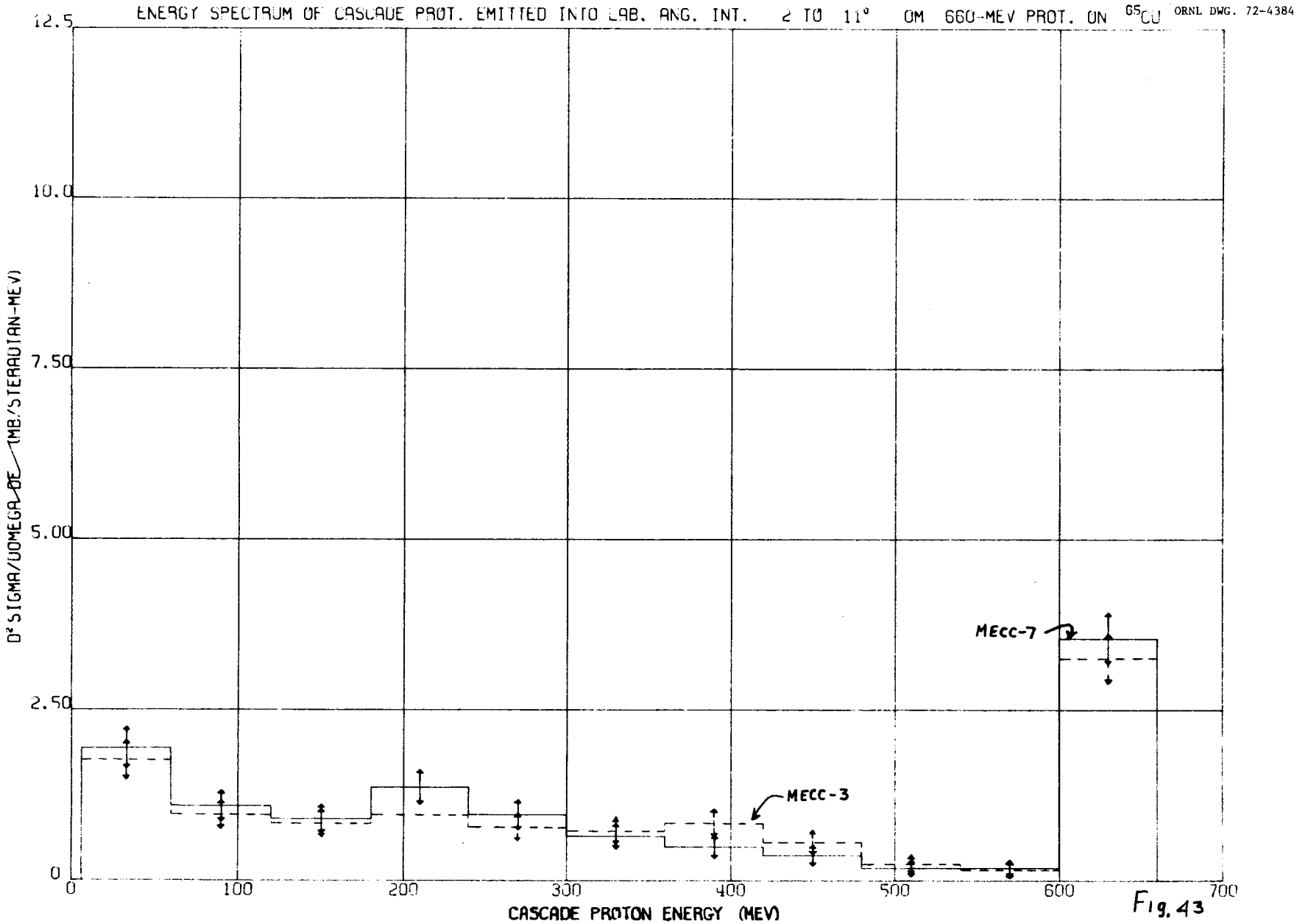
ENERGY SPECTRUM OF CASCADE PROT. EMITTED INTO LAB. ANG. INT. 2 TO 11° ON 660-MEV PROT. ON ^{65}CU
ORNL DWG. 72-4384
D²SIGMA/DOMEGA DE (MB/STERADIAN-MEV)
12.5
10.0
7.50
5.00
2.50
0
0
100
200
300
400
500
600
700
CASCADE PROTON ENERGY (MEV)
MECC-7
MECC-3

Fig. 43

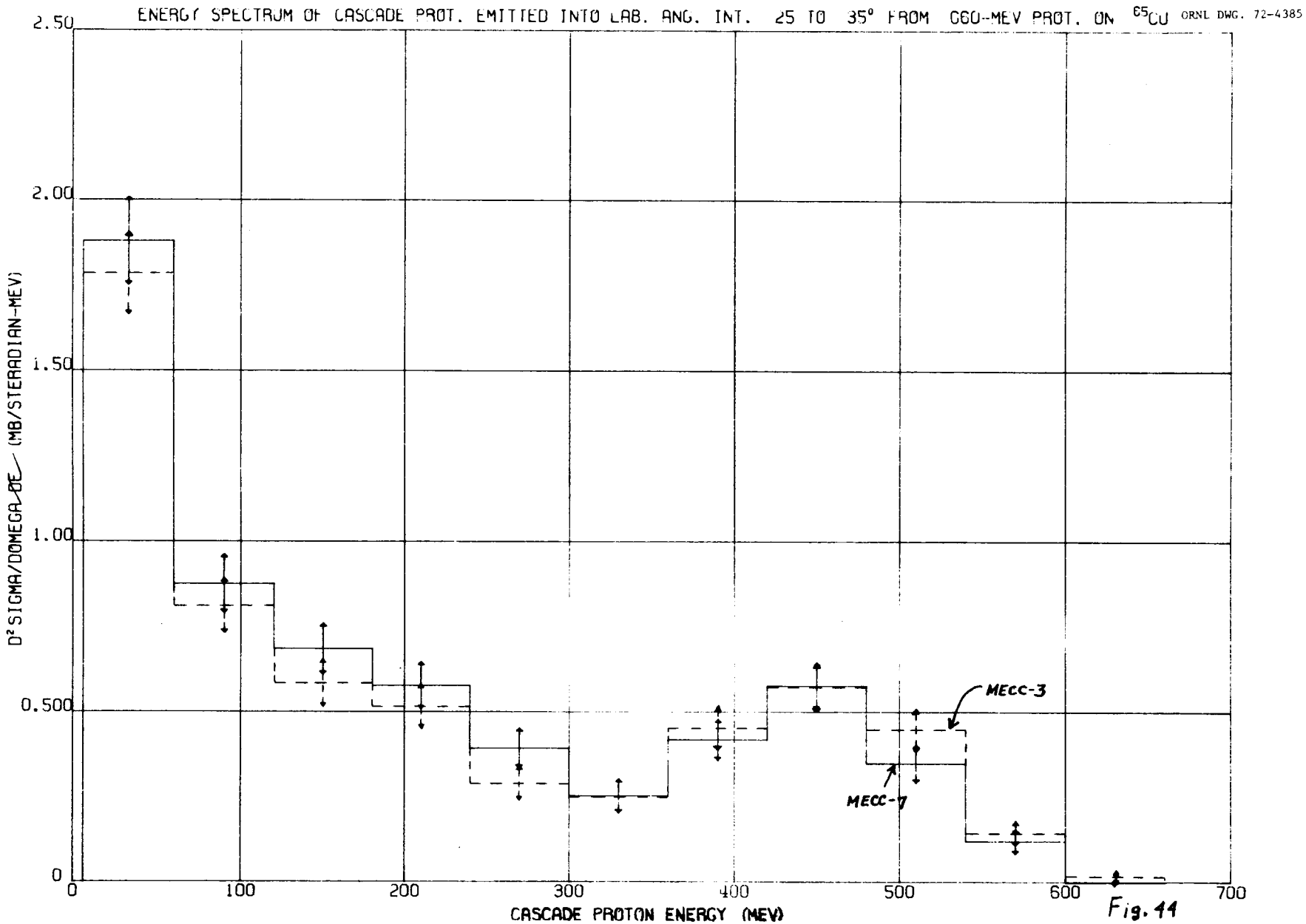
ENERGY SPECTRUM OF CASCADE PROT. EMITTED INTO LAB. ANG. INT. 25 TO 35° FROM 660-MEV PROT. ON ^{65}CU
ORNL DWG. 72-4385
D²SIGMA/DOMEGA-DE (MB/STERADIAN-MEV)
2.50
2.00
1.50
1.00
0.500
0
0
100
200
300
400
500
600
700
CASCADE PROTON ENERGY (MEV)
MECC-3
MECC-7

Fig. 44

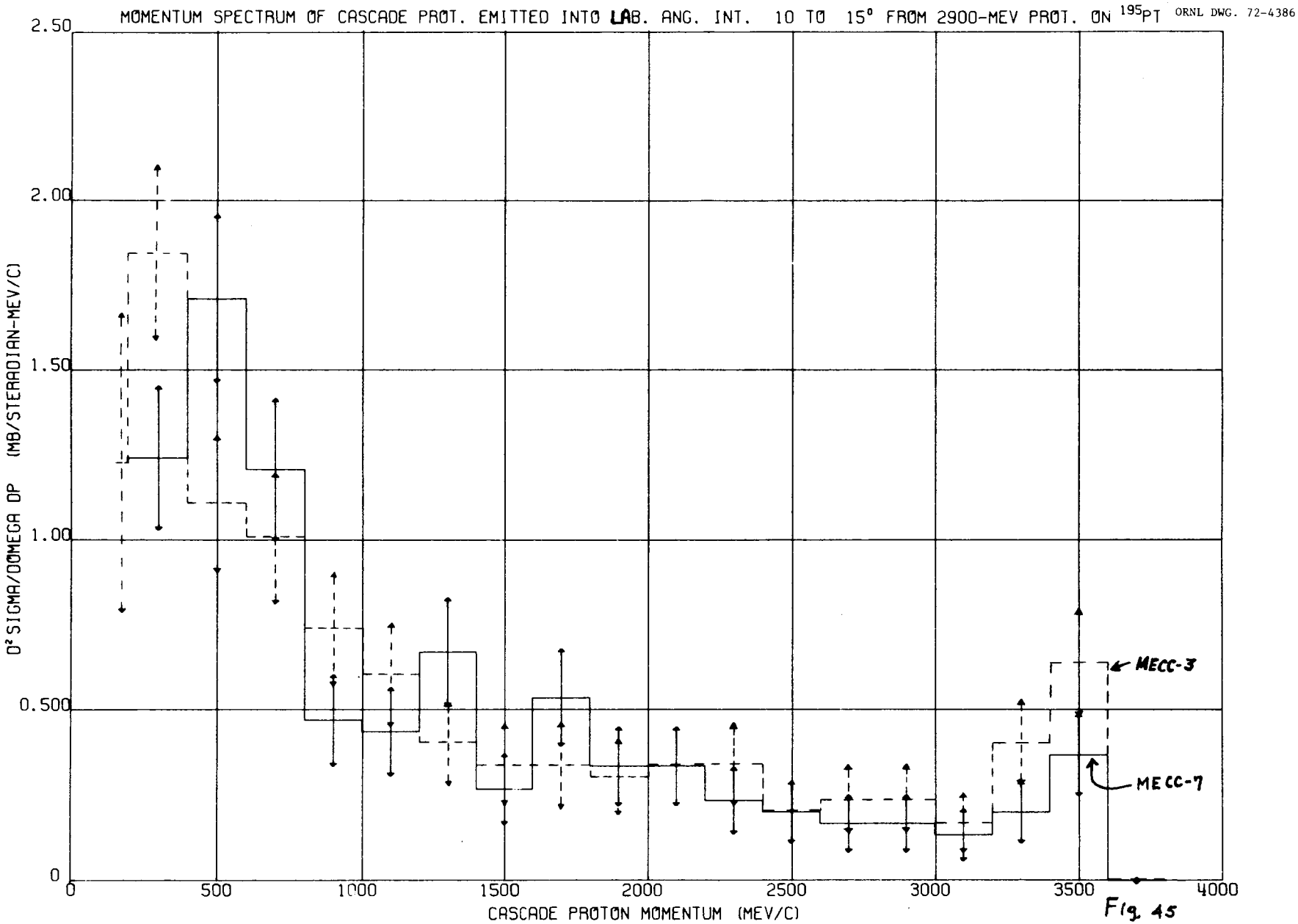
MOMENTUM SPECTRUM OF CASCADE PROT. EMITTED INTO LAB. ANG. INT. 10 TO 15° FROM 2900-MEV PROT. ON 195PT
ORNL DWG. 72-4386
D²SIGMA/DOMEGA DP (MB/STERADIAN-MEV/C)
2.50
2.00
1.50
1.00
0.500
0
0
500
1000
1500
2000
2500
3000
3500
4000
CASCADE PROTON MOMENTUM (MEV/C)
MECC-3
MECC-7

Fig. 45

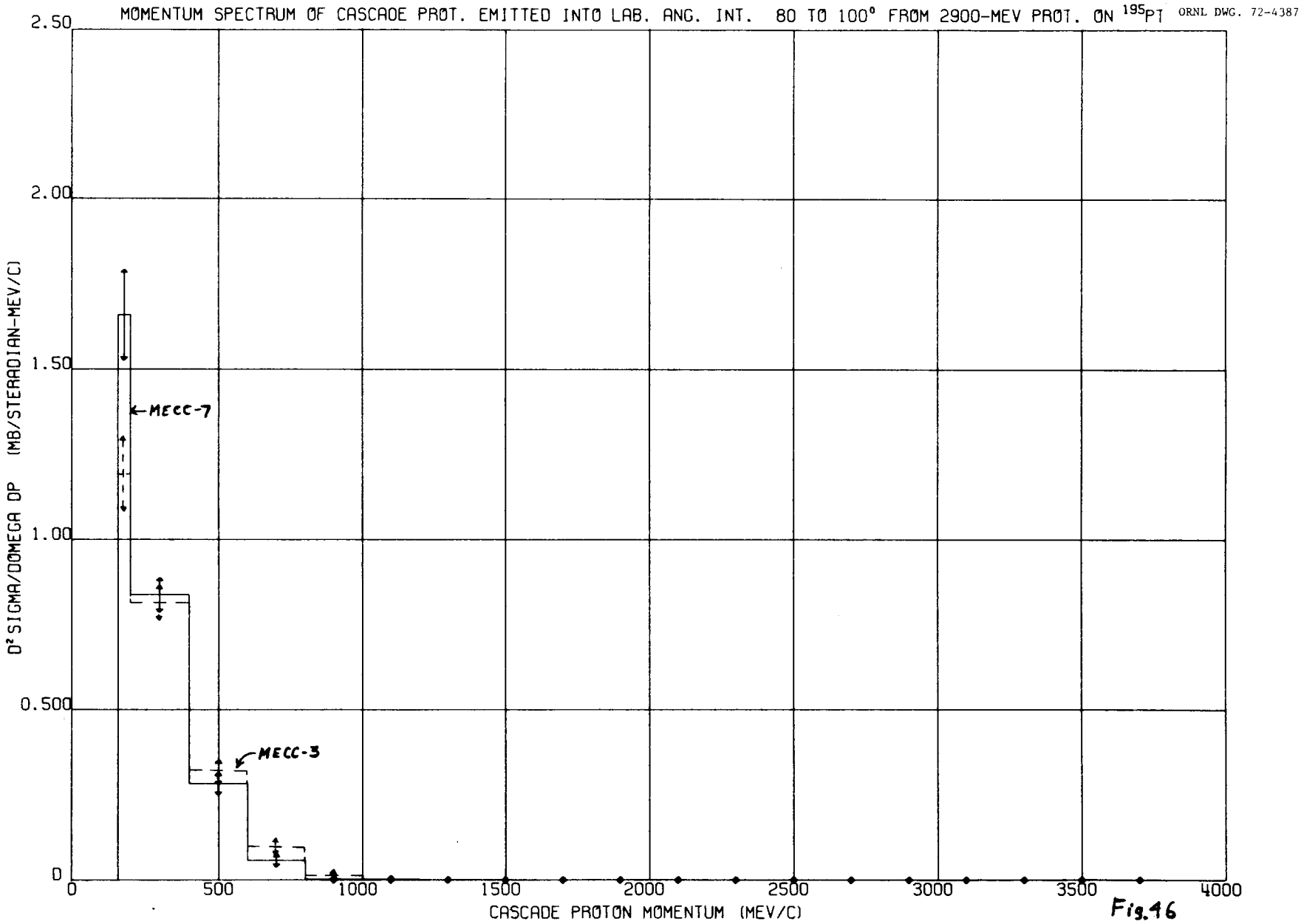
MOMENTUM SPECTRUM OF CASCADE PROT. EMITTED INTO LAB. ANG. INT. 80 TO 100° FROM 2900-MEV PROT. ON 195PT
ORNL DWG. 72-4387
D²SIGMA/DOMEGA DP (MB/STERADIAN-MEV/C)
2.50
2.00
1.50
1.00
0.500
0
MECC-7
MECC-3
0
500
1000
1500
2000
2500
3000
3500
4000
CASCADE PROTON MOMENTUM (MEV/C)

Fig. 46

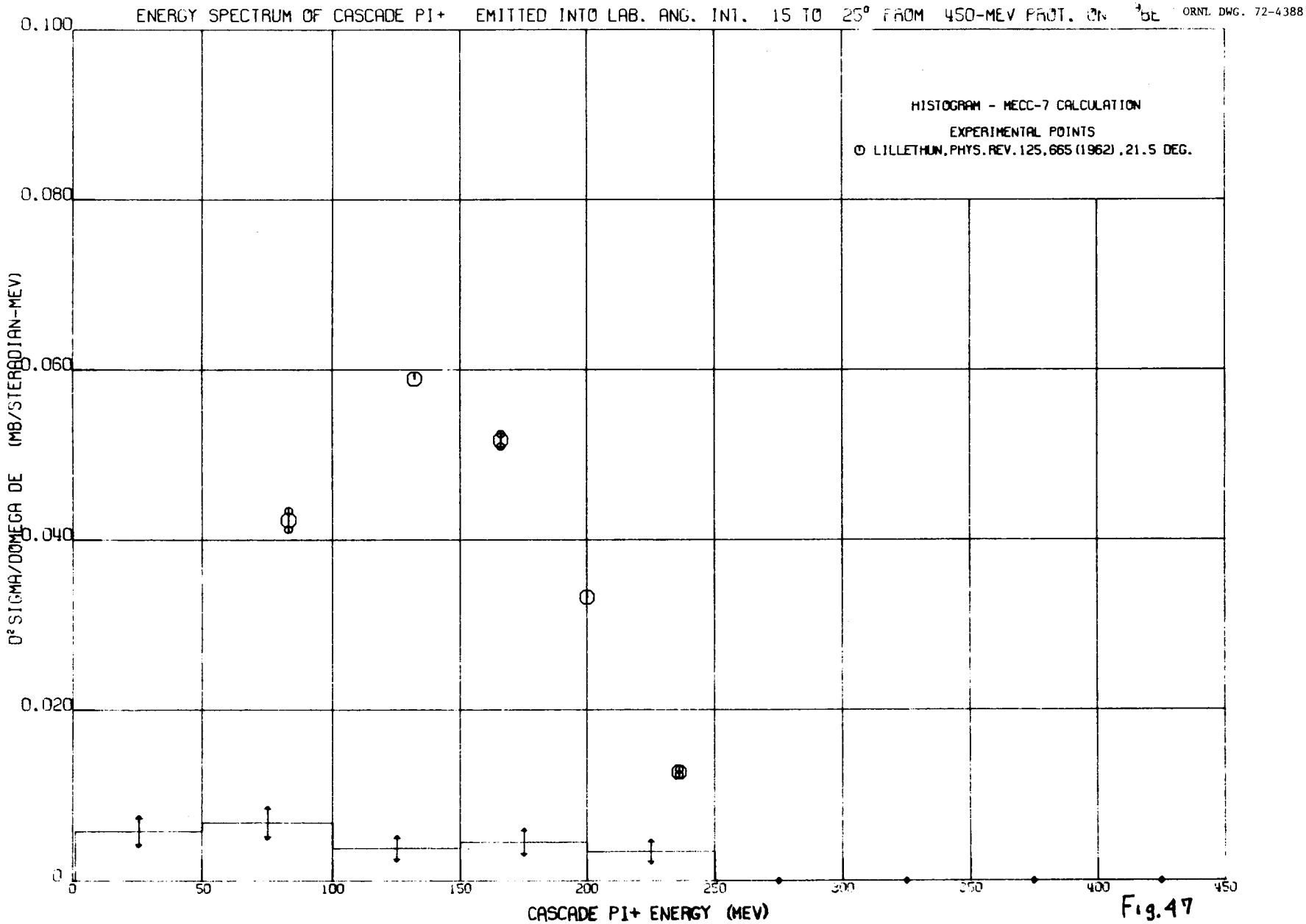
ENERGY SPECTRUM OF CASCADE PI+ EMITTED INTO LAB. ANG. INT. 15 TO 25° FROM 450-MEV PROT. ON
ORNL DWG. 72-4388
HISTOGRAM - MECC-7 CALCULATION
EXPERIMENTAL POINTS
LILLETHUN, PHYS. REV. 125, 665 (1962), 21.5 DEG.
D²SIGMA/DOMEGA DE (MB/STERADIAN-MEV)
0.100
0.080
0.060
0.040
0.020
0
0
50
100
150
200
250
300
350
400
450
CASCADE PI+ ENERGY (MEV)

Fig. 47

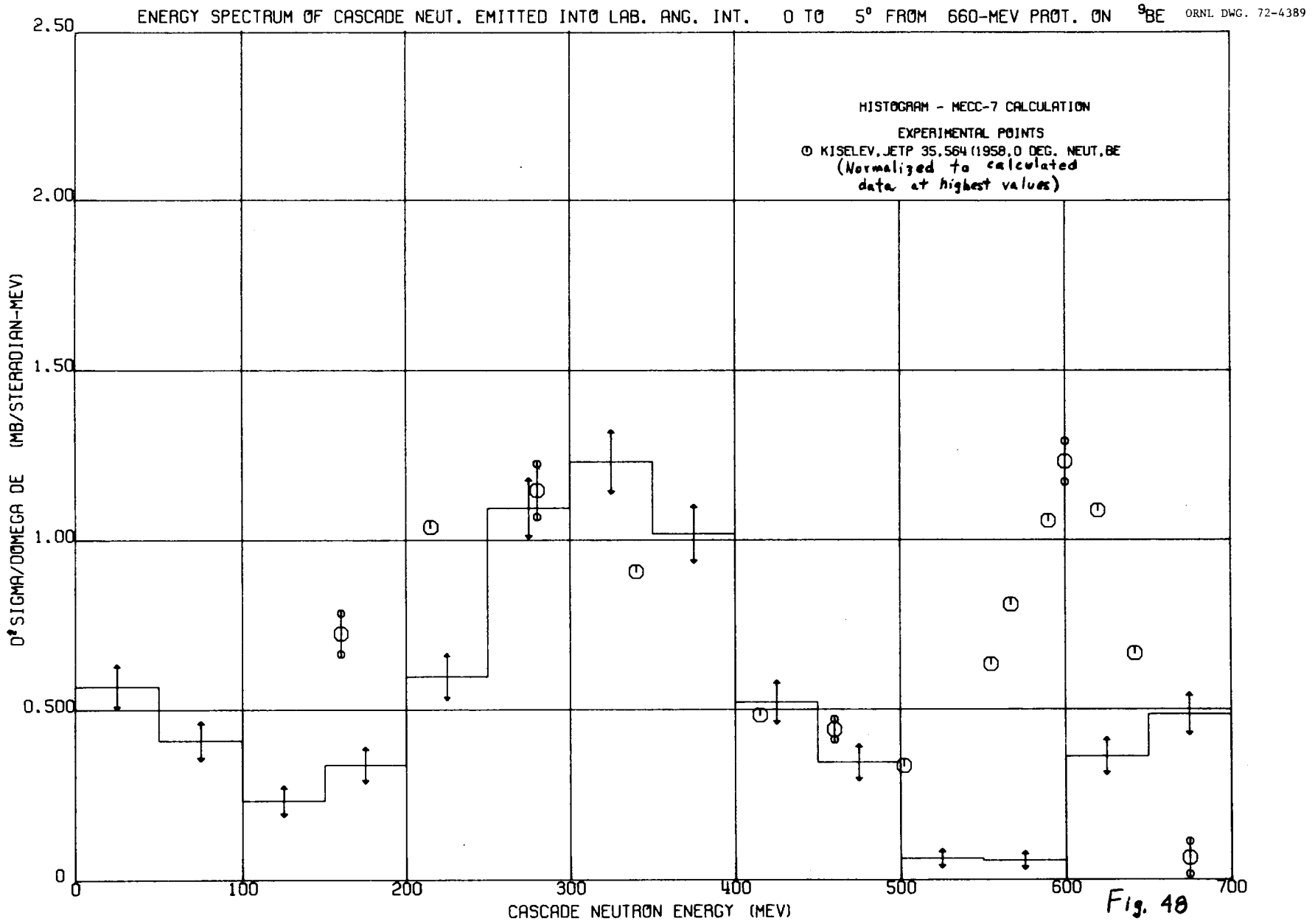
ENERGY SPECTRUM OF CASCADE NEUT. EMITTED INTO LAB. ANG. INT. 0 TO 5° FROM 660-MEV PROT. ON ^{9}BE
ORNL DWG. 72-4389
HISTOGRAM - MECC-7 CALCULATION
EXPERIMENTAL POINTS
KISELEV, JETP 35, 564 (1958, 0 DEG. NEUT, BE
(Normalized to calculated data at highest values)
D²SIGMA/DOMEGA DE (MB/STERADIAN-MEV)
2.50
2.00
1.50
1.00
0.500
0
0
100
200
300
400
500
600
700
CASCADE NEUTRON ENERGY (MEV)

Fig. 48

ORNL DWG. 72-4390

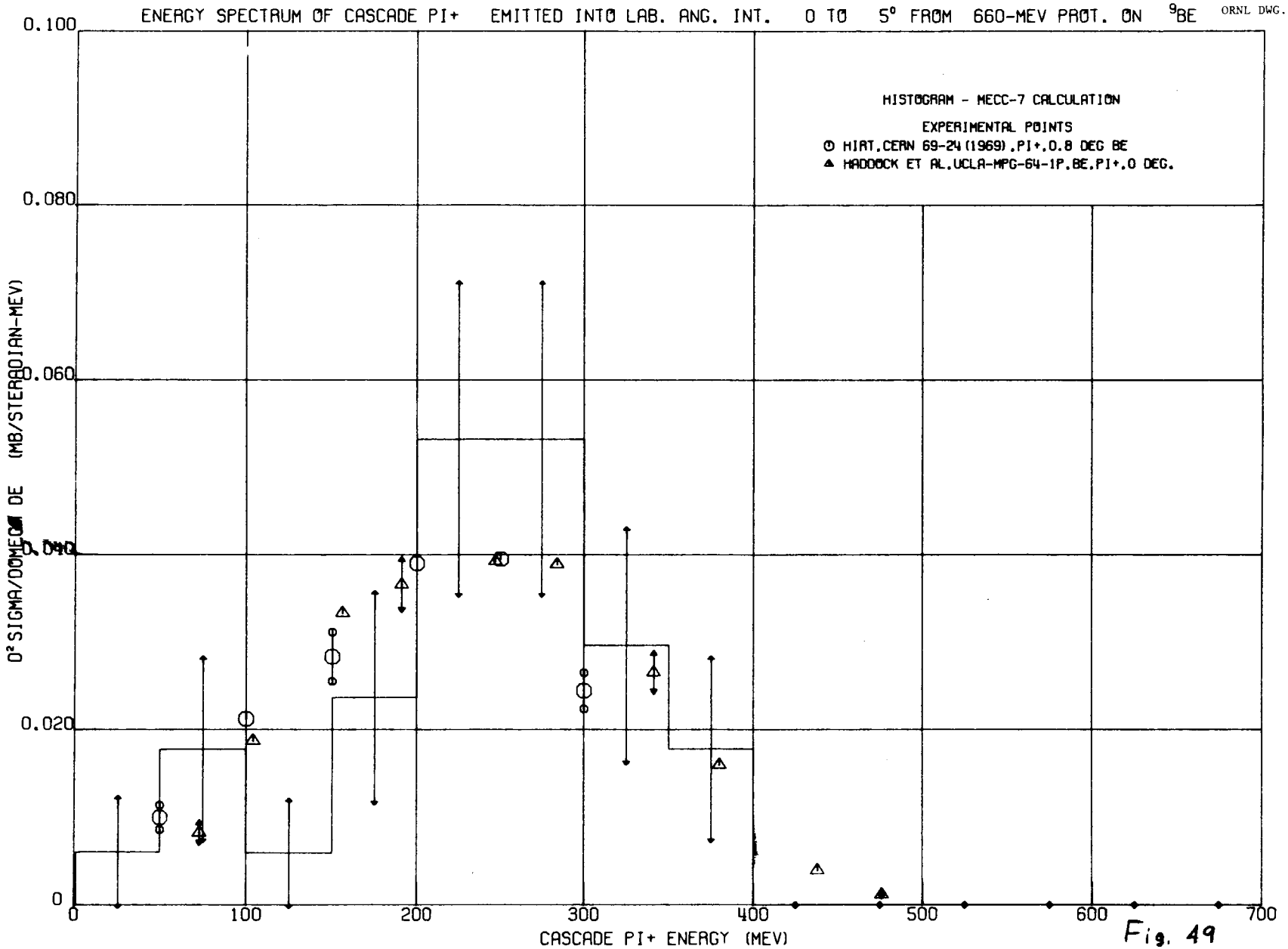

Fig. 49

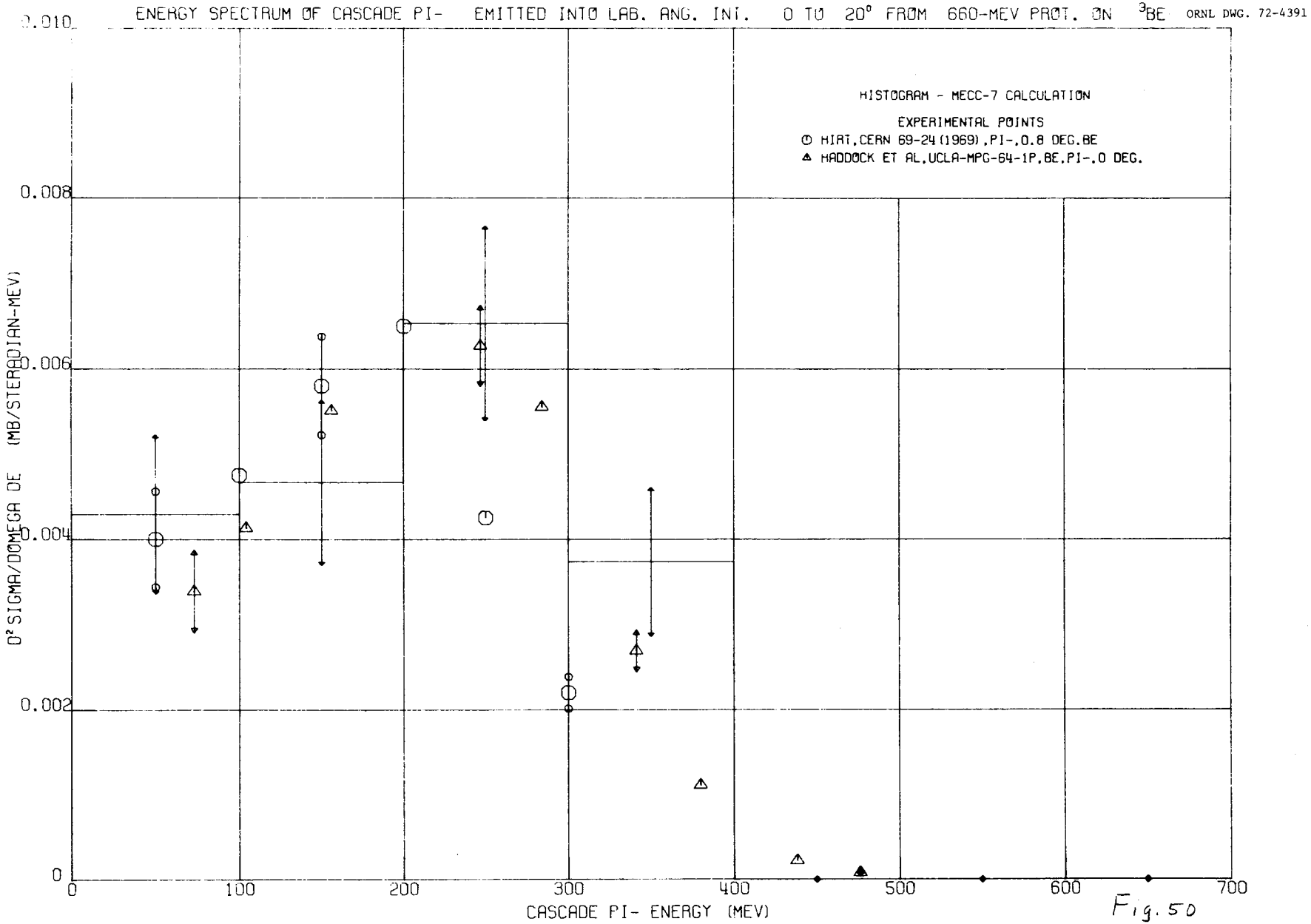
ENERGY SPECTRUM OF CASCADE PI- EMITTED INTO LAB. ANG. INT. 0 TO 20° FROM 660-MEV PROT. ON ^{3}BE
ORNL DWG. 72-4391
HISTOGRAM - MECC-7 CALCULATION
EXPERIMENTAL POINTS
HIRT,CERN 69-24(1969),PI-,0.8 DEG.BE
HADDOCK ET AL,UCLA-MPG-64-1P,BE,PI-,0 DEG.
D² SIGMA/DOMEGA DE (MB/STERADIAN-MEV)
0.010
0.008
0.006
0.004
0.002
0
0
100
200
300
400
500
600
700
CASCADE PI- ENERGY (MEV)

Fig. 50

ORNL DWG. 72-4392

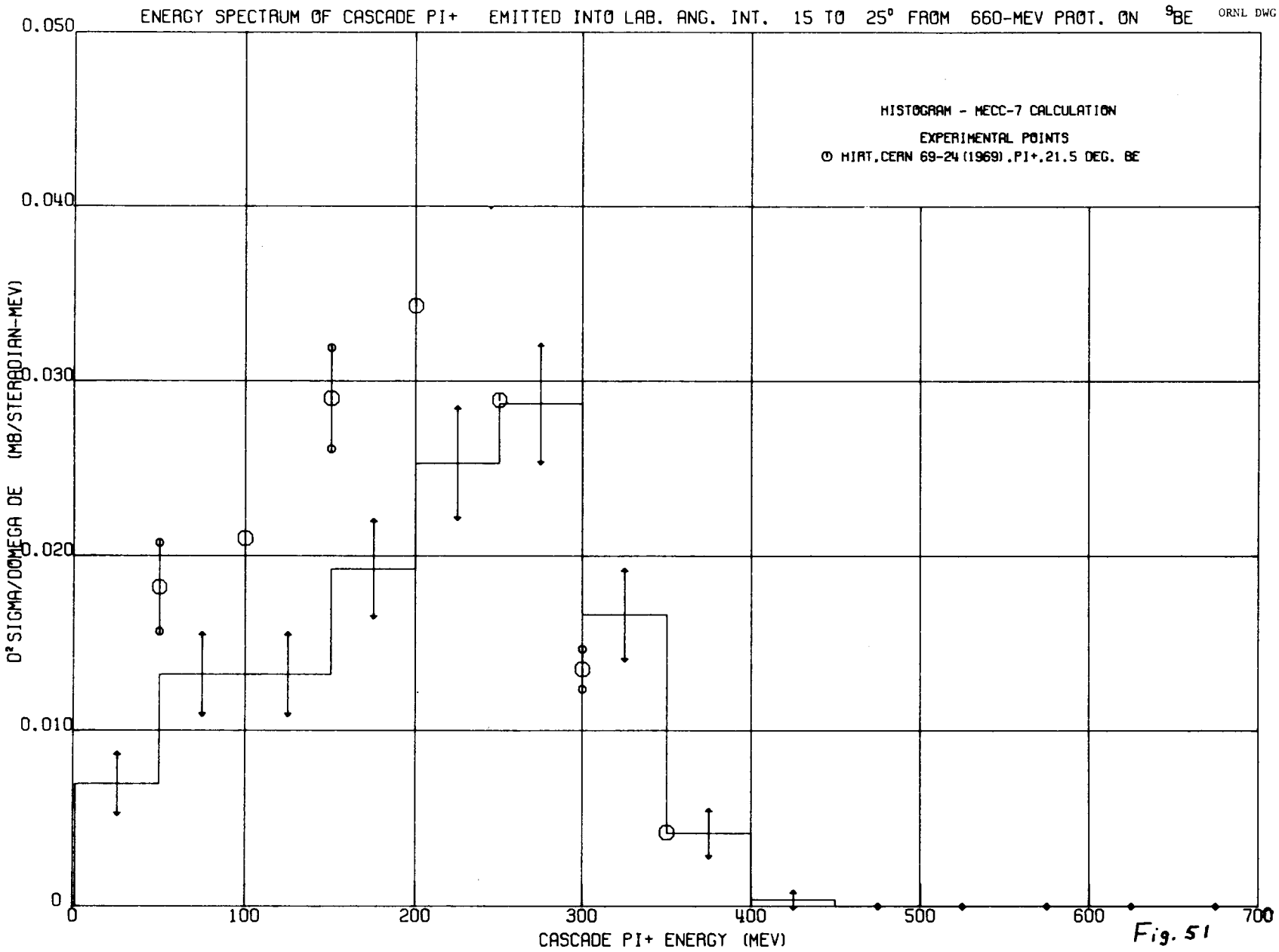

Fig. 51

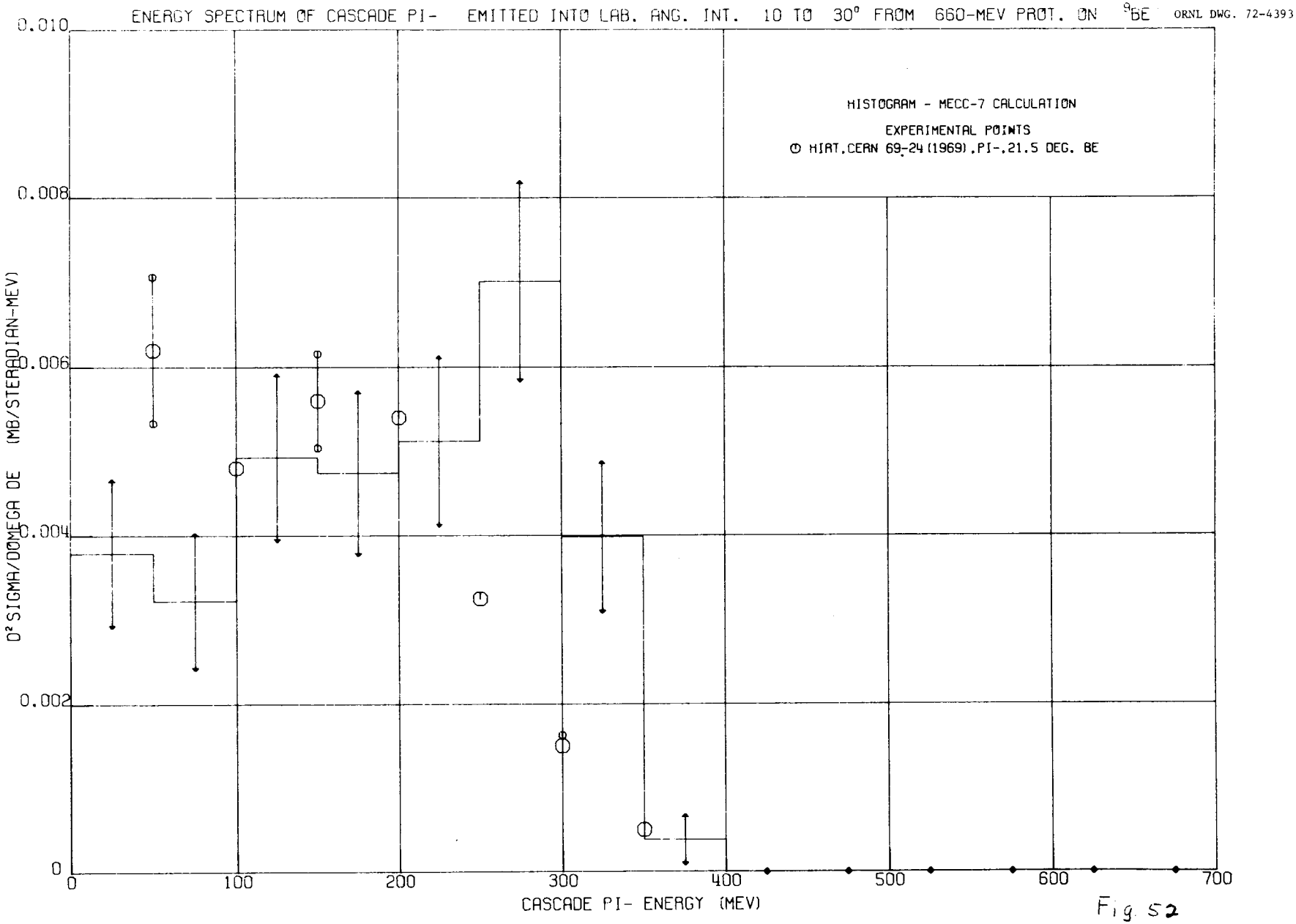
ENERGY SPECTRUM OF CASCADE PI- EMITTED INTO LAB. ANG. INT. 10 TO 30° FROM 660-MEV PROT. ON 9BE
ORNL DWG. 72-4393
HISTOGRAM - MECC-7 CALCULATION
EXPERIMENTAL POINTS
HIRT,CERN 69-24 (1969),PI-,21.5 DEG. BE
D² SIGMA/DOMEGA DE (MB/STERADIAN-MEV)
0.010
0.008
0.006
0.004
0.002
0
0
100
200
300
400
500
600
700
CASCADE PI- ENERGY (MEV)

Fig. 52

ORNL DWG. 72-4394

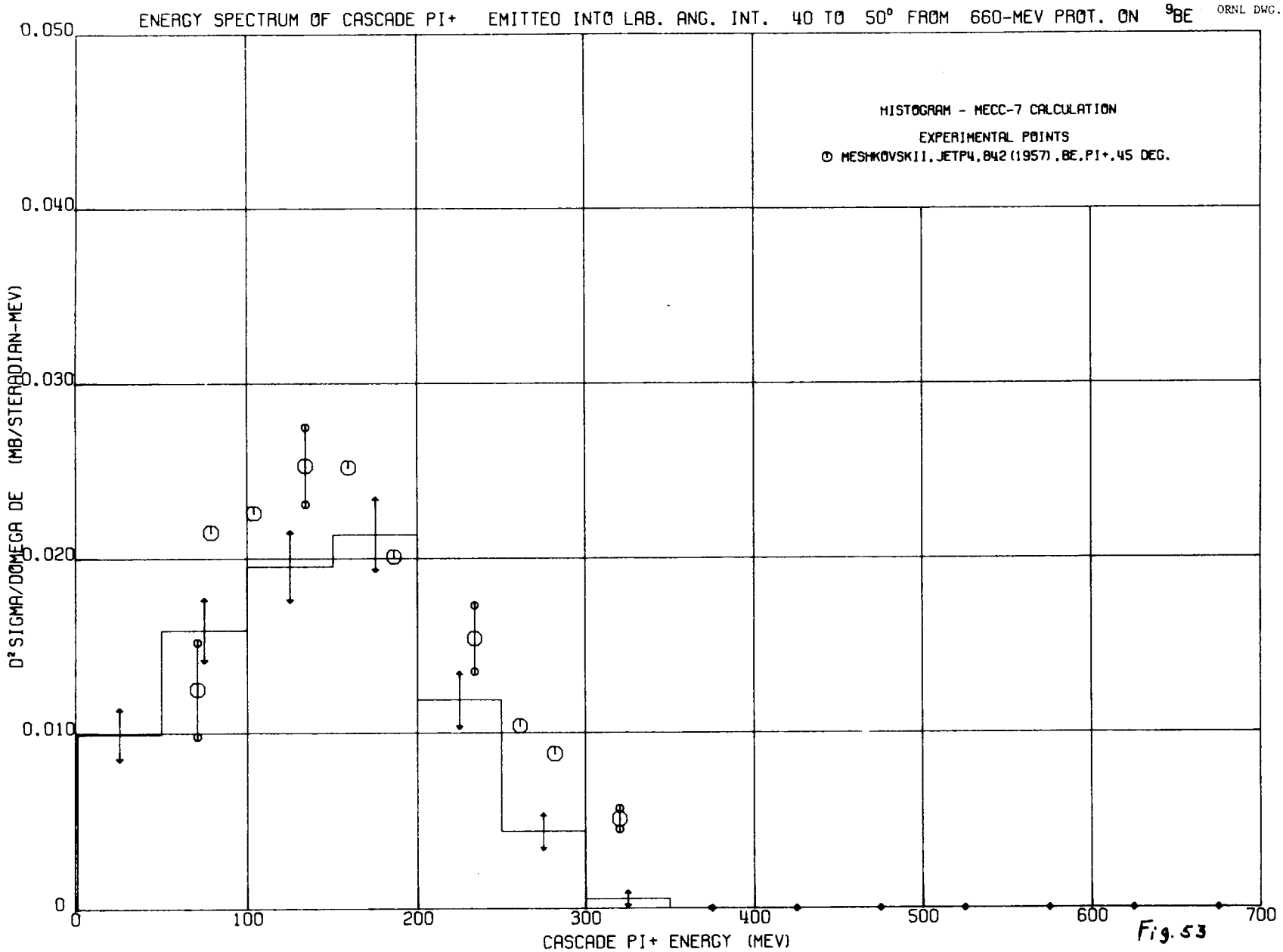

Fig. 53

ORNL DWG. 72-4395

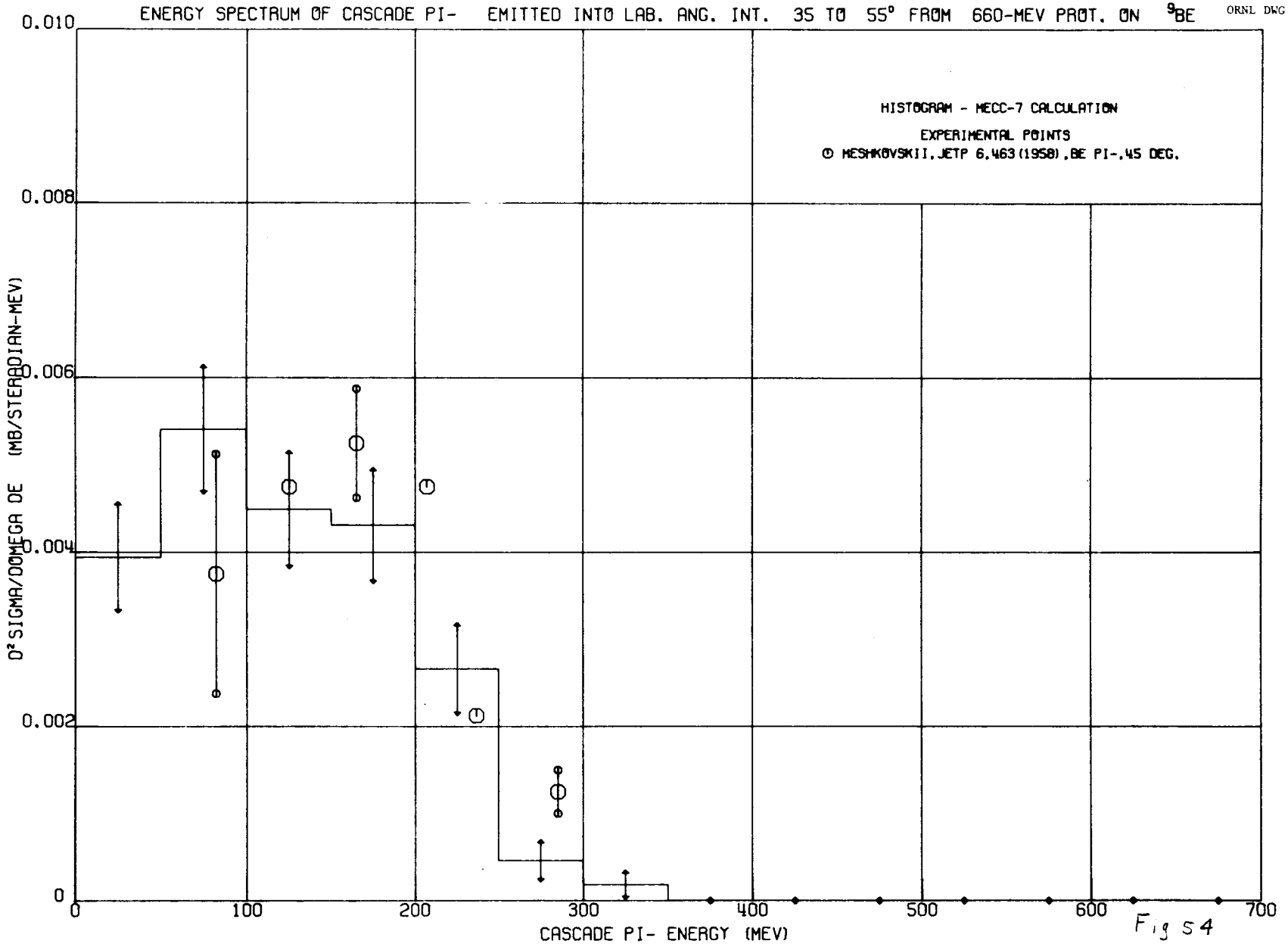

Fig 54

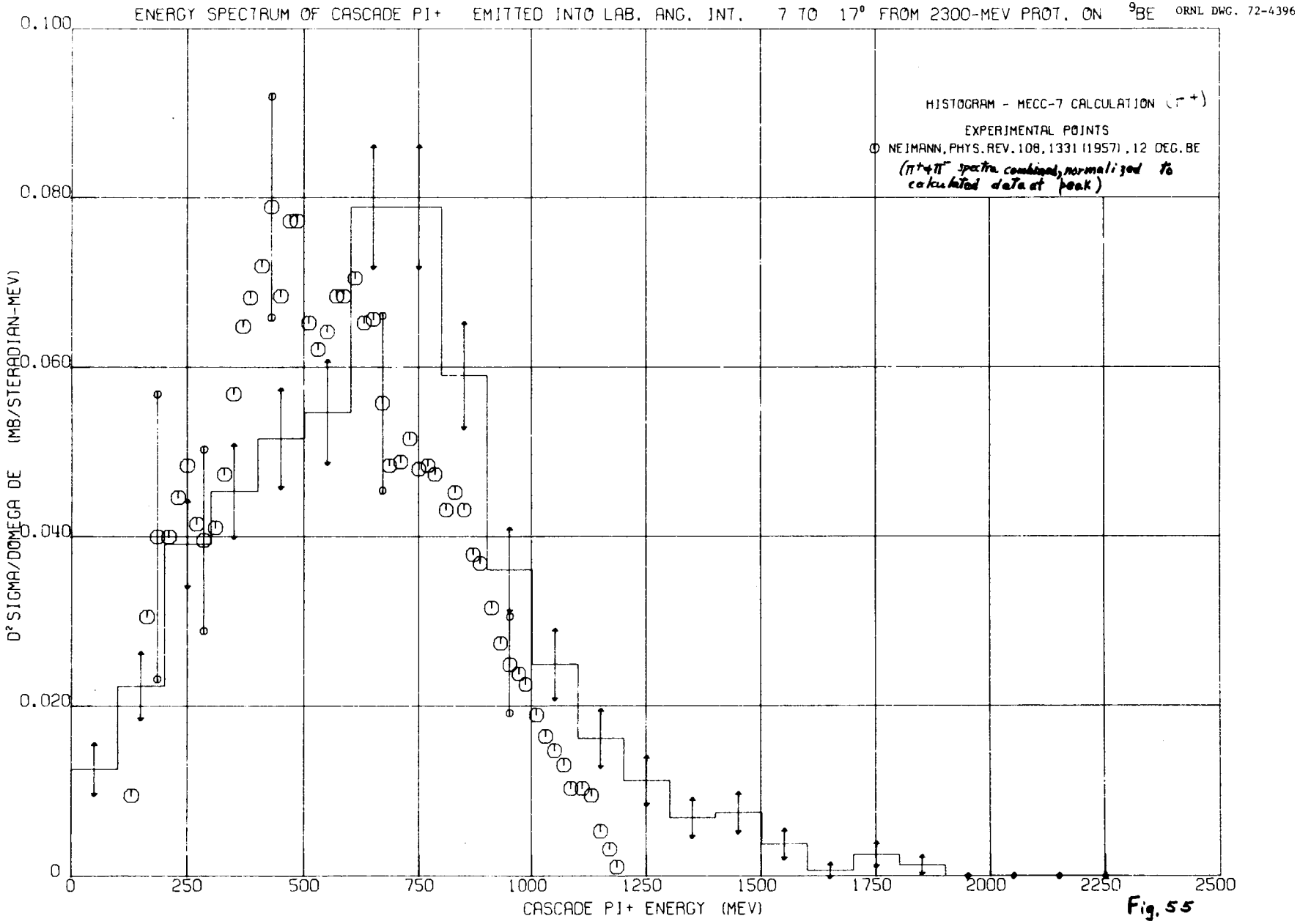
ENERGY SPECTRUM OF CASCADE PI+ EMITTED INTO LAB. ANG. INT. 7 TO 17° FROM 2300-MEV PROT. ON 9BE
ORNL DWG. 72-4396
HISTOGRAM - MECC-7 CALCULATION (π+)
EXPERIMENTAL POINTS
NEIMANN, PHYS. REV. 108, 1331 (1957), 12 DEG. BE
(π+ + π− spectra combined, normalized to calculated data at peak)
D² SIGMA/DOMEGA DE (MB/STERADIAN-MEV)
0.100
0.080
0.060
0.040
0.020
0
0
250
500
750
1000
1250
1500
1750
2000
2250
2500
CASCADE PI+ ENERGY (MEV)

Fig. 55

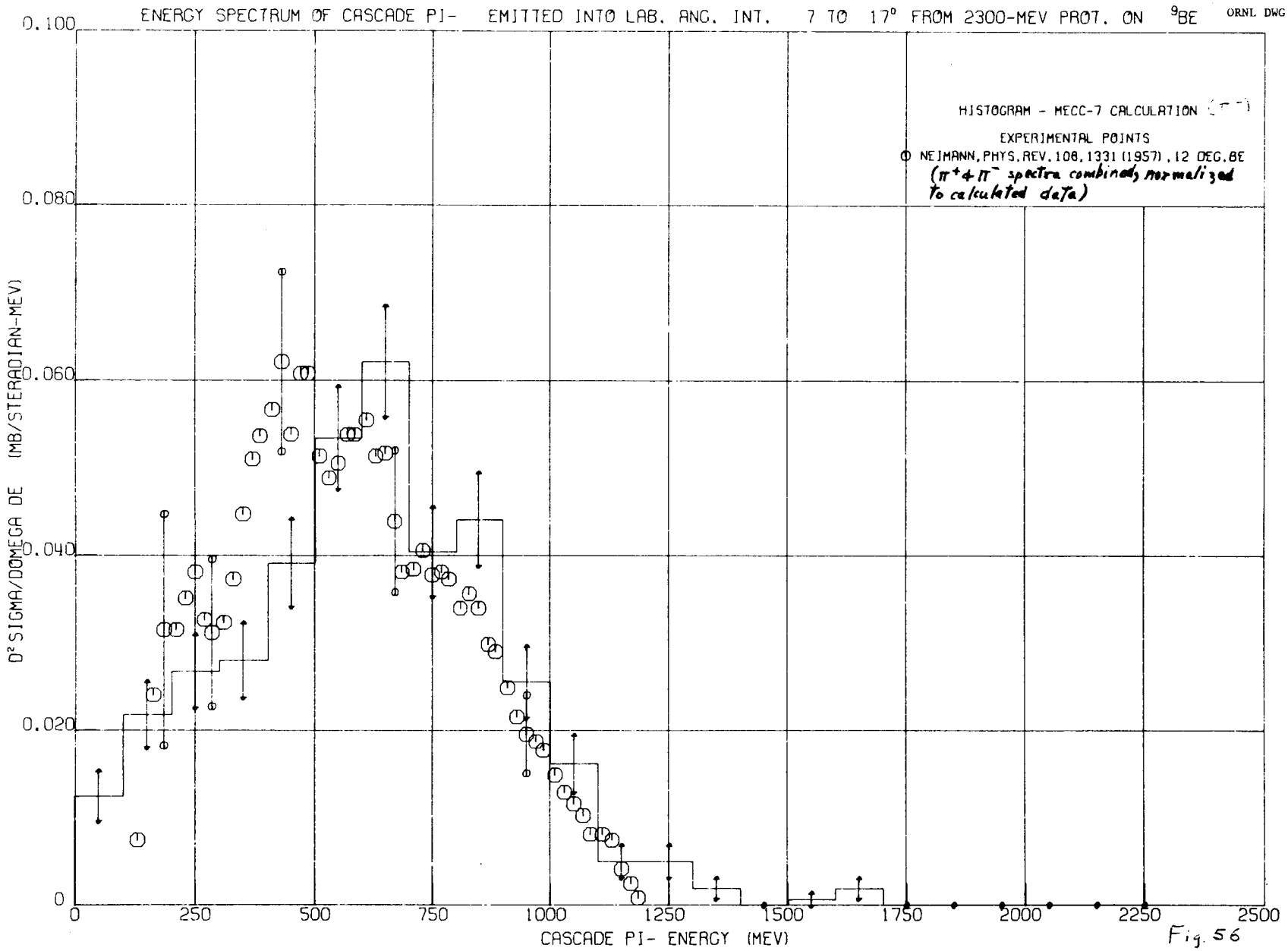
ENERGY SPECTRUM OF CASCADE PI- EMITTED INTO LAB. ANG. INT. 7 TO 17° FROM 2300-MEV PROT. ON ^{9}BE
ORNL DWG. 72-4397
HISTOGRAM - MECC-7 CALCULATION
EXPERIMENTAL POINTS
NEIMANN, PHYS. REV. 108, 1331 (1957), 12 DEG. BE
($\pi^+ + \pi^-$ spectra combined, normalized to calculated data)
D² SIGMA/DOMEGA DE (MB/STERADIAN-MEV)
0.100
0.080
0.060
0.040
0.020
0
0
250
500
750
1000
1250
1500
1750
2000
2250
2500
CASCADE PI- ENERGY (MEV)

Fig. 56

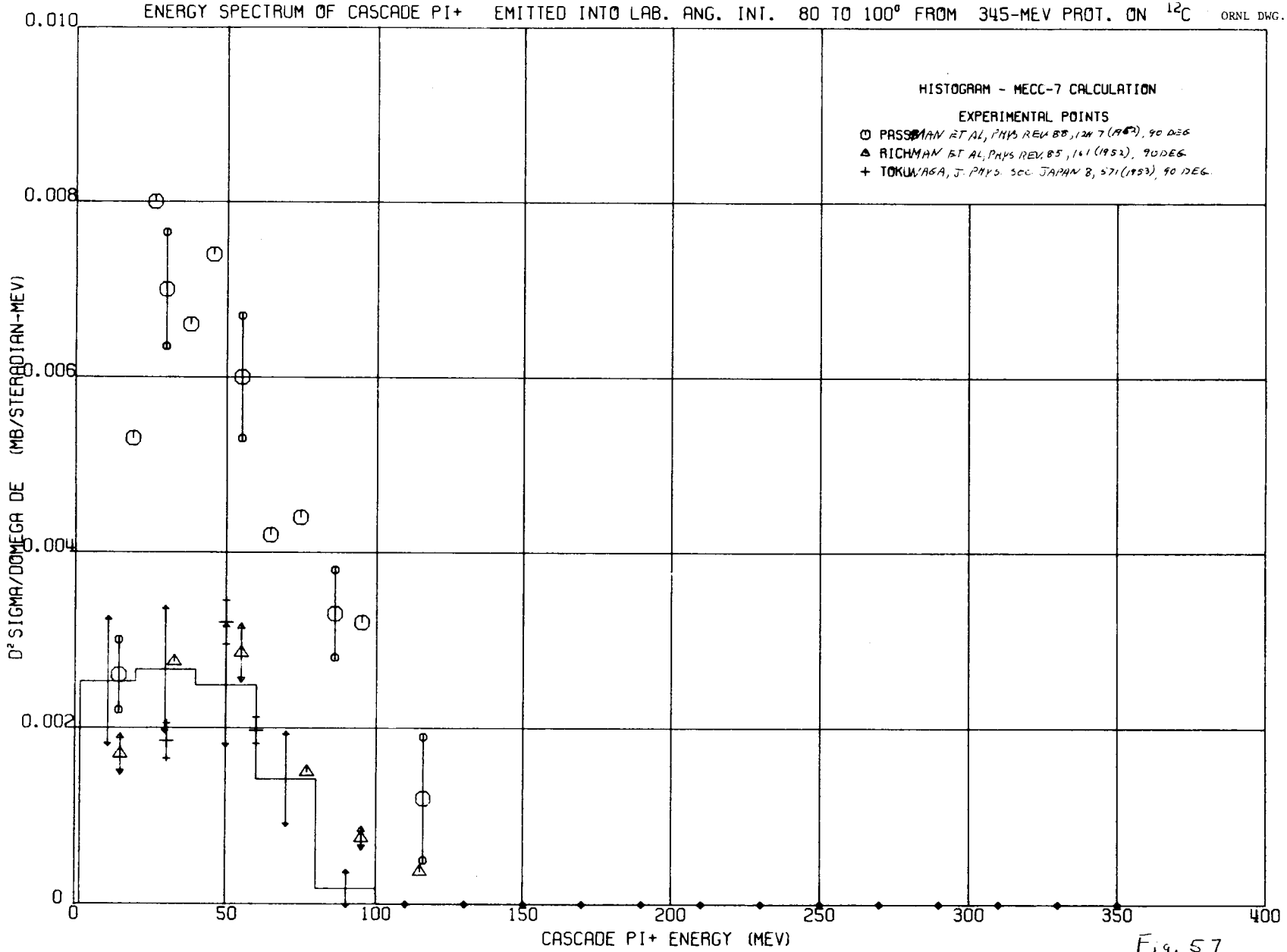
ENERGY SPECTRUM OF CASCADE PI+ EMITTED INTO LAB. ANG. INT. 80 TO 100° FROM 345-MEV PROT. ON 12C
ORNL DWG. 72-4398
HISTOGRAM - MECC-7 CALCULATION
EXPERIMENTAL POINTS
PASSMAN ET AL, PHYS REV 88, 1247 (1952), 90 DEG
RICHMAN ET AL, PHYS REV, 85, 161 (1952), 90 DEG
TOKUNAGA, J. PHYS. SOC. JAPAN 8, 571 (1953), 90 DEG.
D²SIGMA/DOMEGA DE (MB/STERADIAN-MEV)
0.010
0.008
0.006
0.004
0.002
0
0
50
100
150
200
250
300
350
400
CASCADE PI+ ENERGY (MEV)

Fig. 57

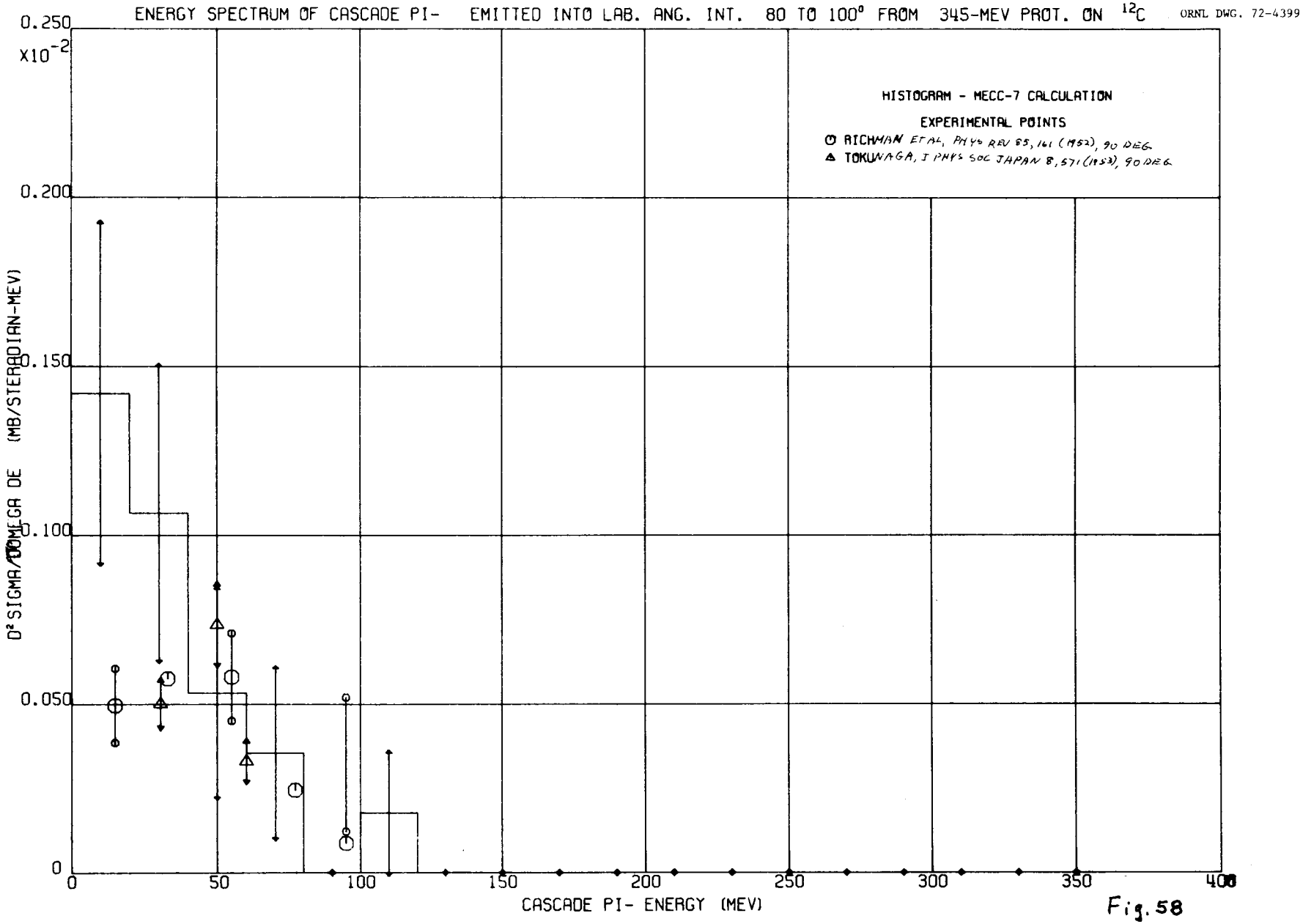
ENERGY SPECTRUM OF CASCADE PI- EMITTED INTO LAB. ANG. INT. 80 TO 100° FROM 345-MEV PROT. ON 12C
ORNL DWG. 72-4399
HISTOGRAM - MECC-7 CALCULATION
EXPERIMENTAL POINTS
RICHMAN ET AL, PHYS REV 85, 161 (1952), 90 DEG
TOKUNAGA, J PHYS SOC JAPAN 8, 571 (1953), 90 DEG
D²SIGMA/DOMEGA DE (MB/STERADIAN-MEV)
X10⁻²
0.250
0.200
0.150
0.100
0.050
0
0
50
100
150
200
250
300
350
400
CASCADE PI- ENERGY (MEV)

Fig. 58

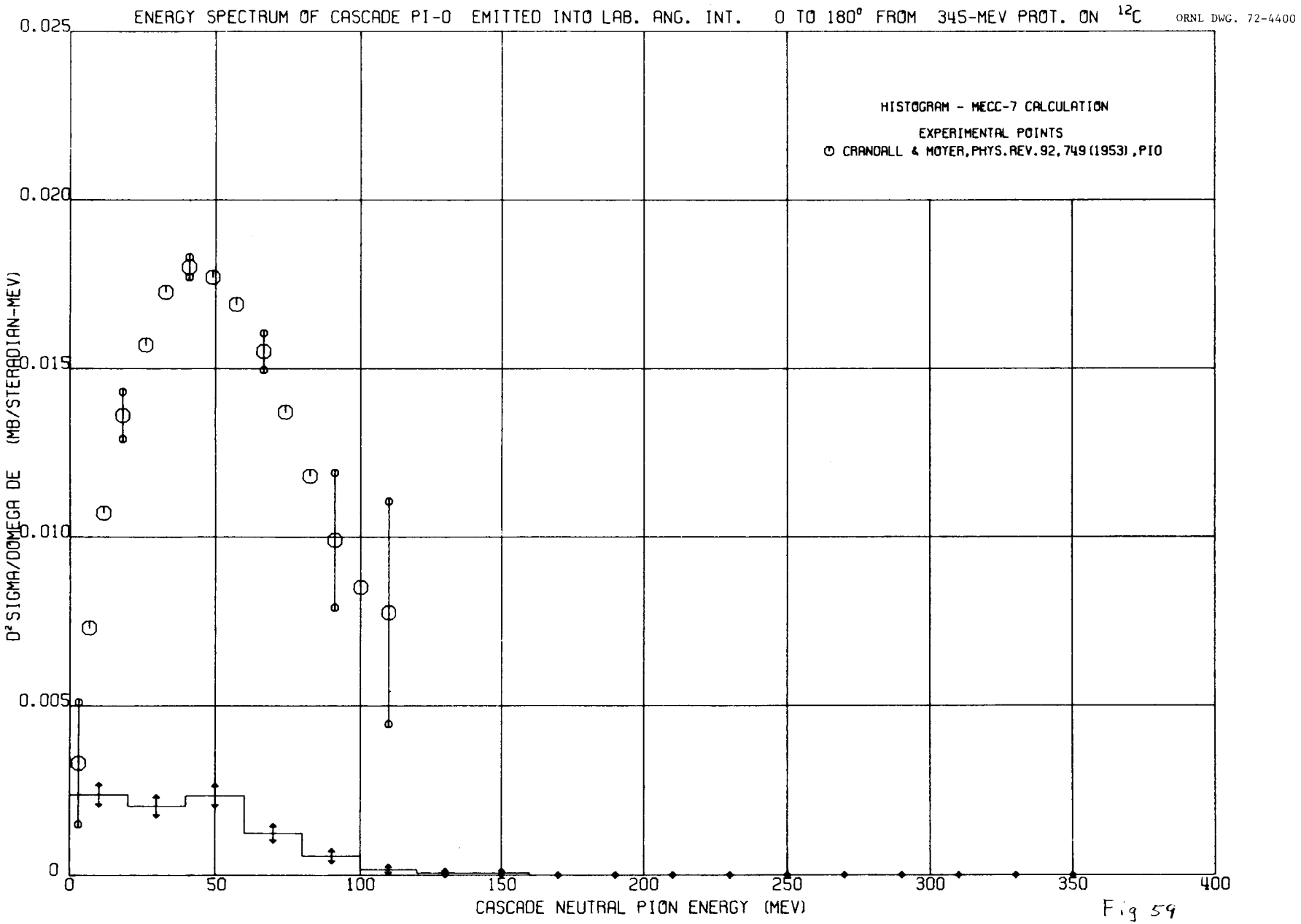
ENERGY SPECTRUM OF CASCADE PI-0 EMITTED INTO LAB. ANG. INT. 0 TO 180° FROM 345-MEV PROT. ON 12C
ORNL DWG. 72-4400
HISTOGRAM - MECC-7 CALCULATION
EXPERIMENTAL POINTS
CRANDALL & MOYER, PHYS. REV. 92, 749 (1953), PIO
D²SIGMA/DOMEGA DE (MB/STERADIAN-MEV)
0.025
0.020
0.015
0.010
0.005
0
0
50
100
150
200
250
300
350
400
CASCADE NEUTRAL PION ENERGY (MEV)

Fig 59

ENERGY SPECTRUM OF CASCADE PI+ EMITTED INTO LAB. ANG. INT. 15 TO 25° FROM 450-MEV PROT. ON ^{12}C ORNL DWG. 72-4401

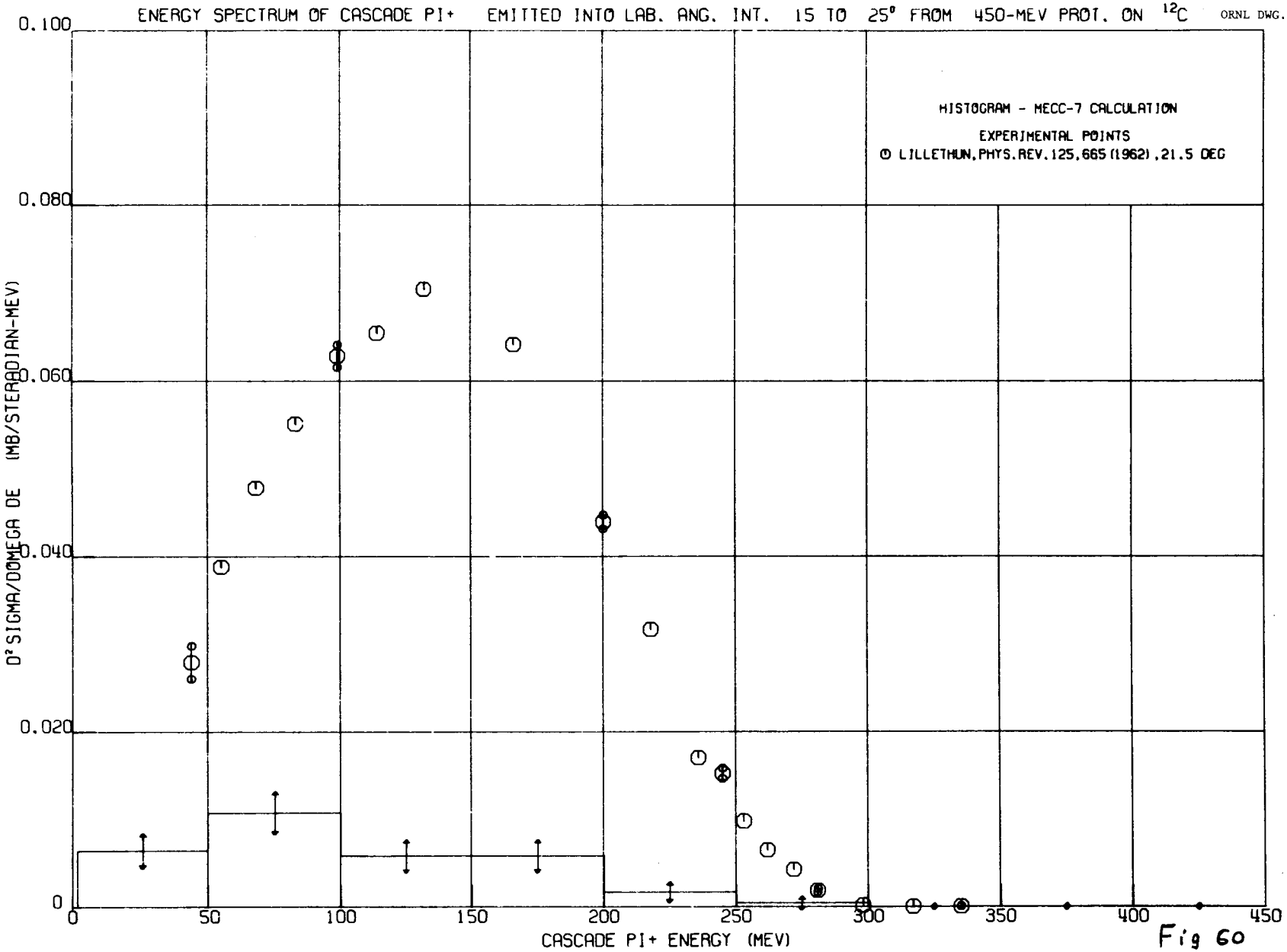

Fig 60

ORNL DWG. 72-4402

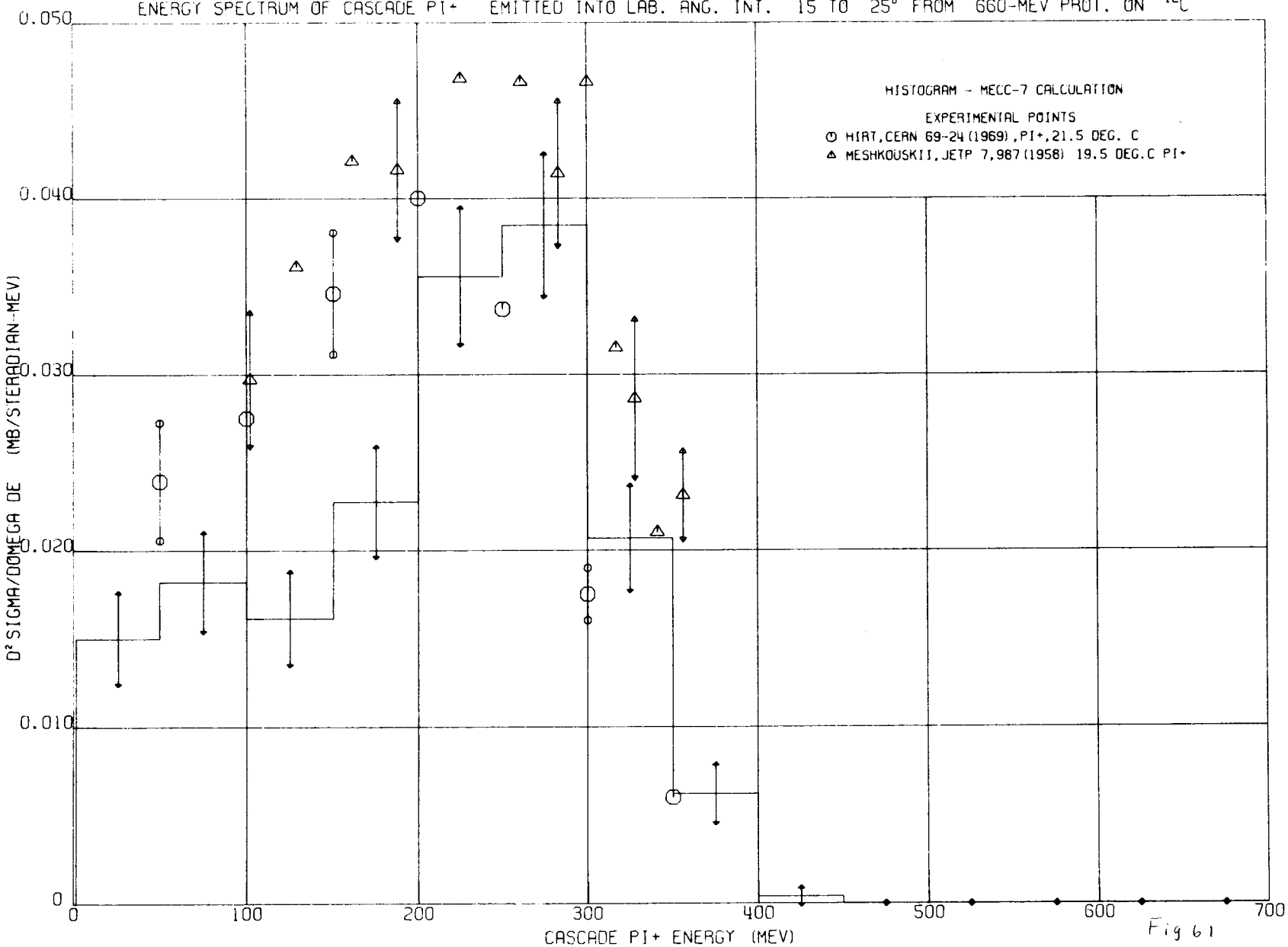

Fig 61

ORNL DWG. 72-4403

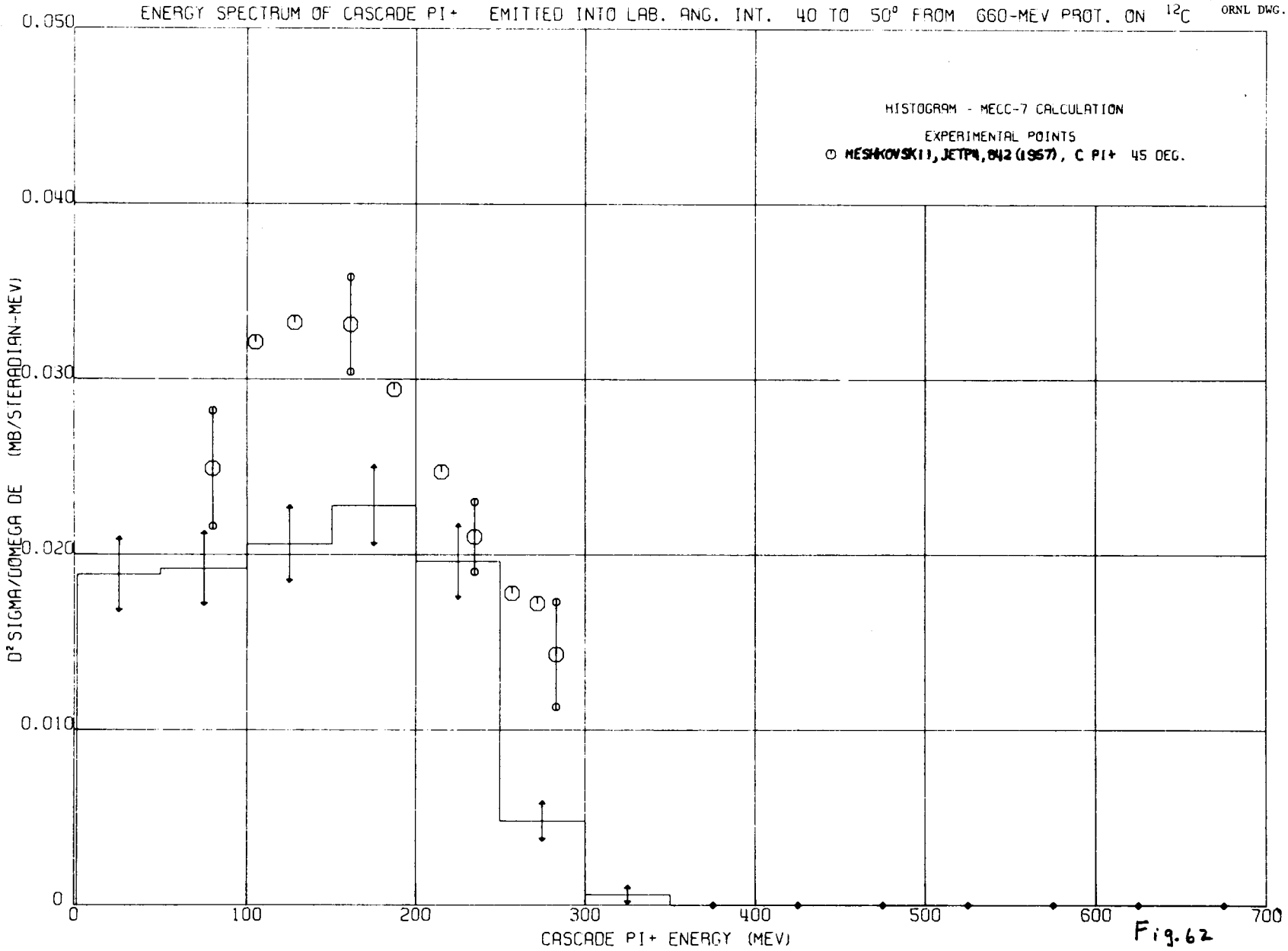

Fig. 62

ORNL DWG. 72-4404

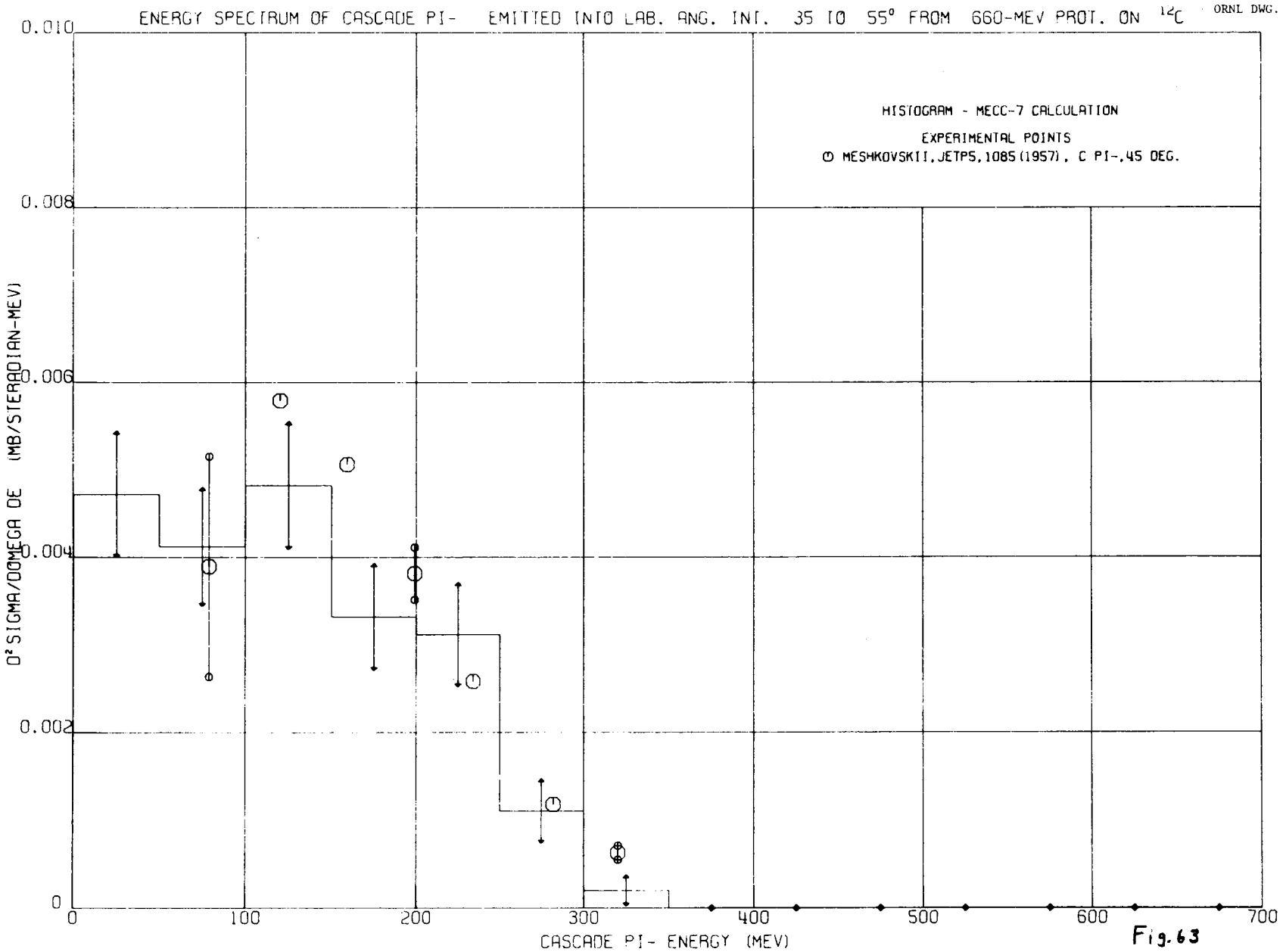

Fig. 63

ORNL DWG. 72-4405

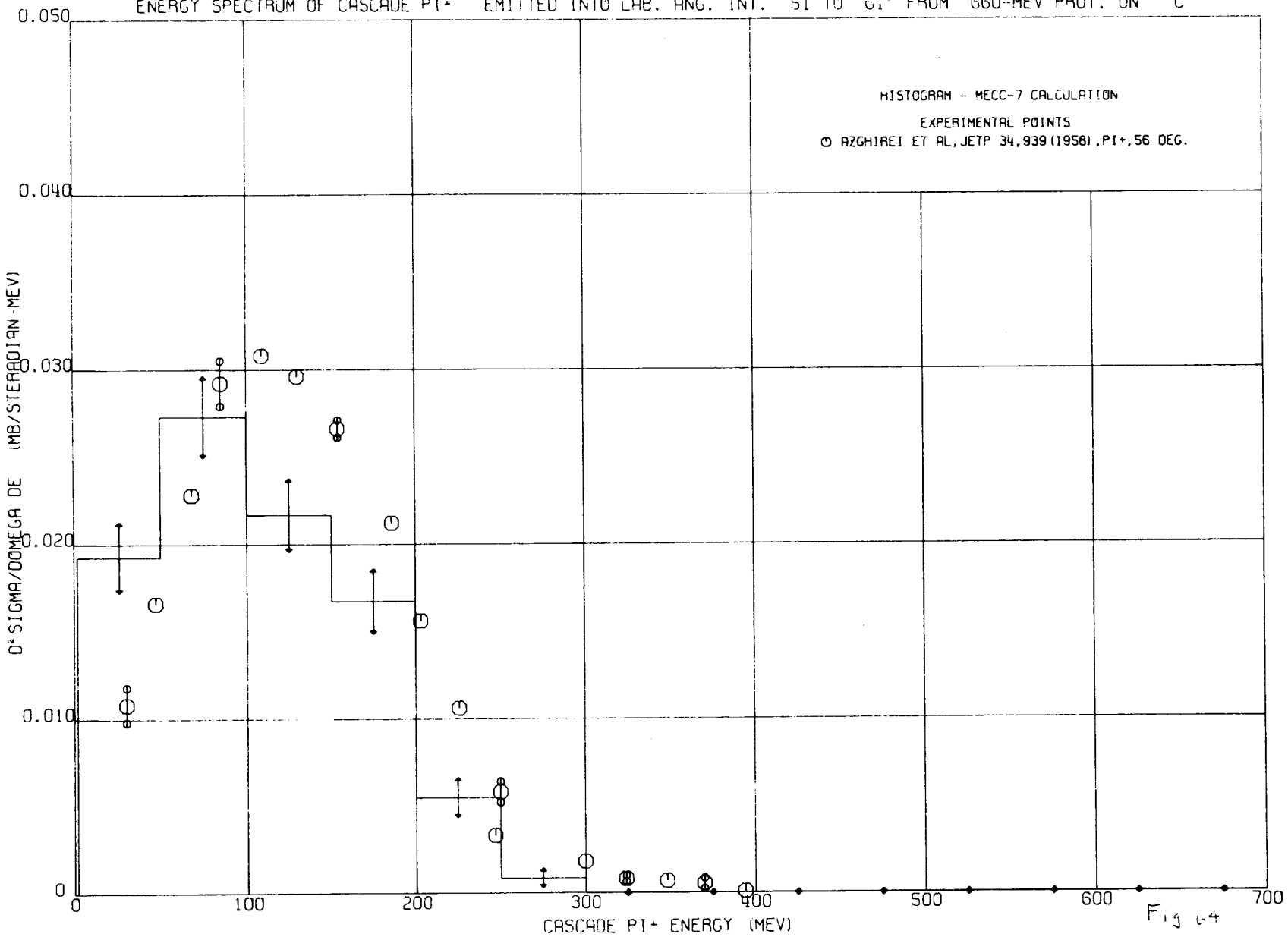

Fig 64

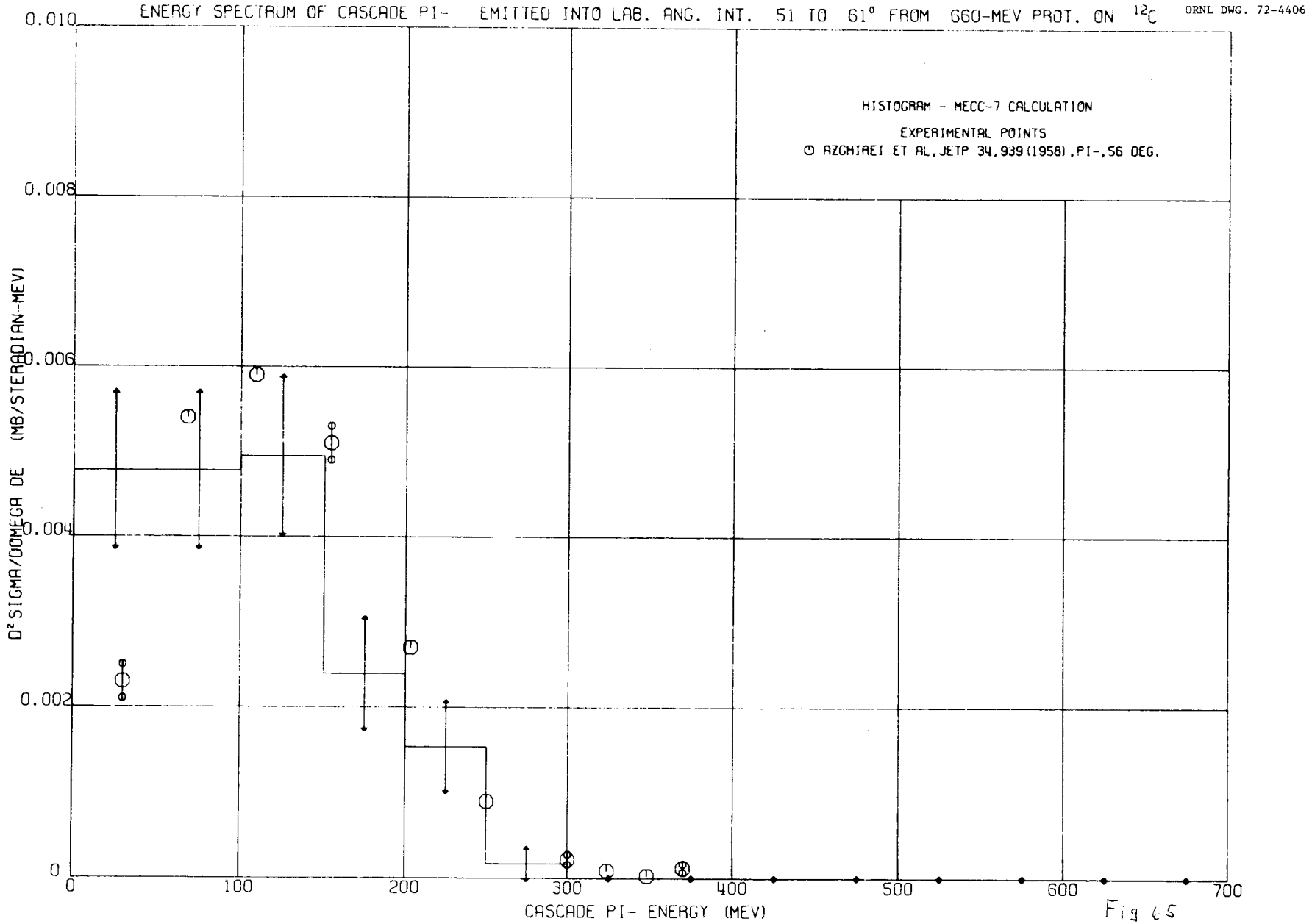
ENERGY SPECTRUM OF CASCADE PI- EMITTED INTO LAB. ANG. INT. 51 TO 61° FROM 660-MEV PROT. ON 12C
ORNL DWG. 72-4406
HISTOGRAM - MECC-7 CALCULATION
EXPERIMENTAL POINTS
AZGHIREI ET AL, JETP 34,939(1958), PI-, 56 DEG.
D²SIGMA/DOMEGA DE (MB/STERADIAN-MEV)
0.010
0.008
0.006
0.004
0.002
0
0
100
200
300
400
500
600
700
CASCADE PI- ENERGY (MEV)

Fig 65

ORNL-DWG 70-12873

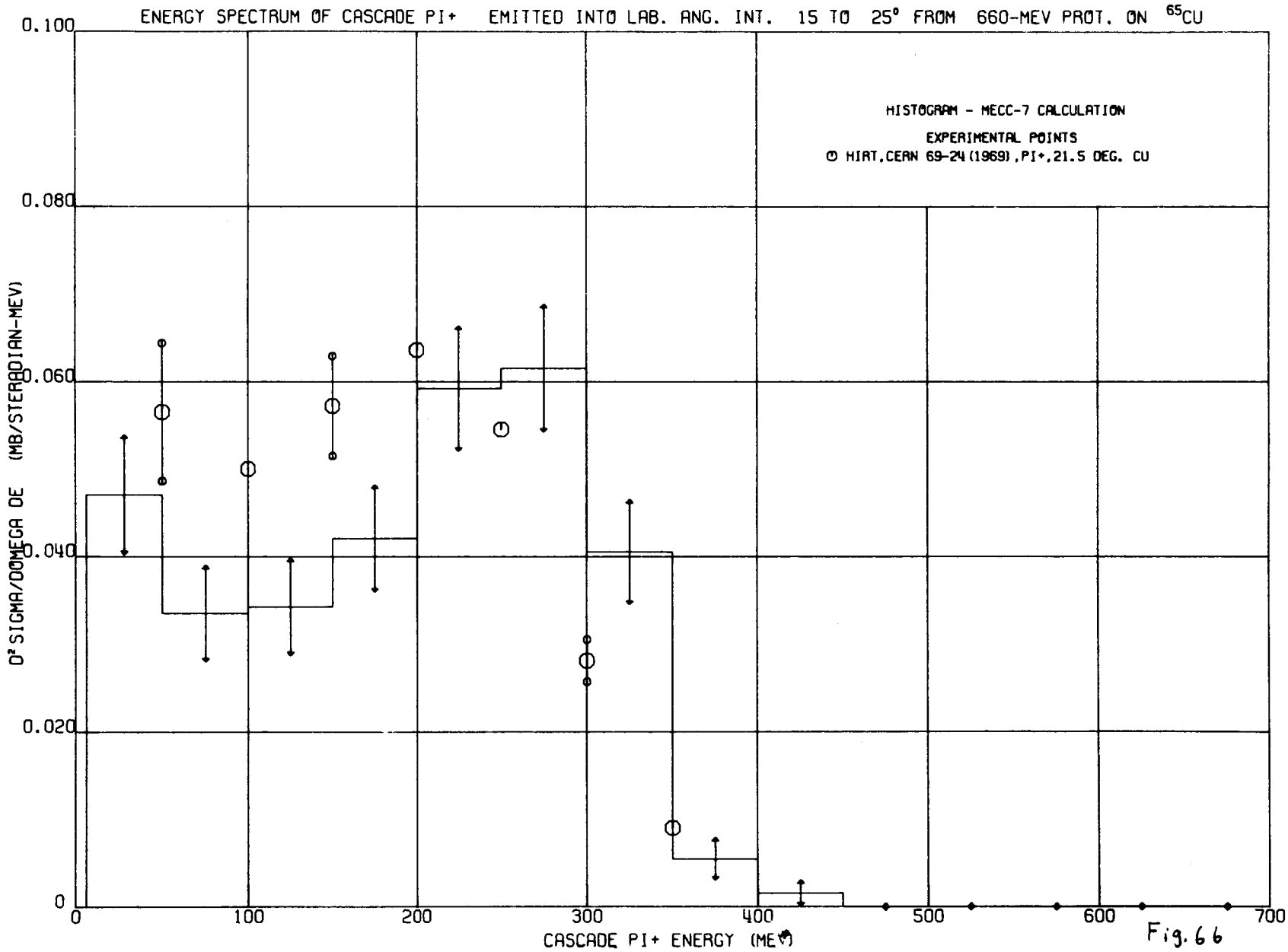

Fig. 66

ORNL-DWG 70-12872

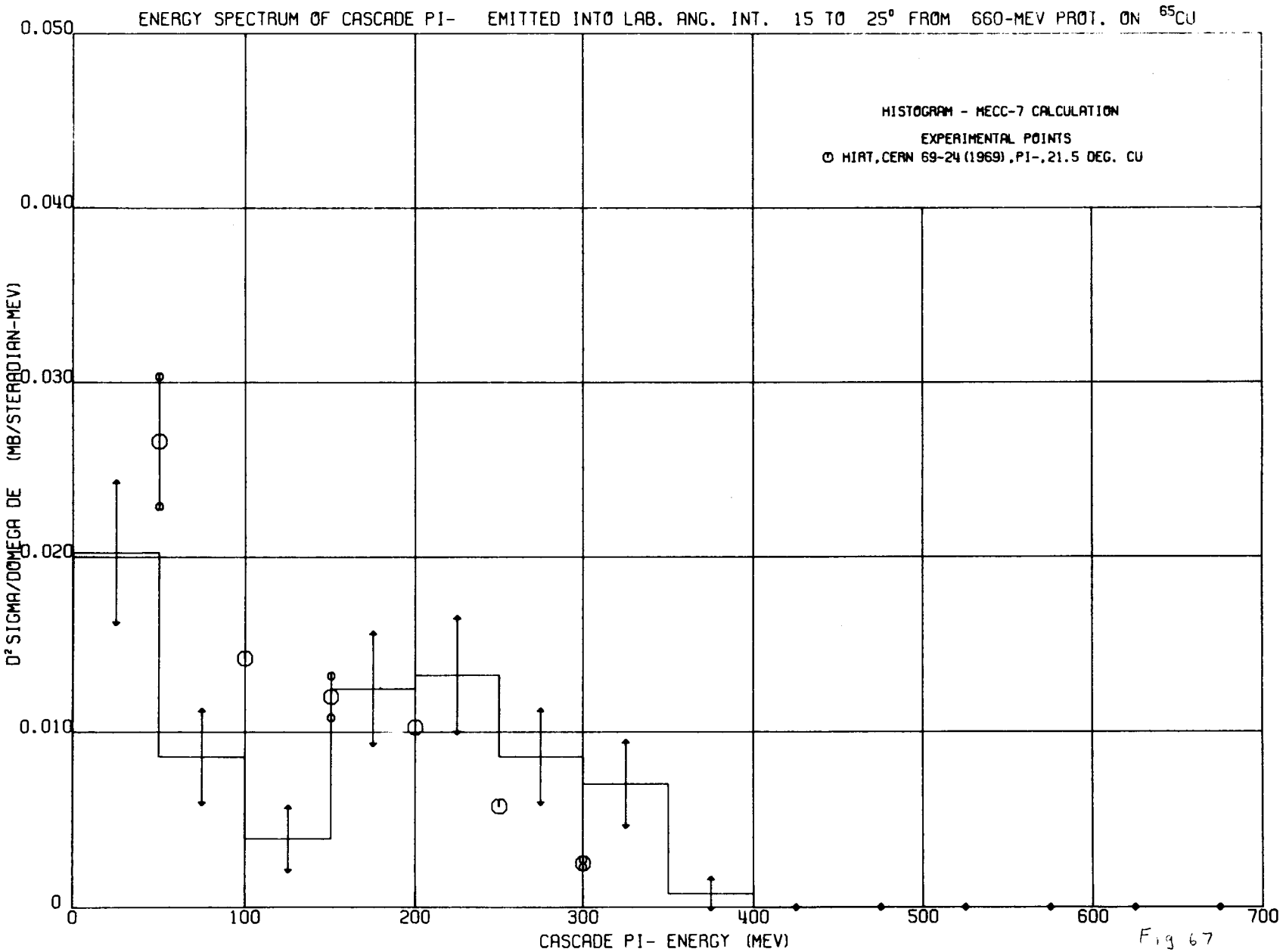

Fig 67

ORNL-DWG 70-12871

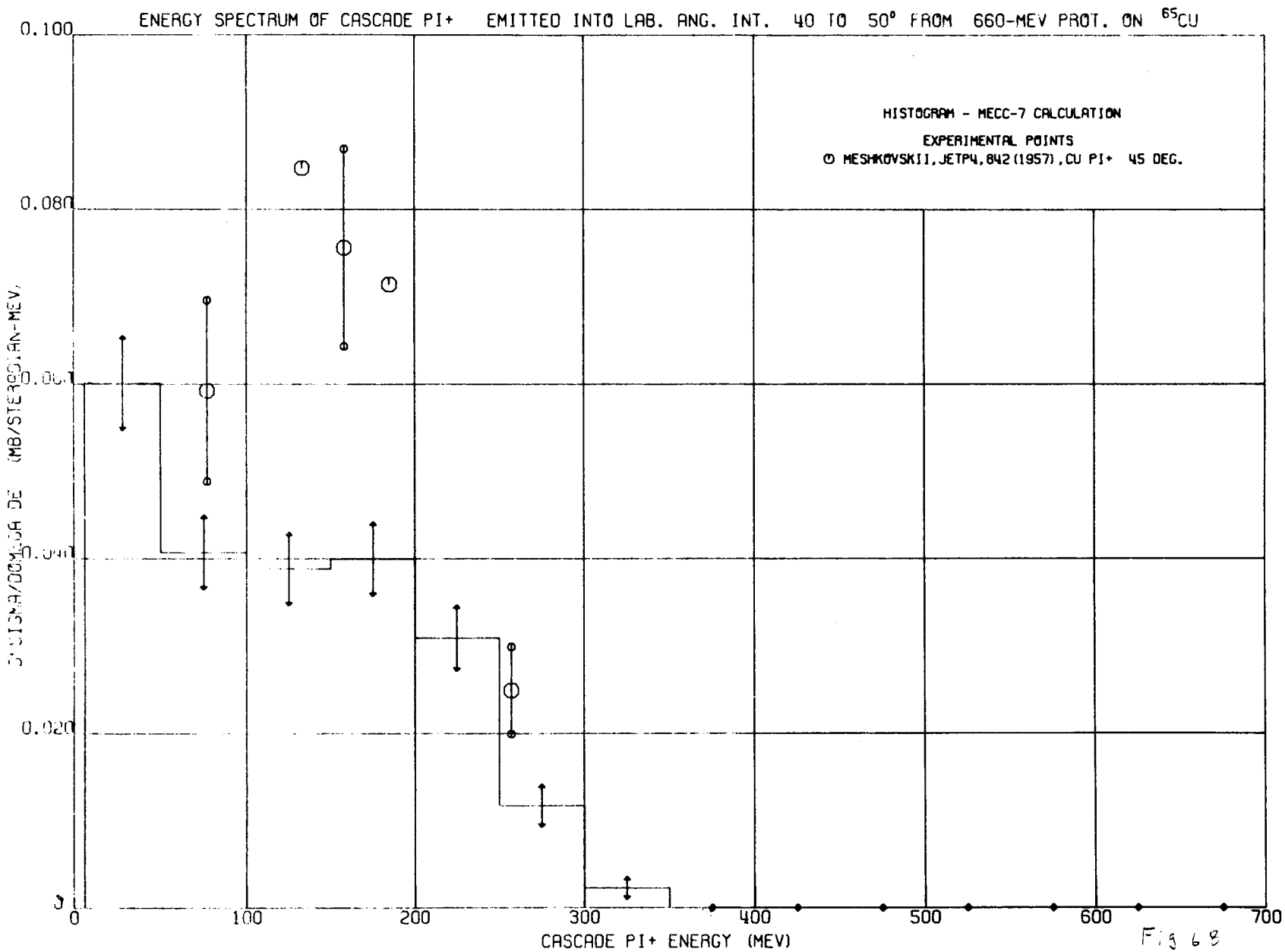

Fig 68

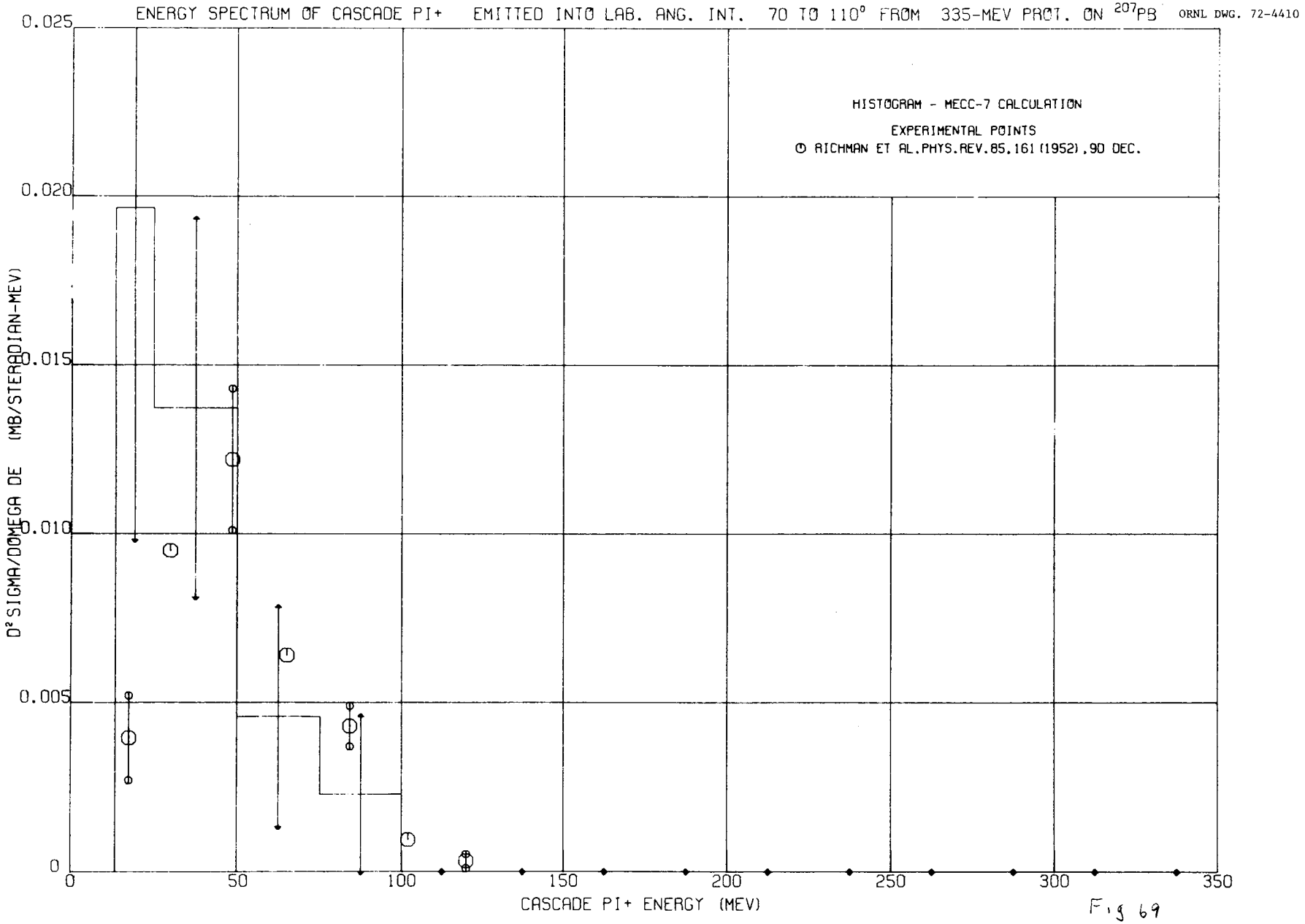
ENERGY SPECTRUM OF CASCADE PI+ EMITTED INTO LAB. ANG. INT. 70 TO 110° FROM 335-MEV PROT. ON 207PB
ORNL DWG. 72-4410
HISTOGRAM - MECC-7 CALCULATION
EXPERIMENTAL POINTS
RICHMAN ET AL.PHYS.REV.85,161(1952),90 DEC.
D²SIGMA/DOMEGA DE (MB/STERADIAN-MEV)
0.025
0.020
0.015
0.010
0.005
0
0
50
100
150
200
250
300
350
CASCADE PI+ ENERGY (MEV)

Fig 69

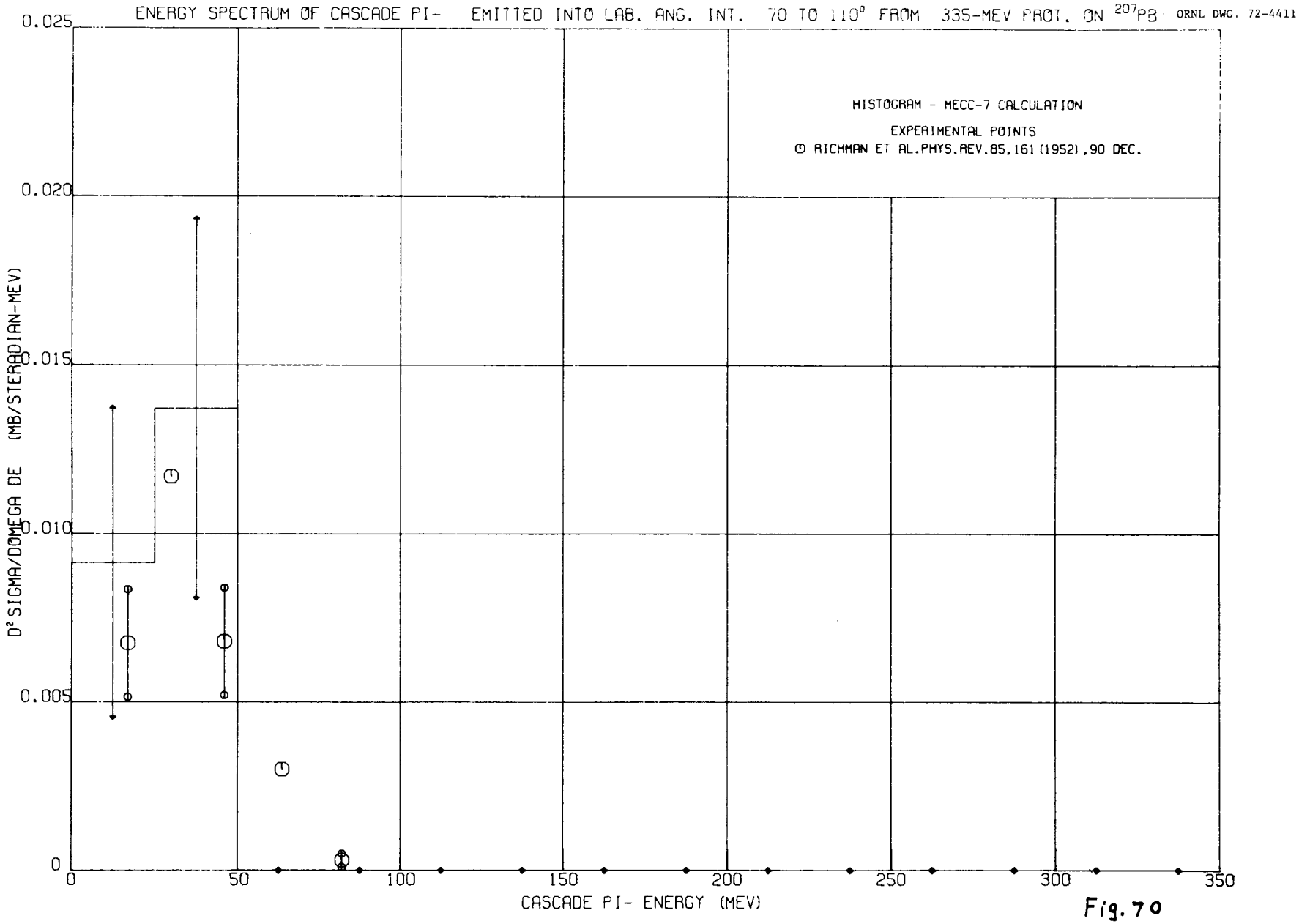
ENERGY SPECTRUM OF CASCADE PI- EMITTED INTO LAB. ANG. INT. 70 TO 110° FROM 335-MEV PROT. ON 207PB
ORNL DWG. 72-4411
HISTOGRAM - MECC-7 CALCULATION
EXPERIMENTAL POINTS
RICHMAN ET AL.PHYS.REV.85,161 (1952),90 DEC.
D²SIGMA/DOMEGA DE (MB/STERADIAN-MEV)
0.025
0.020
0.015
0.010
0.005
0
0
50
100
150
200
250
300
350
CASCADE PI- ENERGY (MEV)

Fig. 70

ORNL DWG. 72-4412

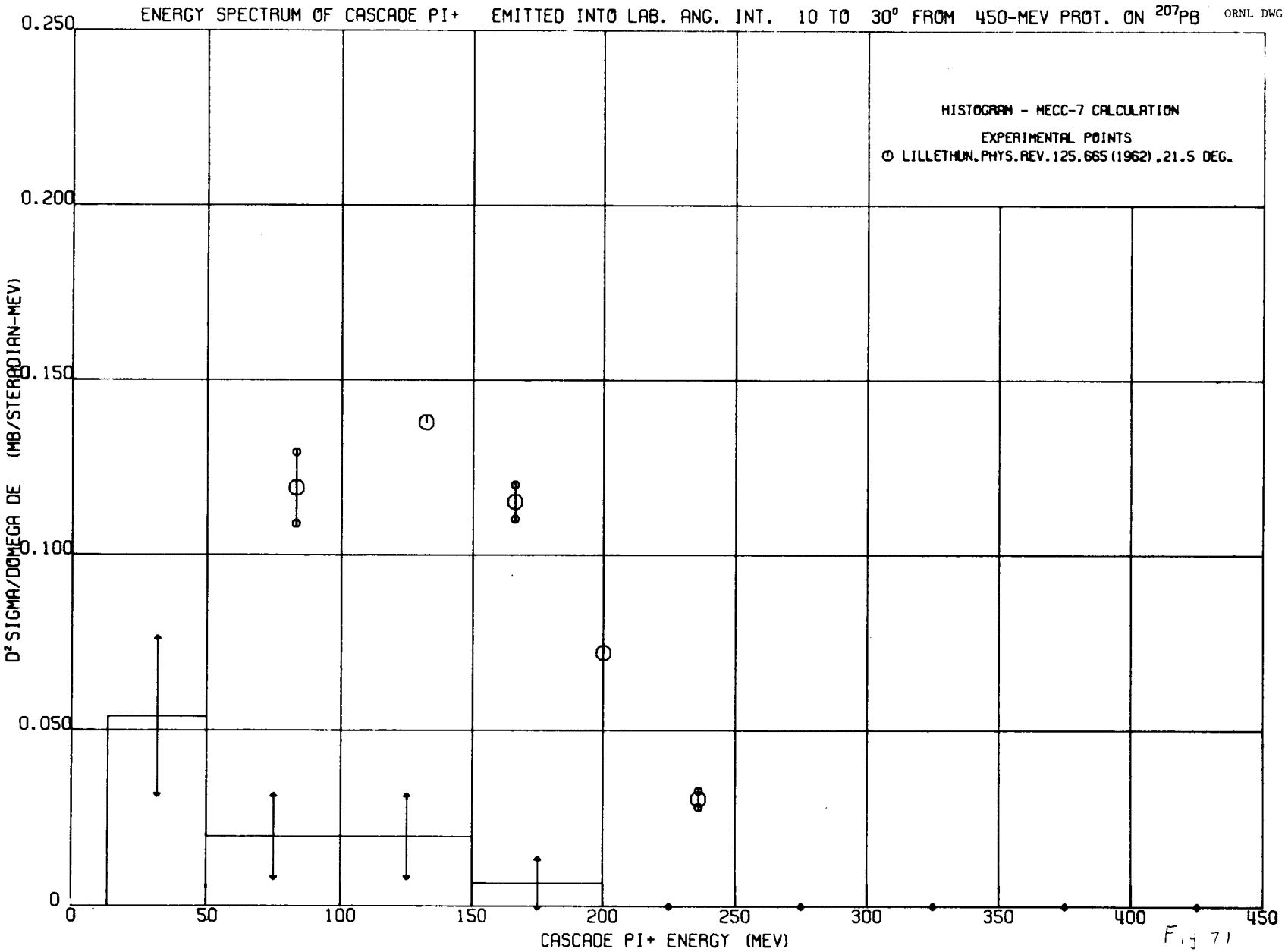

Fig 71

ORNL DWG. 72-4413

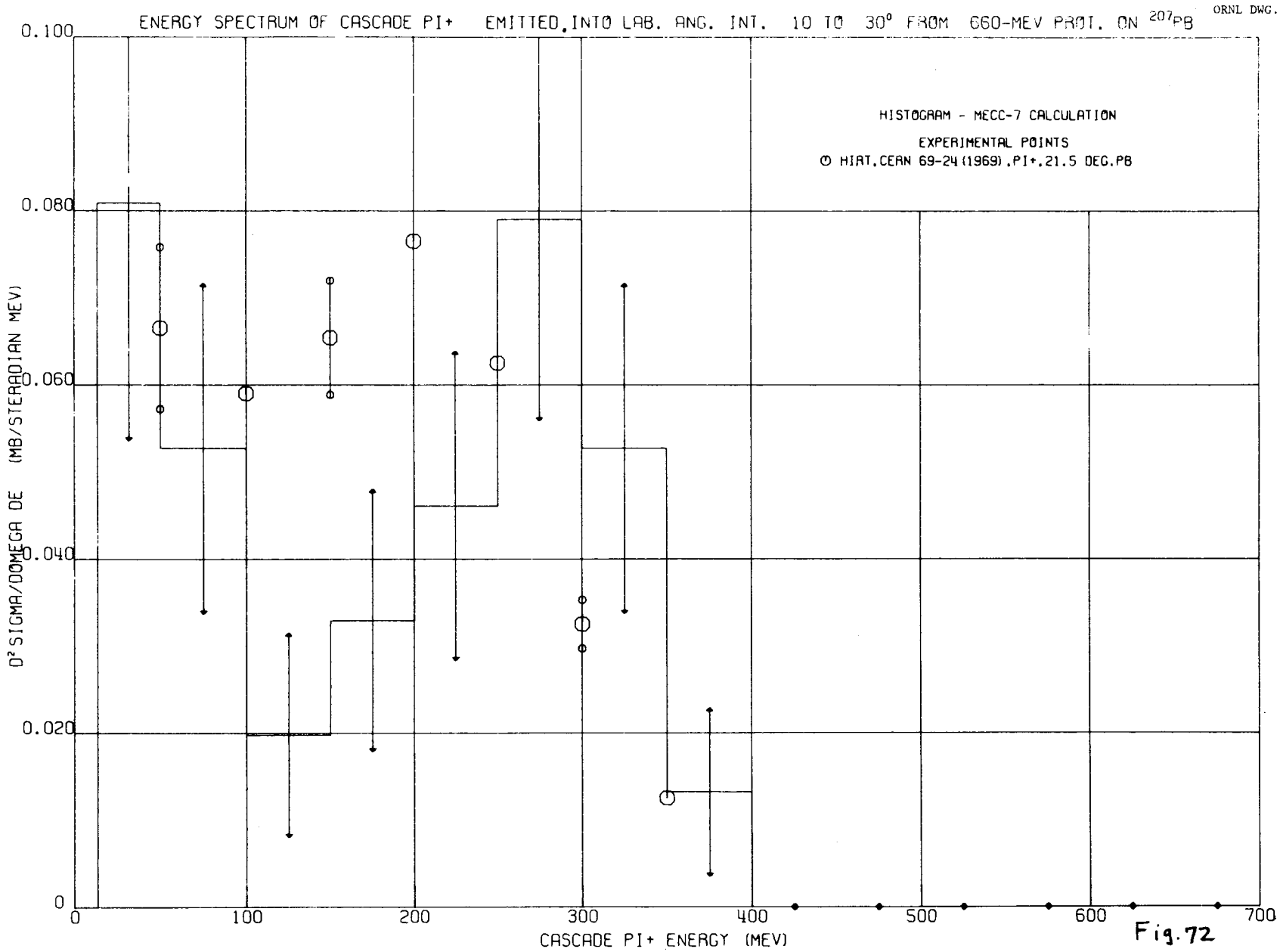

Fig. 72

ORNL DWG. 72-4414

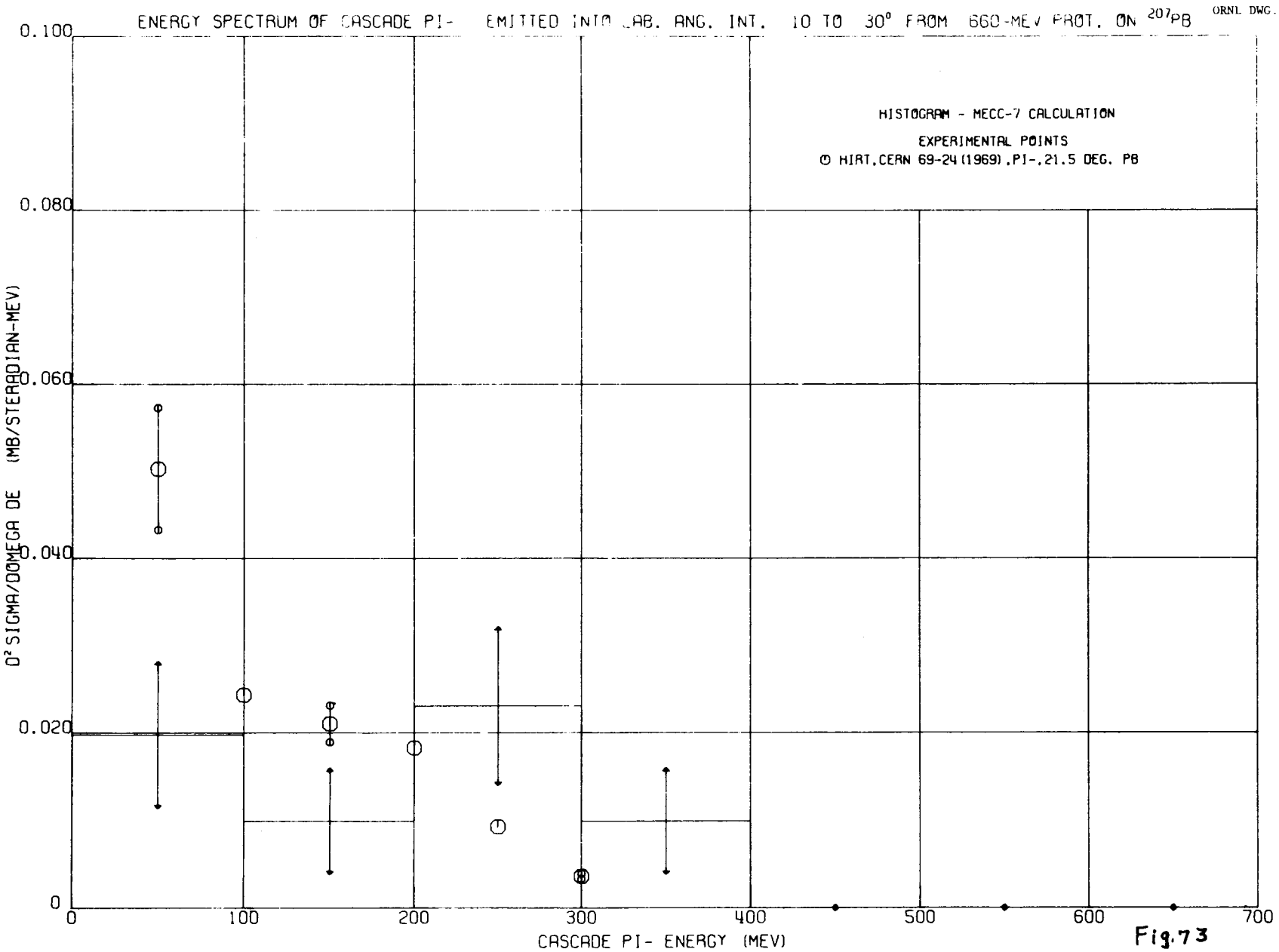

Fig. 73

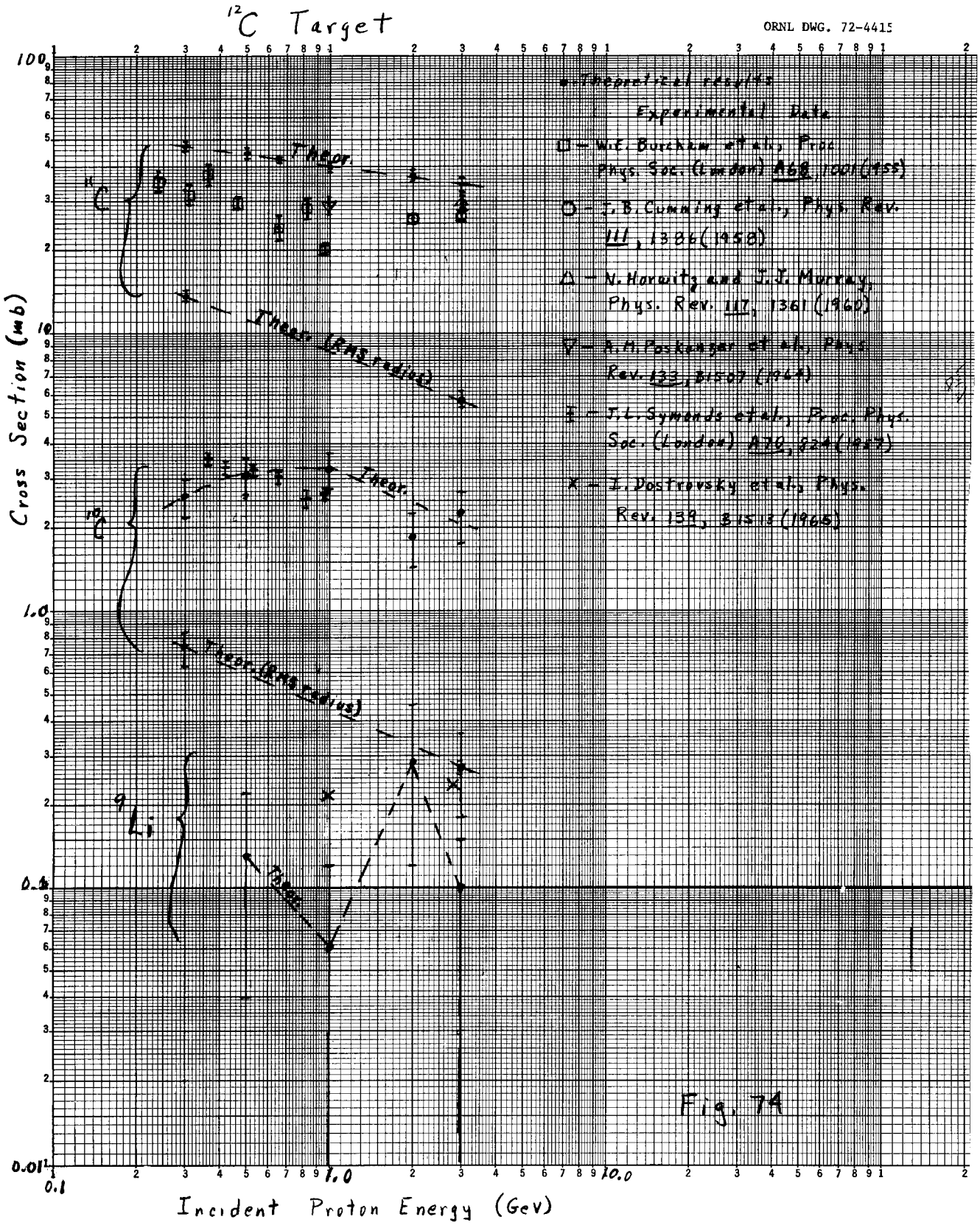
^{12}C Target
ORNL DWG. 72-4415
Theoretical results
Experimental Data
□ – W.E. Burcham et al., Proc. Phys. Soc. (London) A68, 1001 (1955)
○ – J.B. Cumming et al., Phys. Rev. 111, 1386 (1958)
△ – N. Horwitz and J.J. Murray, Phys. Rev. 117, 1361 (1960)
▽ – R.M. Poskanzer et al., Phys. Rev. 133, B1507 (1964)
X – J.L. Symonds et al., Proc. Phys. Soc. (London) A70, 824 (1957)
× – I. Dostrovsky et al., Phys. Rev. 139, B1115 (1965)
Theor.
Theor. (RMS radius)
^{12}C
^{10}C
^{9}Li
Cross Section (mb)
Incident Proton Energy (GeV)

Fig. 74

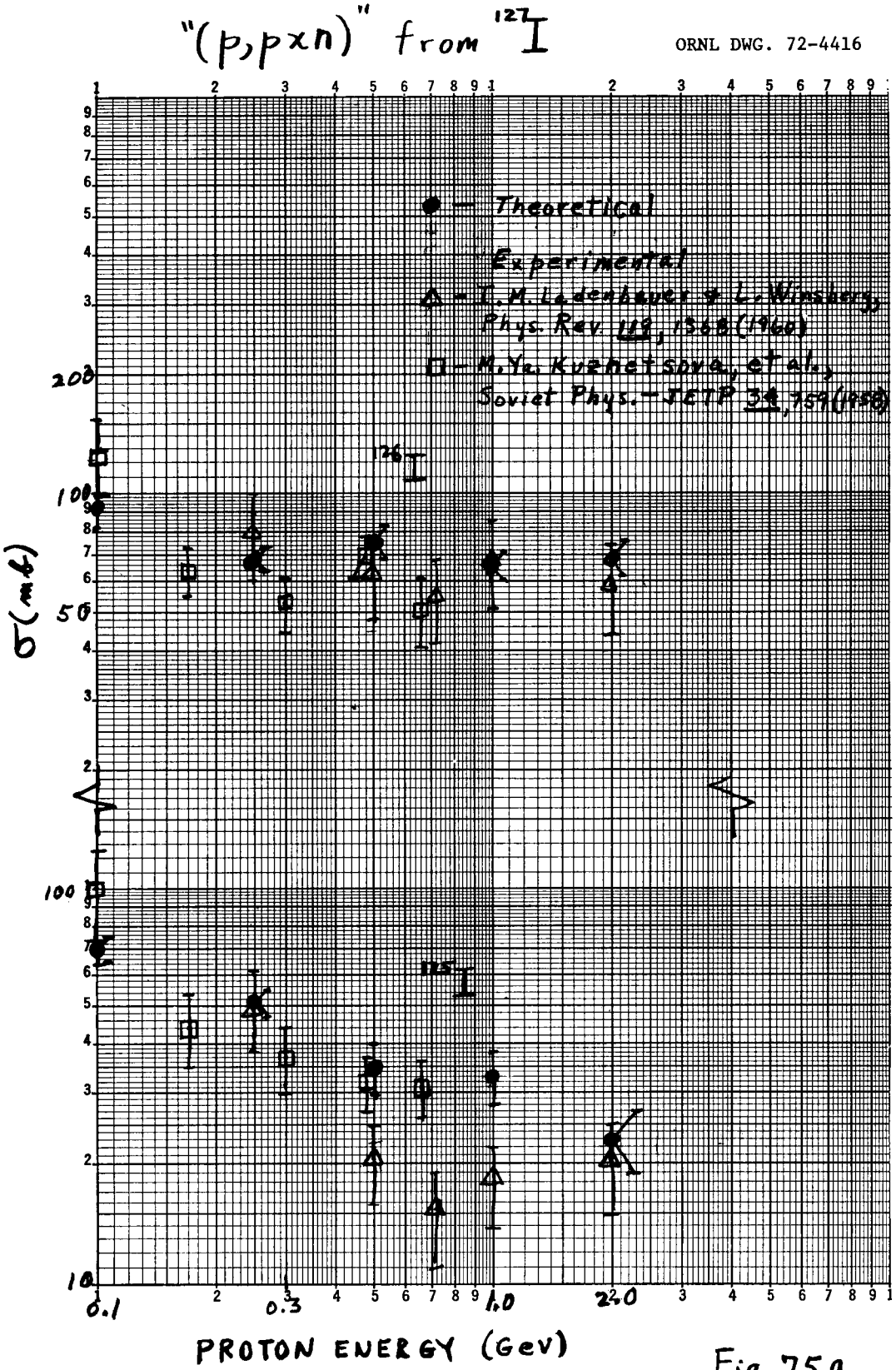
"(p,pxn)" from 127 I
ORNL DWG. 72-4416
● — Theoretical
Experimental
△ - I. M. Ladenbauer & L. Winsberg, Phys. Rev. 119, 1368 (1960)
□ - M. Ya. Kuznetsova, et al., Soviet Phys.-JETP 34, 759 (1958)
126 I
125 I
σ (mb)
PROTON ENERGY (GeV)
0.1
0.3
1.0
2.0

Fig. 75a

ORNL DWG. 72-4417

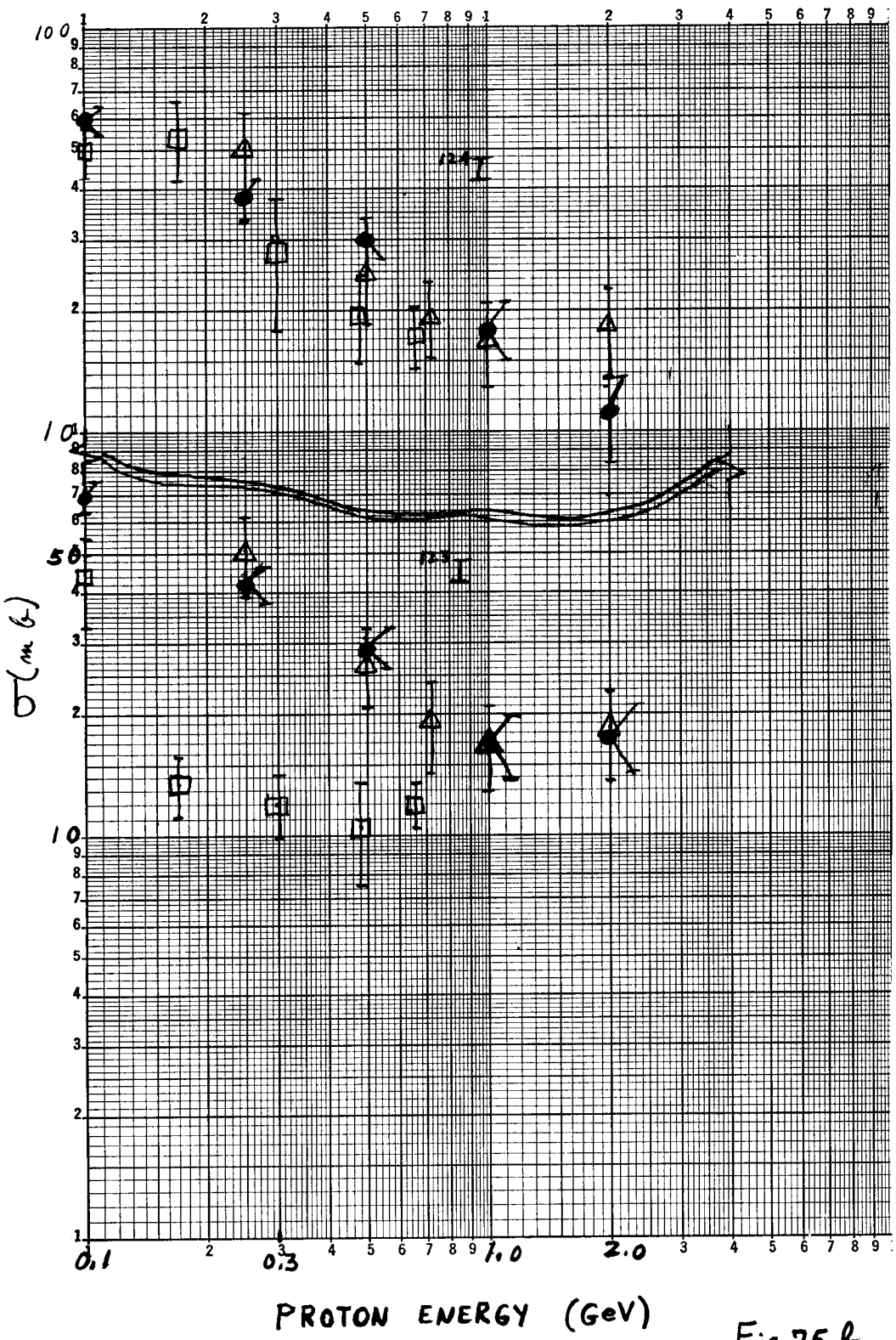

Fig. 75 b

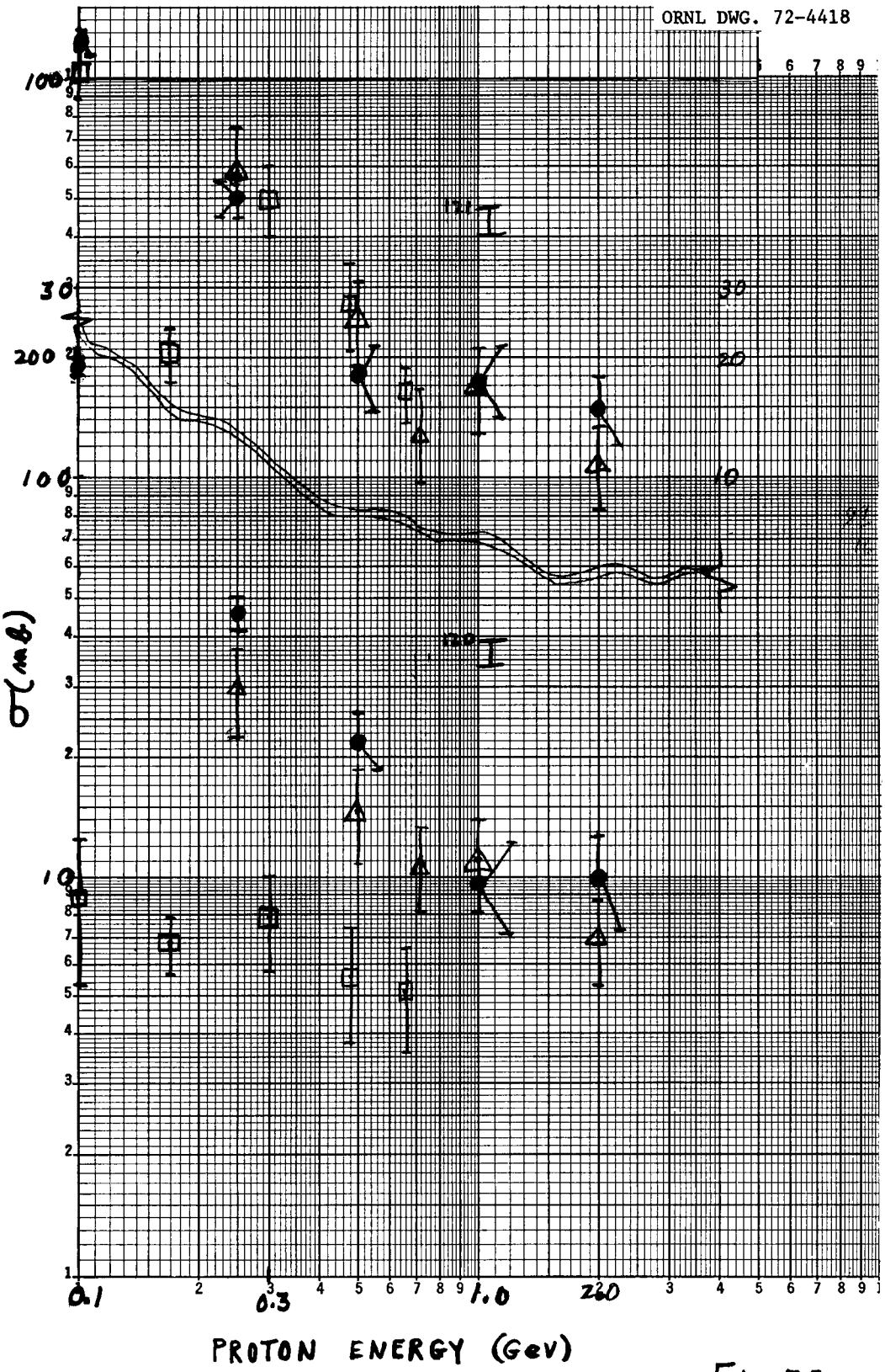
ORNL DWG. 72-4418
σ (mb)
PROTON ENERGY (GeV)
0.1
0.3
1.0
2.0
100
30
200
100
10
30
20
10

Fig. 75c

Internal Distribution

1-3. L. S. Abbott
4. F. S. Alsmiller
5. R. G. Alsmiller, Jr.
6. T. W. Armstrong
7-46. H. W. Bertini
47. H. P. Carter
48. C. E. Clifford
49. A. H. Culkowski
50. T. A. Gabriel
51. M. P. Guthrie
52. R. L. Hahn
53. W. E. Kinney
54. T. A. Love
55. F. C. Maienschein
56. R. W. Peelle
57. R. W. Roussin
58. R. T. Santoro
59. D. Sundberg
60. J. E. Turner
61. J. W. Wachter
62. H. A. Wright
63. W. Zobel
64. H. Feshbach (consultant)
65. H. Goldstein (consultant)
66. C. R. Mehl (consultant)
67. H. T. Motz (consultant)
68-69. Central Research Library
70. ORNL Y-12 Technical Library, Document Reference Section
71-72. Laboratory Records Department
73. Laboratory Records ORNL RC
74. ORNL Patent Office

External Distribution

75. P. B. Hemmig, Division of Reactor Development & Technology, U. S. Atomic Energy Commission, Washington, D. C., 20545.
76. W. H. Hannum, Division of Reactor Deve opment & Technology, U. S. Atomic Energy Commission, Washington, D. C., 20545.
77. Kermit O. Laughon, AEC Site Representative.
78. Robert Burman, MP-7, Los Alamos Scientific Laboratory, P. O. Box 1663, Los Alamos, New Mexico, 87544.
79. Bruce Dropesky, J-11, Los Alamos Scientific Laboratory, P. O. Box 1663, Los Alamos, New Mexico, 87544.
80. A. F. Dunaitsev, Joint Institute for Nuclear Research, Dubna, USSR.
81. Z. Fraenkel, Weizmann Institute for Science, Rehovath, Israel.
82. Gerhart Friedlander, Chemistry Division, Brookhaven National Laboratory, Upton, New York, 11973.
83. J. Robb Grover, Chemistry Division, Brookhaven National Laboratory, Upton, New York, 11973.
84. R. P. Haddock, Physics Department, University of California, Los Angeles, California, 90024.
85. George Harp, Chemistry Division, Brookhaven National Laboratory, Upton, New York, 11973.
86. D. R. Harris, Los Alamos Scientific Laboratory, P. O. Box 1663, Los Alamos, New Mexico, 87544.
87. Sheldon Kaufman, Argonne National Laboratory, 9700 South Cass Avenue, Argonne, Illinois, 60439.
88. Robert Macek, MP-7, Los Alamos Scientific Laboratory, P. O. Box 1663, Los Alamos, New Mexico, 87544.
89. S. S. Markowitz, Department of Chemistry, University of California, Berkeley, California, 94720.
90. E. G. Michaelis, Division de la Machine, Synchro-cyclotron, CERN, Geneva 23, Switzerland.
91. Brian D. Pate, Chemistry Department, Simon Fraser University, Burnaby 2, British Columbia, Canada.

External Distribution (cont'd)

92. Arthur M. Poskanzer, Lawrence Berkeley Laboratory, Berkeley, California, 94720.
93. L. P. Remsberg, Chemistry Department, Brookhaven National Laboratory, Upton, New York, 11973.
94. Mario Schillaci, MP-7, Los Alamos Scientific Laboratory, P. O. Box 1663, Los Alamos, New Mexico, 87544.
95. Anthony Turkevich, Chemistry Department, University of Chicago, Chicago, Illinois, 60637.
96. R. G. Vasil'kov, Joint Institute for Nuclear Research, Dubna, USSR.
97. L. Yaffe, Department of Chemistry, McGill University, Montreal, Quebec, Canada.

98-235. Given AEC High-Energy Accelerator Shielding and NASA Space Shielding Distribution.*

236-237. Technical Information Center (TIC).

238. Laboratory and University Division (ORO).

*A copy of this distribution list is available on request.